To the Graduate Council:

I am submitting herewith a thesis written by Gerald Henderson Springer entitled "FTIR, Raman and Polarimetric Studies of Organic Compounds in Solution and on Alumina." I have examined the final copy of this thesis for form and content and recommend that it be accepted in partial fulfillment of the requirements for the degree of Master of Science, with a major in Chemistry.

Richard M. Pagni, Major Professor

We have read this thesis
and recommend its acceptance:

Accepted for the Council:

Associate Vice Chancellor and
Dean of the Graduate School

FTIR, RAMAN AND POLARIMETRIC STUDIES OF ORGANIC COMPOUNDS IN SOLUTION AND ON ALUMINA

A Thesis

Presented for the

Master of Science

Degree

The University of Tennessee, Knoxville

Gerald Henderson Springer

May, 1997

Dedication

This thesis is lovingly dedicated to the memory of my mother, who taught me, both by precept and example what love is all about and to my father, who always insisted that "a hill of hard work is worth more than a mountain of unused talent."

Acknowledgments

I would like to thank my major professor, Dr. R .M. Pagni for his leadership, expertise and patience without which this study would have been impossible. I would also like to thank The University of Tennessee for providing the teaching assistantship. I am deeply indebted to Dr. Anna Edwards from whom I learnt FTIR and Raman spectroscopy. The spectroscopic work done for this study would have been impossible without her help. I would also like to thank Dr. T. F. Williams, distinguished professor in the chemistry department at The University of Tennessee, Knoxville, for making physical chemistry exciting and understandable and for the many delightful conversations we had. Many thanks are extended to my father, teacher, mentor and friend Dr. Emerson Cooper, professor emeritus of chemistry and former president of Oakwood College, for all the help and encouragement that he has given me over the last seven years. Thanks also to Dr. D. Kleinfelter for use of his lab and for bringing me so much laughter. I am also grateful to Dr. Garth Baker of the University of Tennessee and Dr. Carlos Lee of Tennessee State University for ensuring that I was comfortable while here in Knoxville. Dr. Shirley Beary, my amazing college piano teacher, also deserves special thanks. The music we studied together added joy to living. To my adopted mother, Joni Pierre-Louis, on whom I could always call for support and encouragement, I say a very special thank you. To my sisters Miriam and Margaret I say thanks for a lifetime of great memories. Finally, to my brother and friend, Stephen Balfour I say thanks for all the times that we shared and for the richness that we brought to each other's lives.

Abstract

An attempt was made to follow the kinetics of the hydrolysis of benzonitrile on unactivated alumina. Calibration curves were constructed using DRIFTS data. An attempt was also made to follow the reaction *in situ* by Raman spectroscopy. Poor calibration curves were obtained, however, with some modification in the experimental protocol it should be possible to follow the kinetics of the hydrolysis.

The complexation of the Lewis acid, Li^+, to crotonaldehyde, benzonitrile and camphor was studied using spectroscopic (FTIR) and polarimetric techniques. Using band resolution, it was found that within certain concentration ranges that the complexation of the Lewis acid to the Lewis base gives rise to 1:1 complexes. The equilibrium constants for the complexation to each substrate were calculated. The experimental IR shifts of the crotonaldehyde and benzonitrile complexes were compared to those obtained using MNDO calculations.

The effect of thirteen solvents on the optical rotatory power of (1R)(+) camphor were studied. These effects were compared to several solvent parameters. A linear relationship was found to exist between the amount of camphor used and the extent of the optical rotation. The magnitude of the slopes of the Rotation vs Camphor (g) curves were found to be dependent on the nature of the solvent. No simple correlation was found to exist between the degree of optical rotation and the solvent parameters.

TABLE OF CONTENTS

PART 1: DRIFTS and Raman Studies of the Kinetics of Benzonitrile Hydrolysis on Unactivated Alumina.

CHAPTER Page

I. Introduction 2

II. Results and Discussion 4

III. Experimental Section 24

A. General 24

B. Infrared Analysis 24

C. Raman Analysis 24

D. Sample Preparation 25

References 27

Part 2: FTIR and Polarimetric Studies of the Lithium Ion Complexation to Carbonyl and Nitrile Functional Groups, using Crotonaldehyde, Benzonitrile and Camphor in a $LiClO_4$/Diethyl Ether System.

I. Introduction 29

II. Results and Discussion 37

III. Experimental Section 77

A. Preparation of Reagents and Solutions 77

Chapter Page

B. Acquisition and Spectral Manipulation of IR Data 78

C. Polarimetric Data 80

D. MO Calculations 81

References 82

PART 3: An Investigation of the Influence of Solvent Effects on the Optical Rotation of Camphor.

I. Introduction 86

II. Results and Discussion 89

A. Definitions of the Selected Solvent Parameters in Table 3-17 96

III Experimental Section 111

A. General 111

B. Preparation of Solutions 111

C. Polarimetric Data 111

References 113

Vita 114

LIST OF TABLES

PART 1: DRIFTS and Raman Studies of the Kinetics of Benzonitrile Hydrolysis on Unactivated Alumina.

Table — Page

1-1. Results of DRIFTS Analysis of Benzonitrile Standards in Absorbance Units 5

1-2. Results of DRIFTS Analysis of Benzonitrile Standards in K-M Units 6

1-3. Results of Test for Reproducibility in Sample Preparation 12

Part 2: FTIR and Polarimetric Studies of the Lithium Ion Complexation to Carbonyl and Nitrile Functional Groups, Using Crotonaldehyde, Benzonitrile and Camphor in a $LiClO_4$/Diethyl Ether System.

2-1. ^{1}H Chemical Shift Differences ($\Delta\delta$) of Crotonaldehyde on Complexation with Various Lewis Acids 32

2-2. ^{13}C Chemical Shift Differences ($\Delta\delta$) of Crotonaldehyde on Complexation with Various Lewis Acids 33

2-3. Lewis Acid Scale Based On $\Delta\delta$-values of H3 Resonances of Crotonaldehyde 34

2-4. Induced Chemical Shifts of Crotonaldehyde (H3) and Diethyl Ether in Solutions of CA in LPDE at -20 °C 35

2-5. Peak Centers and Widths at Half-Max as a Function of LP Conc. For 0.10 M to 3.00 M LP-CA Complexes 52

2-6. Band-Fitting Results for 0.04 M to 0.10 M LP-CA Complexes in DE (Lorentzian Fit) 53

2-7. Band-Fitting Results for 0.04 M to 0.10 M LP-CA Complexes in DE (Pearson Fit) 54

2-8. Band-Fitting Results for 0.10 M to 2.00 M LP-CA Complexes in DE (Lorentzian Fit) 58

Table Page

2-9. Band-Fitting Results for 0.10 M to 2.00 M LP-CA Complexes in DE (Pearson Fit) 56

2-10. Band-Fitting Results for 0.10 M to 3.00 M LP-CA Complexes in DE (Lorentzian Fit) 57

2-11. Band-Fitting Results for 1.00 M to 3.00 M LP-CA Complexes in DE (Pearson Fit) 58

2-12. Resolved Bands of 0.04 M to 0.10 M LP-CA Complexes in DE 61

2-13. Equilibrium Constants for the Formation of 0.04 to 0.10 M LP-CA Complexes 61

2-14. Peak Center and Widths at Half-Max as a Function of LP Conc. for 0.10 M to 2.00 M LP-BN Complexes 62

2-15. Band-Fitting Results for 0.10 M to 2.00 M LP-BN Complexes in DE (Lorentzian Fit) 65

2-16. Band-Fitting Results for the 0.10 M to 2.00 M LP-BN Complexes in DE (Pearson Fit) 66

2-17. Resolved Bands of the 0.10 M to 2.00 M LP-BN Complexes in DE 67

2-18. Equilibrium Constants for the Formation of 0.10 M to 2.00 M LP-BN Complexes in DE 68

2-19. Camphor Rotations in Diethyl Ether as a Function of LP Conc. 69

2-20. Camphene Rotations in Diethyl Ether as a Function of LP Conc. 69

2-21. Results for the Calculation of K_{eq} for the LP-CM Complexation 73

2-22. Comparison of IR Stretching Frequencies 74

Part 3: An Investigation of the Influence of Solvent Effects on the Optical Rotation of Camphor.

Table Page

3-1. Observed Rotations in Diethyl ether 90

3-2. Observed Rotations in Toluene 90

3-3. Observed Rotations in Acetone 90

3-4. Observed Rotations in Acetonitrile 90

3-5. Observed Rotations in Methylene chloride 91

3-6. Observed Rotations in Methanol 91

3-7. Observed Rotations in Benzene 91

3-8. Observed Rotations in Cyclohexane 91

3-9. Observed Rotations in Carbon disulfide 92

3-10. Observed Rotations in Dimethyl sulfoxide 92

3-11. Observed Rotations in Nitrobenzene 92

3-12. Observed Rotations in N,N-Dimethylformamide 92

3-13. Observed Rotations in Hexafluorobenzene 93

3-14. Summary of Optical Rotations of Camphor in Various Solvents 93

3-15. Intercepts (b), Slopes (m), and Correlation Coefficients (r) for Curves (Rot. Vs g) Using the five Lowest Data Sets Obtained in a Given Solvent ... 94

3-16. Intercepts (b), Slopes (m), and Correlation Coefficients (r) for Rot. Vs Camphor (g) Curves Obtained Using "Cricket Graph". 94

3-17. A Selection of Solvent Parameters 95

3-18. Observed Rotations of Camphor in Benzene and Methanol as a Function of Camphor's Molarity 98

LIST OF FIGURES

Part 1: DRIFTS and Raman Studies of the Kinetics of Benzonitrile Hydrolysis on Unactivated Alumina.

Figure — Page

1-1. A calibration curve using benzonitrile calibration standards. The integrated area under the nitrile stretching band is plotted as a function of the number of millimoles of the calibration standard on 15 g of unactivated alumina. Absorbance units are used for the plot 8

1-2. A calibration curve using benzonitrile calibration standards. The height of the nitrile stretching band is plotted as a function of the number of millimoles of the calibration standard on 15 g of unactivated alumina. Absorbance units are used for the plot 9

1-3. A calibration curve using benzonitrile calibration standards. The integrated area under the nitrile stretching band is plotted as a function of the number of millimoles of the calibration standard on 15 g of unactivated alumina. Kubelka-Munk units are used for the plot 10

1-4. A calibration curve using benzonitrile calibration standards. The height of the nitrile stretching band is plotted as a function of the number of millimoles of the calibration standard on 15 g of unactivated alumina. Kubelka-Munk units are used for the plot 11

1-5. Raman spectra of benzonitrile on alumina centered at 1600 cm^{-1} 15

1-6. Raman spectra of benzonitrile on alumina centered at 2300 cm^{-1} 16

1-7. Raman spectra of benzonitrile on alumina centered at 3000 cm^{-1} 17

1-8 Savitsky-Golay treated Raman spectrum of benzonitrile on alumina centered at 1600 cm^{-1} 19

1-9 Savitsky-Golay treated Raman spectrum of benzonitrile on alumina centered at 2300 cm^{-1} 20

Figure Page

1-10 Savitsky-Golay treated Raman spectrum of benzonitrile on alumina centered at 3000 cm^{-1} 21

Part 2: FTIR and Polarimetric Studies of the Lithium Ion Complexation to Carbonyl and Nitrile Functional Groups, using Crotonaldehyde, Benzonitrile and Camphor in a $LiClO_4$/Diethyl Ether System.

2-1. The results of a curvefit and a plot of the residuals. 39

2-2. FTIR of crotonaldehyde in diethyl ether 41

2-3. FTIR of crotonaldehyde in diethyl ether from which the spectrum of diethyl has been removed 42

2-4. The effect of the addition of 0.10 M $LiClO_4$ to a solution of 0.285 M crotonaldehyde in diethyl ether 43

2-5. The effect of the addition of 0.30 M $LiClO_4$ to a solution of 0.285 M crotonaldehyde in diethyl ether 44

2-6. Superimposed raw FTIR spectra of 0.04 M to 0.10 M LP-CA complexes in diethyl ether 45

2-7. Superimposed raw FTIR spectra of 0.10 M to 2.00 M LP-CA complexes in diethyl ether 46

2-8. Superimposed raw FTIR spectra of 1.00 M to 3.00 M LP-CA complexes in diethyl ether 47

2-9. Superimposed raw FTIR spectra of 1.00 M to 3.00 M LP-CA complexes in diethyl ether with emphasis on the wavenumber region of 1940 cm^{-1} to 1980 cm^{-1} 50

2-10. Superimposed raw FTIR spectra of 1.00 M to 3.00 M LP-BN complexes in diethyl ether 63

2-11. The effect of increasing LP concentration on the optical rotation of 2.00 g of camphor in 25 mL of diethyl ether 71

Part 3: An Investigation of the Influence of Solvent Effects on the Optical Rotation of Camphor.

Figure Page

3-1. Plots of Rotation vs Camphor (g) in thirteen solvents 99

3-2. Plots of Rotation vs Camphor (g) in methylene chloride, methanol, cyclohexane and carbon disulfide 100

3-3. Plots of Rotation vs Camphor (g) in diethyl ether, acetone, acetonitrile, dimethyl sulfoxide and N,N-dimethylformamide 101

3-4. Plots of Rotation vs Camphor (g) in toluene, nitrobenzene and hexafluorobenzene 102

3-5. A bar chart showing the effect of solvents on the rotation of two grams of camphor 103

3-6. Plot of Observed Rotation vs Conc. (M) for the camphor /methanol system 107

3-7. Plot of Observed Rotation vs Conc. (M)(dilute) for the camphor /methanol system 108

3-8. Plot of Observed Rotation vs Conc. (M) for the camphor /benzene system 109

3-9. Plot of Observed Rotation vs Conc. (M)(dilute) for the camphor /benzene system 110

LIST OF ABBREVIATIONS

PART 1: DRIFTS and Raman Studies of the Kinetics of Benzonitrile Hydrolysis on Unactivated Alumina.

DRIFTS	Diffuse Reflectance Infrared Fouier Transform Spectroscopy
K-M	Kubelka-Munk
BCN	Benzonitrile
IR	Infrared Spectroscopy
Abs.	Absorbance
CCD	Charge Coupled Device

Part 2: FTIR and Polarimetric Studies of the Lithium Ion Complexation to Carbonyl and Nitrile Functional Groups, using Crotonaldehyde, Benzonitrile and Camphor in a $LiClO_4$/Diethyl Ether System.

$LiClO_4$	Lithium Perchlorate
FTIR	Fourier Transform Infrared Spectroscopy
LPDE	Lithium Perchlorate in Diethyl Ether
NMR	Nuclear Magnetic Resonance Spectroscopy
MO	Molecular Orbital
CA	Crotonaldehyde
LP	Lithium Perchlorate
LP-CA	Lithium-Crotonaldehyde Complex
LP-BN	Lithium-Benzonitrile Complex
BN	Benzonitrile
CM	Camphor
LP-CM	Lithium-Camphor Complex
ATR-FTIR	Attenuated Total Reflectance Fourier Transform Infrared Spectroscopy
MNDO	Modified Neglect of Differential Overlap

Part 3: An Investigation of the Influence of Solvent Effects on the Optical Rotation of Camphor.

Rot.	Rotation
AN	Acceptor Number
DN	Donor Number
CRC	Chemical Rubber Company
HBA	Hydrogen Bond Acceptor
HBD	Hydrogen Bond Donor

PART 1

DRIFTS and Raman Studies of the Kinetics of Benzonitrile Hydrolysis on Unactivated Alumina.

CHAPTER I

INTRODUCTION

The conversion of nitriles to amides in solution can be achieved by a relatively facile acid or base-catalyzed hydrolysis. However, it is difficult to produce the amide selectively, since it is usually hydrolyzed a lot more easily than its parent nitrile.[1] It has been shown that the surface of unactivated alumina is also a good environment for the nitrile-to-amide synthesis.[2] This hydrolysis is possible because of the polarity[3] of the alumina surface and also because of the presence of hydroxyl groups (about 3.7 mmol of hyroxyls/g)[4] which serve as the source of water for the reaction. In solution the reaction is thought to proceed as shown below (eq. 1).[5]

$$RCN \xrightarrow{H_2O} RCONH_2 \xrightarrow{H_2O} RCOOH \qquad (1)$$

The surface reaction works well for both aliphatic and aryl nitriles. Hydrolysis occurs under acid-catalyzed and uncatalyzed conditions, but the uncatalyzed hydrolysis was shown to be more efficient than the acid-catalyzed reaction. It is the uncatalyzed reaction on unactivated alumina which was of interest to this study.

In this study an attempt was made to understand the mechanism of the surface nitrile hydrolysis. A likely mechanism by which the hydrolysis occurs is shown below:

$$RCN + \text{Surface } OH^- \rightarrow \text{Adsorbed } RC(OH)=N^- \qquad (2)$$

$$\text{Adsorbed } RC(OH)=N^- + OH^- \rightarrow \text{Adsorbed } RC(OH)=NH + \text{Surface } O^{2-} \qquad (3)$$

$$\text{Adsorbed } RC(OH)=NH \rightarrow \text{Adsorbed } RCONH_2 \qquad (4)$$

In order to study the mechanism an *in situ* kinetic study was attempted. This study focused on the disappearance of the nitrile stretching band as a function of time. The disappearance of the band was followed using both Diffuse Reflectance Infrared Spectroscopy (DRIFTS) and Raman spectroscopy. These spectroscopic methods proved to have great utility in that the reaction can be studied *in situ.*

Previously, in order to quantify the products of the reaction, the reactions were worked up and the products extracted from the solid with methanol. Product analysis was then done using gas chromatography. In principle much less effort is required when using the aforementioned spectroscopic techniques. An attempt was made to construct a reliable calibration curve using DRIFTS data. The reaction was also followed *in situ* by Raman spectroscopy.

CHAPTER II

RESULTS AND DISCUSSION

Obtaining a calibration curve for the nitrile stretching band was a pivotal part of the DRIFTS analysis. If a reliable and reproducible curve could be obtained, it would be an easy matter to plot the disappearance of the nitrile band as a function of time. Thus, we would gain greater insight into the kinetics of the reaction.

Several samples of various millimolar concentrations of benzonitrile on 15 g of unactivated alumina were prepared and their spectra were obtained. These samples were prepared by adding, via syringe, the appropriate amount of benzonitrile to 15 g of alumina in a round-bottomed flask. This mixture was stirred with a magnetic stir bar for three hours. These samples were then kept in sealed vials until they were ready for analysis. The results were recorded both as the height of the band and also as the integrated area under the band. These results are reported in Table 1-1 and Table 1-2.

Kubelka-Munk units are included because they are preferred when doing quantitative DRIFTS analysis.[6] The Kubelka-Munk (K-M) function [$f(R_\infty)$] is given by:

$$f(R_\infty) = \frac{(1-R_\infty)_2}{2R_\infty} = \frac{k}{s},$$

where R_∞ is the ratio of the reflectance of the sample and the reference in the case of infinitely thick layers, k is the absorption coefficient, and s is the scattering coefficient of the sample.

Table 1-1. Results of DRIFTS analysis of benzonitrile standards

Absorbance File[a]	Frequency cm^{-1}	Height	Integrated Area
BCN1mM	2231.90	0.1001	1.950
BCN2mM	2232.09	0.1516	3.149
BCN3mM	2231.43	0.2968	6.353
BCN5mM	2230.66	0.3657	8.347
BCN6mM	2231.21	0.3432	7.605
BCN9mM	2230.29	0.4511	10.222
BCN10mM	2230.28	0.4011	9.340
BCN12mM	2230.11	0.4036	9.030
BCN15mM	2229.75	0.5855	13.207
BCN20mM	2229.42	0.4362	9.962

[a]BCN1mM = 1 mM PhCN/15 g alumina.

Table 1-2. Results of DRIFTS analysis of benzonitrile standards			
K-M File[a]	**Frequency cm^{-1}**	**Height**	**Area**
BCN1KM	2231.88	1.6465	30.81
BCN2KM	2232.08	2.7510	53.72
BCN3KM	2231.43	6.3400	120.43
BCN5KM	2230.66	8.1460	160.23
BCN6KM	2231.21	6.608	127.53
BCN9KM	2230.30	10.176.	191.73
BCN10KM	2230.29	8.328	165.43
BCN12KM	2223.11	7.086	135.13
BCN15KM	2229.76	18.518	326.17
BCN20KM	2229.43	8.028	152.22
[a]BCN1KM = 1 mM PhCN with Kubleka Munk units.			

The Kubleka-Munk equation is valid under the following conditions:

(1) Both the reference and the sample should have infinitely deep layers when placed in the sample cup. Thus when these layers are thick enough the IR beam will not reach the bottom of the sample cup.

(2) Measures are taken to make surface scattering and specular reflection negligible..

(3) The degree of light scattering should be proportional to the thickness of the layers.

When using the K-M function for quantitative analysis it is assumed that the absorption coefficient is proportional to the sample concentration (c), and the function can now be rewritten as: $f(R_\infty) = \frac{2.303\varepsilon}{s}.c$, where ε is the molar absorptivity of the sample. Thus the K-M function is suitable for quantitative analysis if the scattering coefficient is constant. When these data were plotted (Figs. 1-1 to 1-4) considerable scatter was observed regardless of the units of the data.

The non-linearity observed in these plots indicated that there might be a problem in sample preparation or in the method used on loading the sample. Furthermore there are many inherent difficulties in using DRIFTS for quantitative analysis. Krivacsy and Hlavay[7,8] explored the influence of concentration dependence and sample packing in generating reproducible DRIFTS data. In their attempt to generate a reliable calibration curve for DRIFTS analysis, Griffiths and coworkers,[9] discovered that homogeneous calibration standards are critical to the success of quantitative reflectance measurements, and that analytes should be prepared under conditions identical to those of the calibration

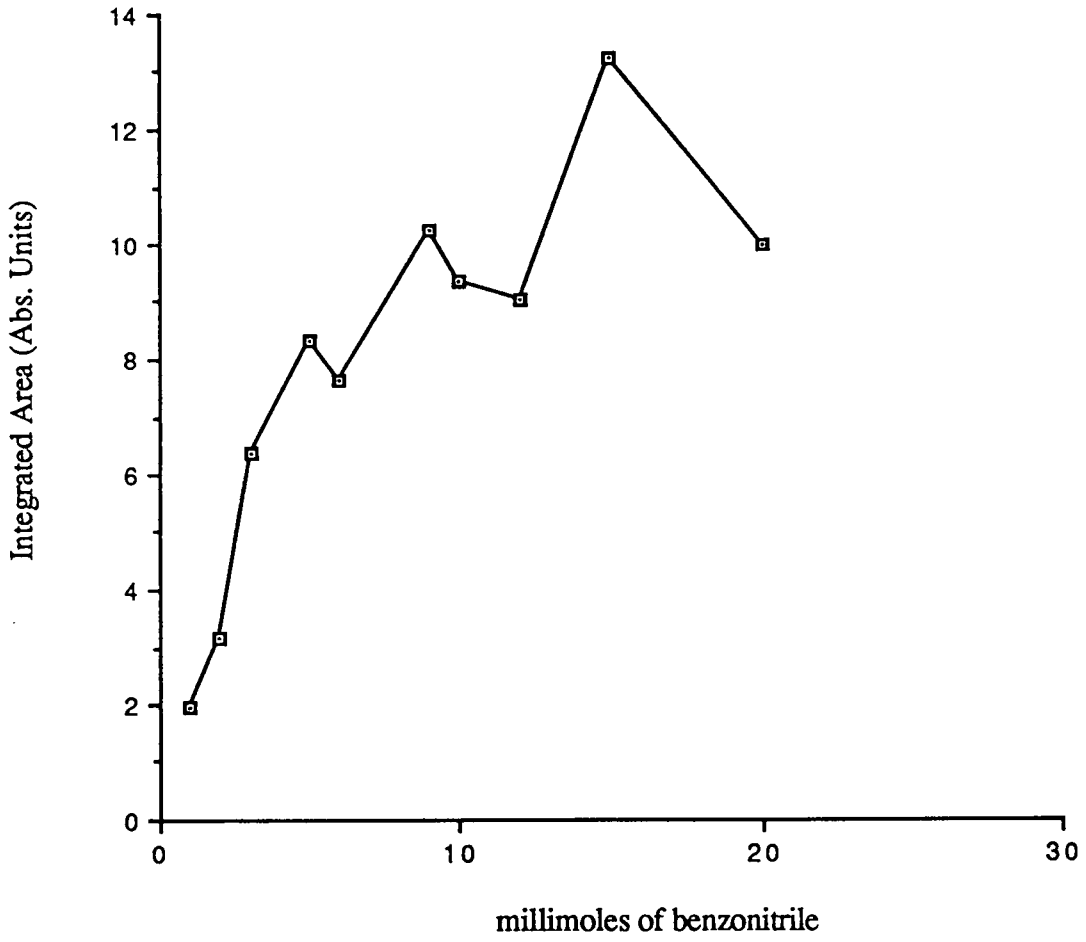


Figure 1-1. A calibration curve using benzonitrile calibration standards. The integrated area under the nitrile stretching band is plotted as a function of the number of millimoles of the calibration standard on 15 g of unactivated alumina. Absorbance units are used for the plot.

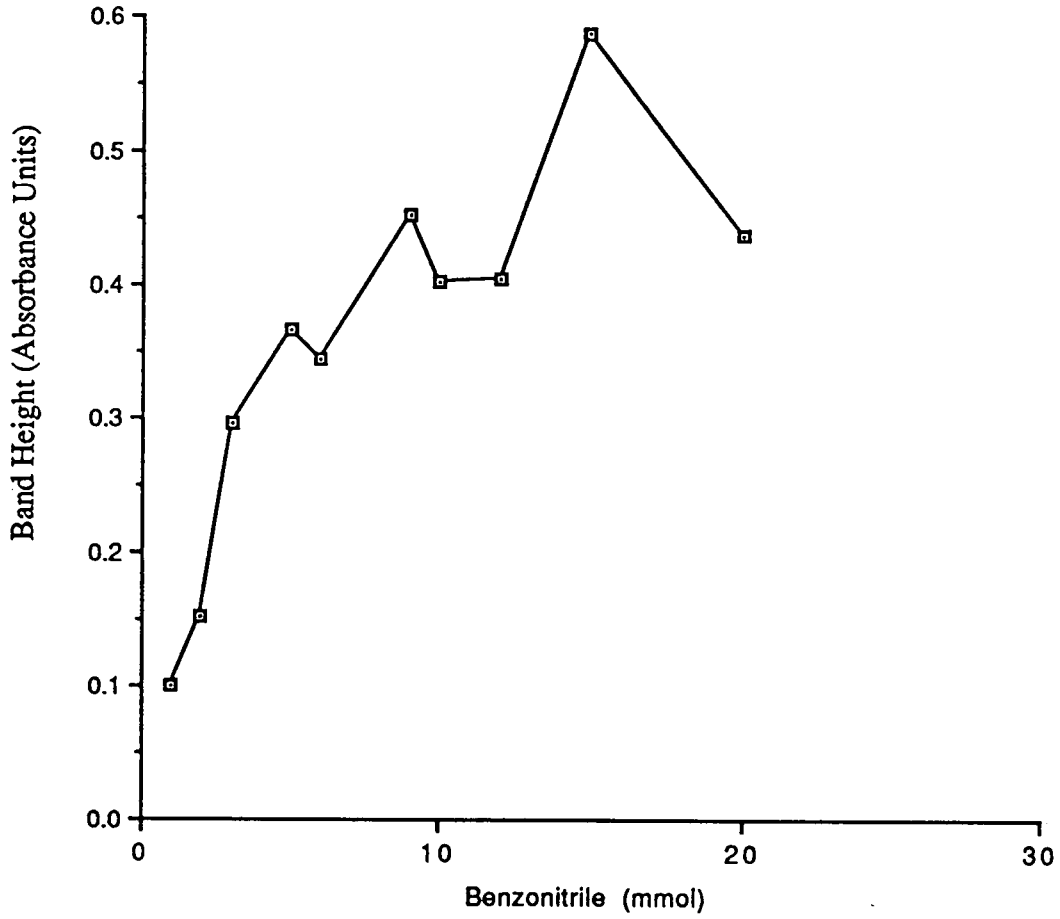


Figure 1-2. A calibration curve using benzonitrile calibration standards. The height the nitrile stretching band is plotted as a function of the number of millimoles of the calibration standard on 15 g of unactivated alumina. Absorbance units are used for the plot.

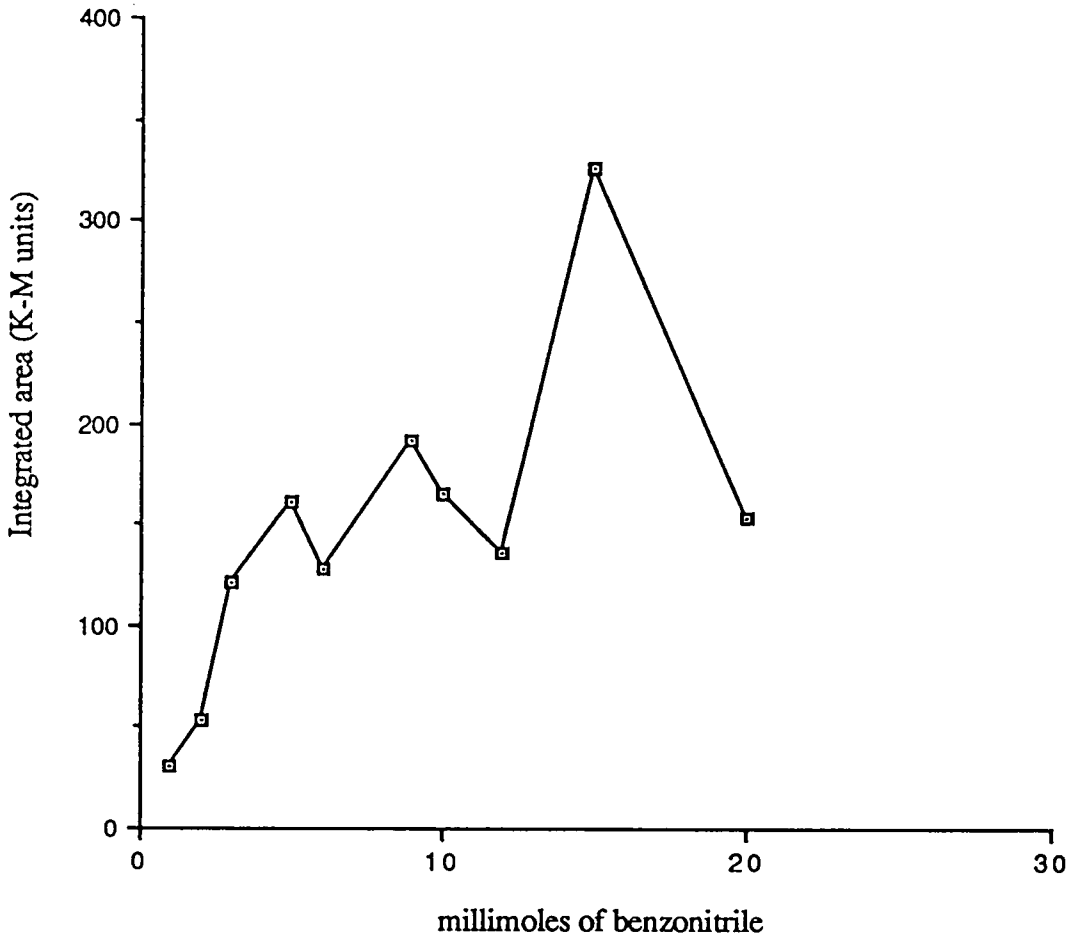


Figure 1-3. A calibration curve using benzonitrile calibration standards. The integrated area under the nitrile stretching band is plotted as a function of the number of millimoles of the calibration standard on 15 g of unactivated alumina. Kubelka-Munk units are used for the plot.

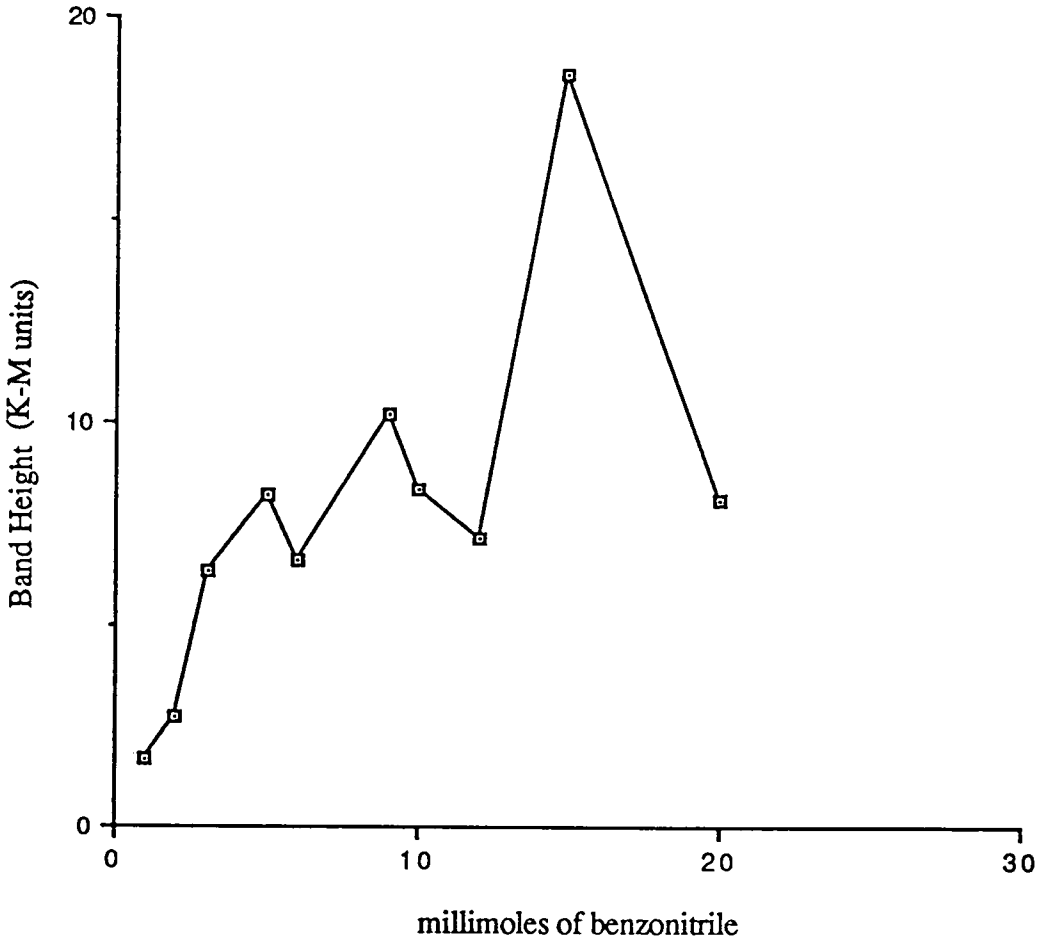


Figure 1-4. A calibration curve using benzonitrile calibration standards. The height of the nitrile stretching band is plotted as a function of the number of millimoles of the calibration standard on 15 g of unactivated alumina. Kubleka-Munk units are used for the plot.

standards. In an attempt to test the homogeneity of the calibration standards three separate samples (6 mM benzonitrile/15 g alumina) were prepared under identical conditions. These samples were then divided into batches A, B and C. DRIFTS data were then acquired for three unique samples taken from each batch. A comparison of the standard deviations with batches for the height and integrated area of the band of interest is shown in Table 1-3

Table 1-3. Results of Test for Reproducibility in Sample Preparation

	Batch A		**Batch B**		**Batch C**	
Trial	Height	Area	Height	Area	Height	Area
1	0.3074	7.221	0.4066	10.141	0.3001	6.880
2	0.3725	8.625	0.3341	8.504	0.3121	7.264.
3	0.3232	7.779	0.3191	7.350	0.3113	7.254

When all nine samples were compared the standard deviation of the band height whose average value is 0.3318 was 0.029. The standard deviation of the integrated area whose average value was 7.891 was 0.996. These results demonstrate how difficult it is prepare reliable calibration curves for use in doing quantitative DRIFTS work. In the face of these difficulties an attempt was made, using Raman spectroscopy, to follow the nitrile hydrolysis reaction *in situ.*

When the Raman spectra of neat benzonitrile and its hydrolysis product benzamide, are compared, similar bands are observed for the aromatic C-H stretches around 3075 cm^{-1}. However, benzonitrile has a distinct band at 2230 cm^{-1} (due to the nitrile stretch).

Samples were mounted in a furnace and kept there for the duration of the experiment. The furnace was set up at the macro stage of the Dilor Raman Spectrometer and data acquired directly on the heated sample. Each sample was heated continuously and analyzed directly in the furnace. The progress of the reaction was followed by ratioing the integrated band intensity at 2230 cm^{-1} to two other bands whose intensity should not change. Several accumulations of a given window were taken since the software package on the Dilor system works best when individual windows are manipulated.

Individual window spectra centered at 1600, 2230 and 3000 cm^{-1} were acquired. Each spectrum recorded was the average of three accumulations (each accumulation was 60 sec. integration). Spectra were acquired at the beginning of the experiment, at several hour intervals afterwards, and then after 24 hours, 35 hours, 144 hours, and 366 hours. The spectra presented here are from the individual windows at the beginning of the experiment, 35 hours, at 6 days, and two weeks later. The software package on the Dilor Raman Spectrometer permits background subtraction and Savitsky-Golay window averaging for the purpose of smoothing the signal. The Savitsky-Golay smooth works by fitting a polynomial to the set of data points in the smoothing window. The higher the

degree of the polynomial used, the lower the amount of smoothing. The accumulated spectra were subjected to a smoothing, background subtraction routine and included here to show band shapes.

The reaction sought here was the conversion of benzonitrile to benzamide on alumina. Spectra of the pure materials, benzonitrile and benzamide, were acquired initially. These two materials each have intense bands which occur at similar wavenumbers. Benzonitrile has a very intense band at 2230 cm^{-1}, due to the nitrile group, which is absent in the spectrum of benzamide. However, benzamide has a medium intensity band at 1572 cm^{-1}, the development of which was hoped to indicate the formation of benzamide.

Figures 1-5 to 1-7 show the spectra of benzonitrile on alumina acquired at three different wavenumber regions. Because the concentration of analyte (PhCN) is greatly reduced between pure sample and application of the benzonitrile analyte to the surface of solid adsorbant the intensities of signal are greatly reduced. Nevertheless, benzonitrile signals were observed on alumina. In general, alumina does not have any Raman signal; however, it has a high background reading.

In each of Figures 1-5 to 1-7 are two benzonitrile spectra, first the acquired spectrum and then the spectrum after application of smoothing and baseline subtraction routines. The main band in Figure 1-5 at 1602 cm^{-1} is due to the C=C stretch in the aromatic ring, At 2230 cm^{-1} in Figure 1-6 is the band due to the nitrile group. Finally, the band due to the C-H stretch occurs at about 3075 cm^{-1} in Figure 1-7. The Dilor

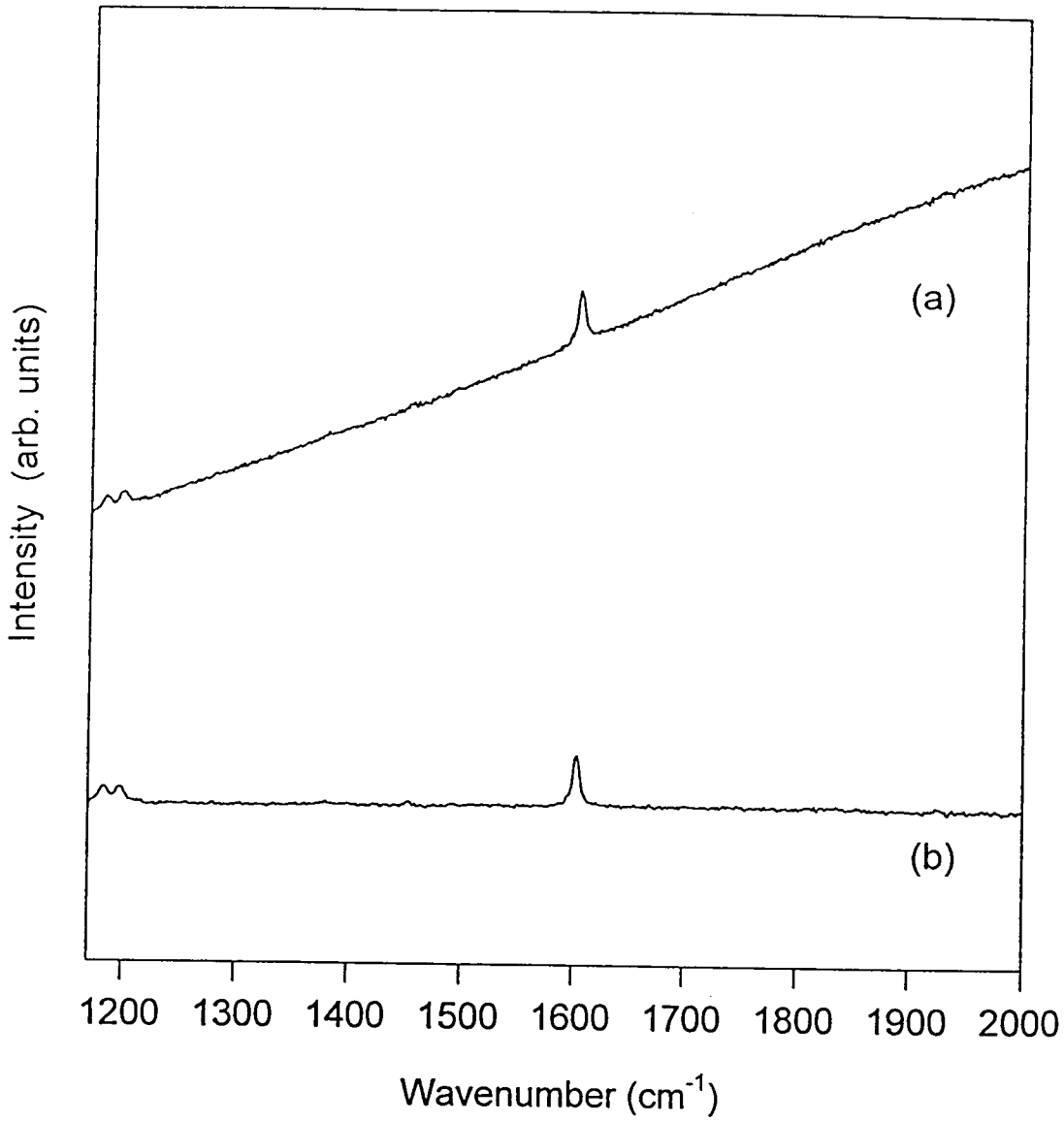


Figure 1-5. Raman spectra of benzonitrile on alumina centered at 1600 cm^{-1}. (a) Spectrum as acquired and (b) Spectrum after Savitsky-Golay smoothing and baseline correction.

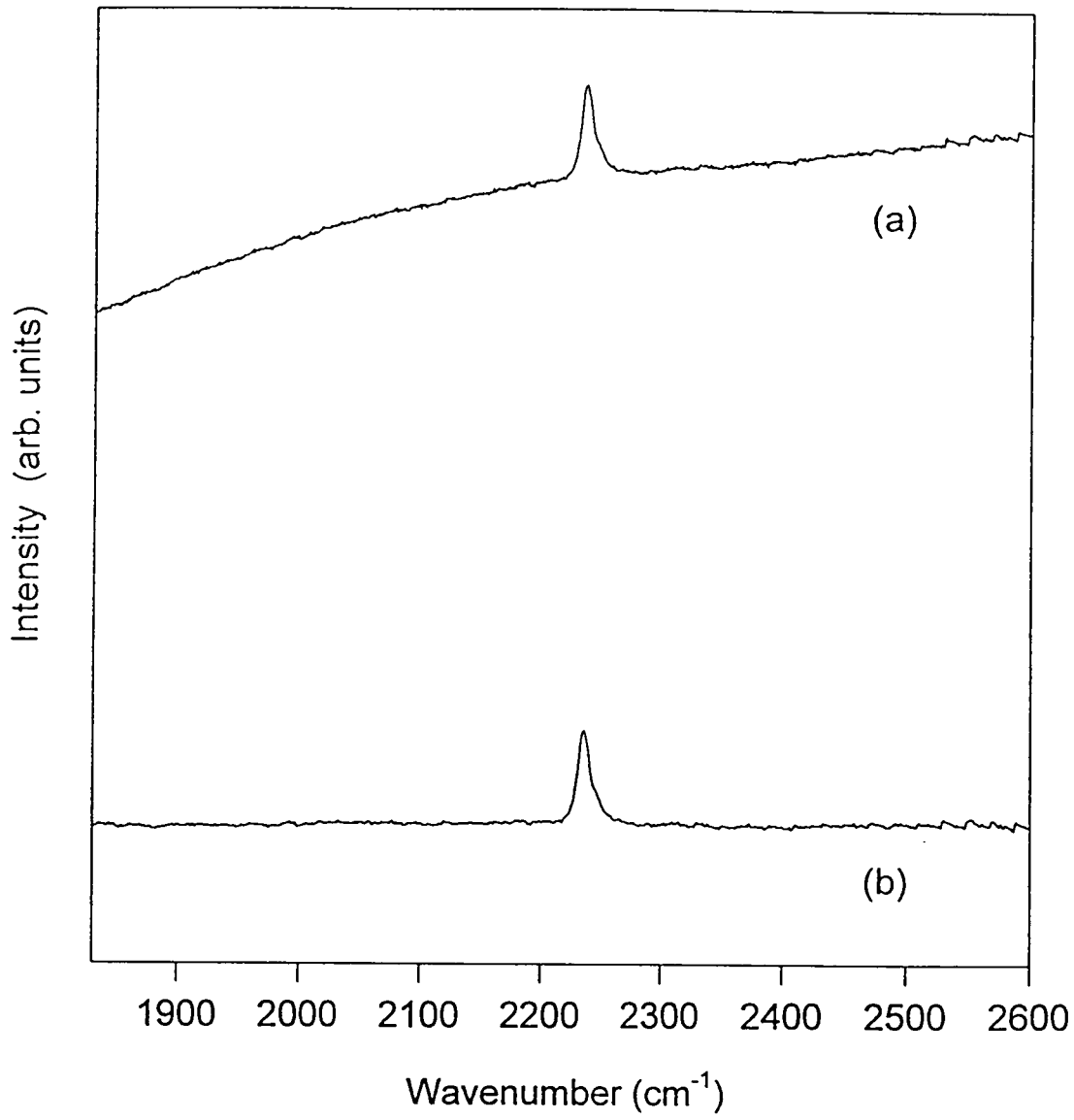


Figure 1-6. Raman spectra of benzonitrile on alumina centered at 2230 cm^{-1}. (a) Spectrum as acquired and (b) Spectrum after Savitsky-Golay smoothing and baseline correction.

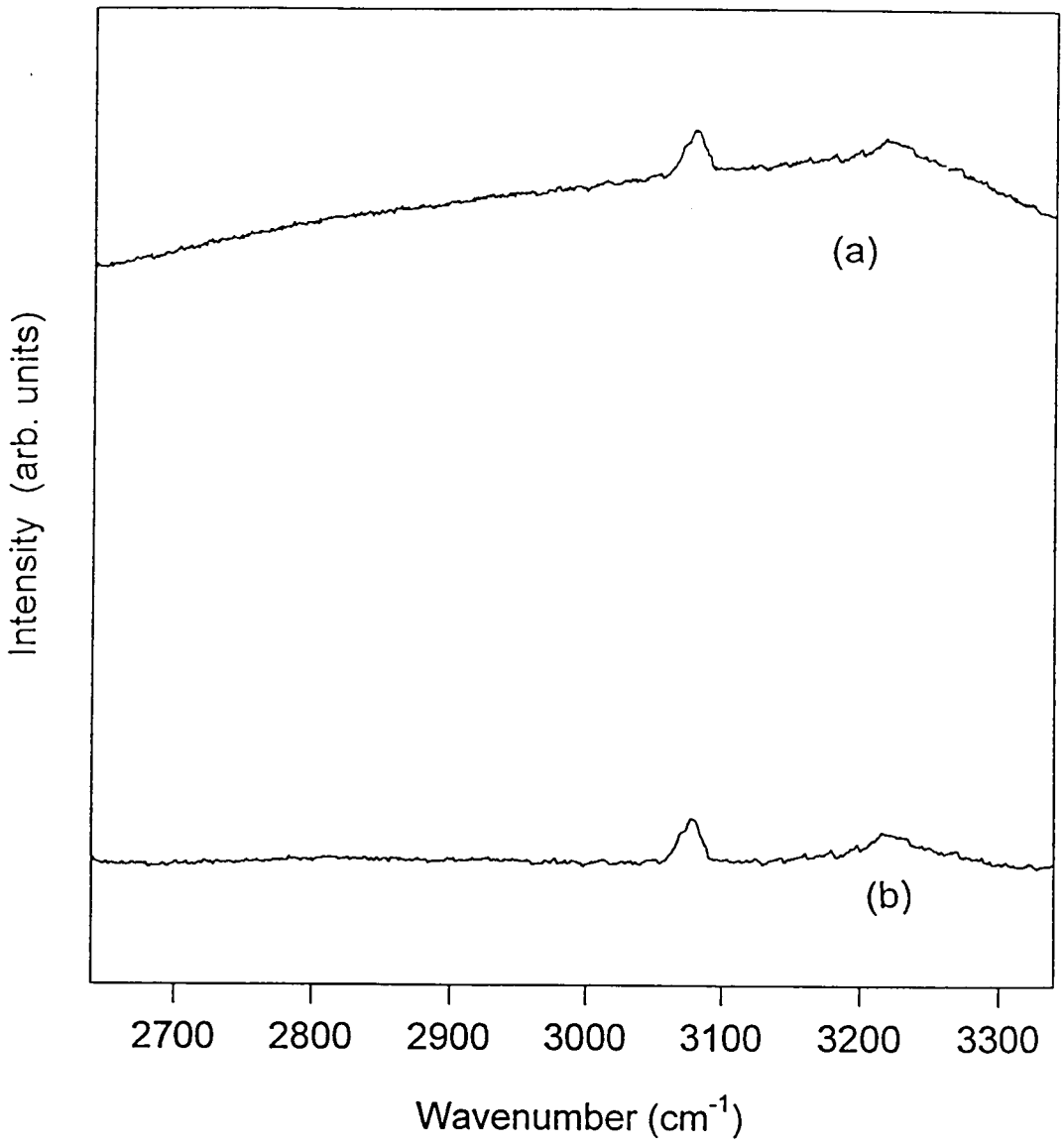


Figure 1-7. Raman spectra of benzonitrile on alumina centered at 3000 cm^{-1}. (a) Spectrum as acquired and (b) Spectrum after Savitsky-Golay smoothing and baseline correction.

Raman Spectrometer has an aberration on its grating which results in the appearance of an apparent band at approximately 3250 cm^{-1} (which is particularly evident in the baseline corrected spectrum) and causes the baseline to change slope.

In Figures 1-8 through Figures 1-10 are the smoothed and baseline subtracted spectra acquired 35 hours after the sample heating at 78 °C was initiated. Overall, the treated spectra in Figures 1-8 to 1-10 are similar to spectra in Figures 1-5 to 1-7. Because the spectra looked similar, it appeared that the reaction may not have occurred. Also no band at 1572 cm^{-1} for benzamide was observed. Therefore, a different approach to determining whether or not some reaction had occurred was taken.

Since the band at 2230 cm^{-1} occurs only for benzonitrile, while the bands at 1602 and 3075 cm^{-1} occur for both starting material and product, it was felt that a decrease in the ratios of the integrated peak areas at 2230 cm^{-1} to the 1602 and 3075 cm^{-1} bands would be an indication that some of the benzonitrile had reacted.

What is noteworthy is that when the integrated peak area at 2230 cm^{-1} was ratioed to the other two peak areas for the 35 hour reaction and these values compared to those at the start of the experiment the ratio had decreased with time. Specifically, when the integrated area for the peak at 2230 cm^{-1} in Figure 1-6, was divided by the integrated peak area for the absorption in Figure 1-5, a value of 3.17 was obtained for the benzonitrile before reaction commenced. When the peak area at 2230 cm^{-1} in Figure 1-6 was ratioed to the integrated peak area in Figure 1-7 a value of 1.39 was obtained. When the same calculations were performed on the bands in Figures 1-8, 1-9 and 1-10, ratios of

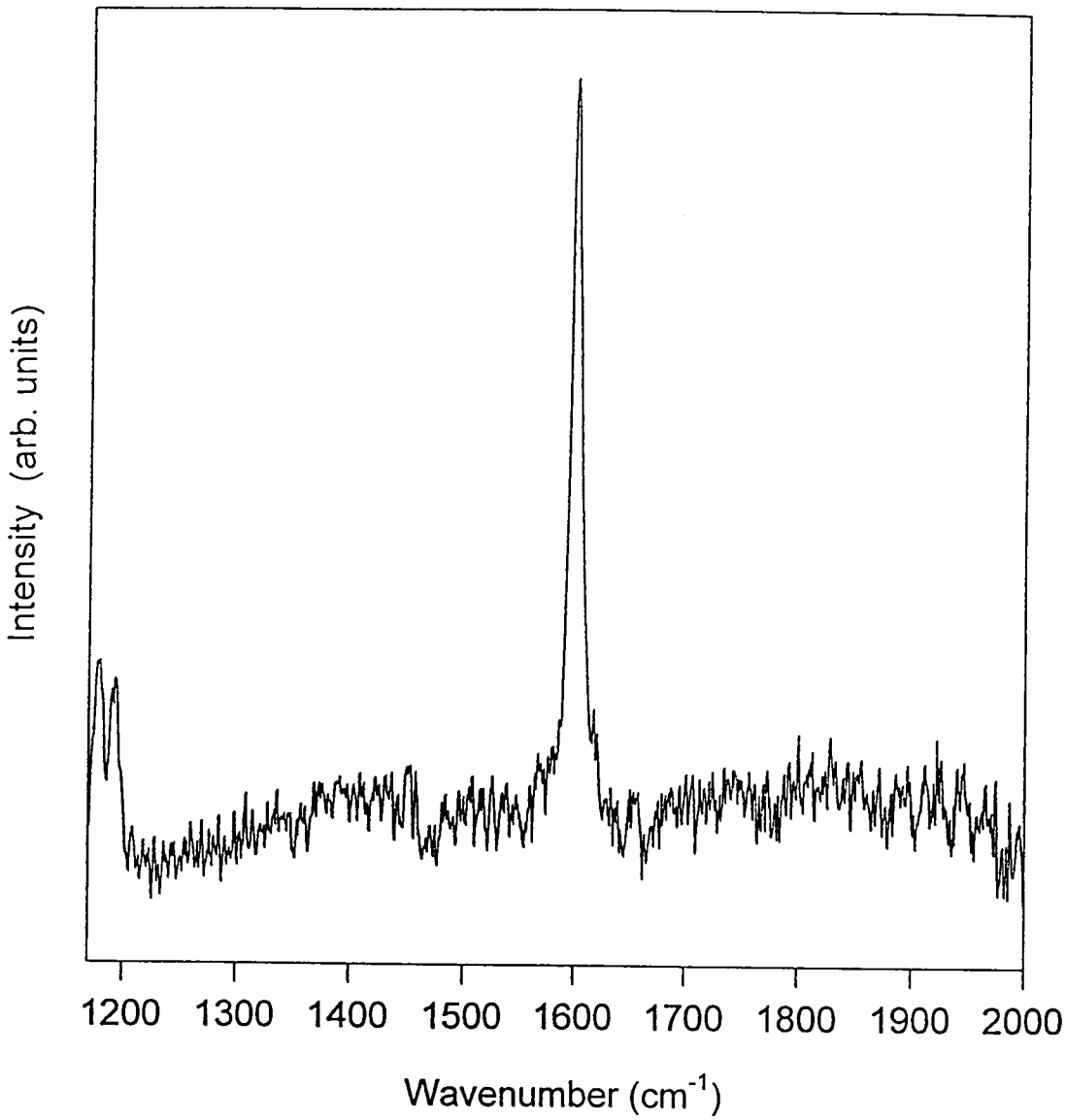


Figure 1-8. Savitsky-Golay treated Raman spectrum of benzonitrile on alumina centered at 1600 cm^{-1}.

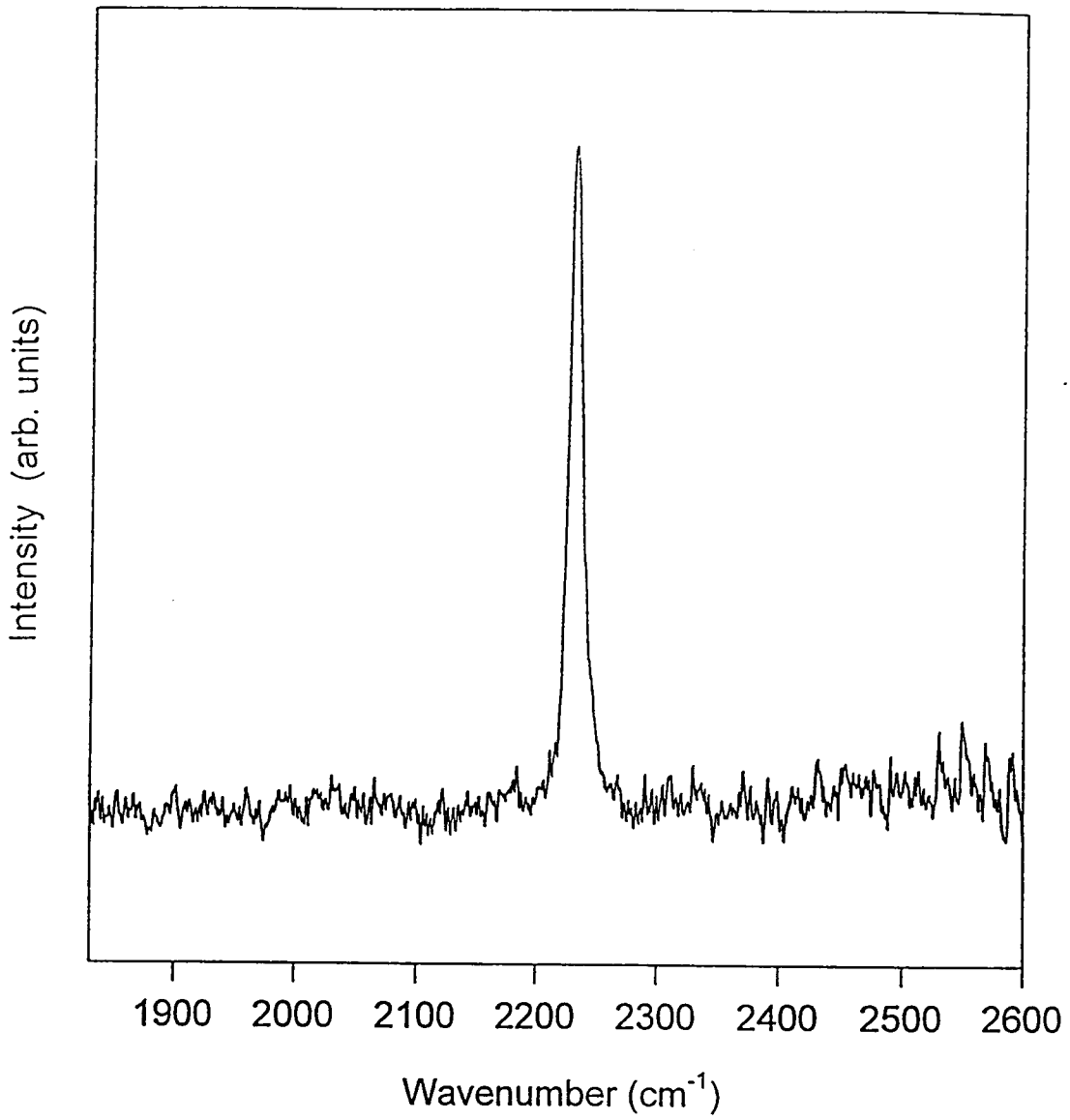


Figure 1-9. Savitsky-Golay treated Raman spectrum of benzonitrile on alumina centered at 2300 cm^{-1}.

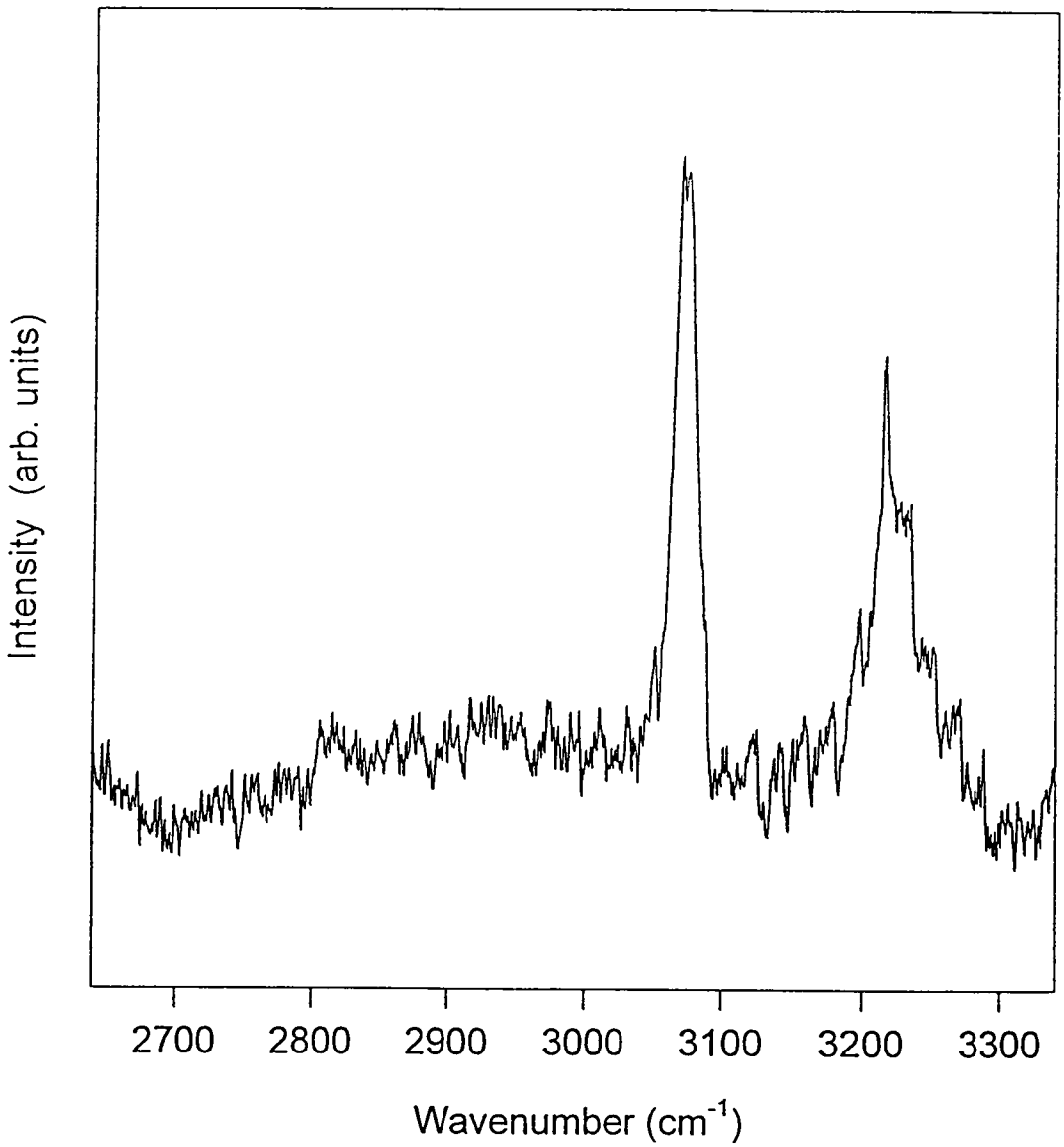


Figure 1-10. Savitsky-Golay treated Raman spectrum of benzonitrile on alumina centered at 3000 cm^{-1}.

2.98 and 1.22, respectively were obtained for the 35 hour reaction. Similar calculations were performed after the sample was heated at 78 °C for 144 hours and the ratios obtained were 2.48 and 1.09. This indirect comparison suggests that the intensity of nitrile band is decreasing with time. The absence of benzamide bands, however, demands an explanation. First of all, both compounds share their most intense Raman bands at very similar cm^{-1}. We would not really expected to see any new features in the spectrum centered at 3000 cm^{-1} or 2230 cm^{-1}. However, the carbonyl absorption centered at 1600 cm^{-1} should have arisen and it did not. First of all, if the band is weak it is possible to integrate for longer time intervals and for such slow kinetics that would make no difference. Also, it would help to work at lower concentrations so that features for the starting material did not obliterate the features for the product.

The data suggest that with some refinement of the experimental procedures it would be possible to construct a reliable and reproducible calibration curve and also to study the reaction *in situ* by Raman spectroscopy.

The results for both the DRIFTS and the Raman experiments are far from perfect, but are encouraging none the less. The data suggest that with some refinement in the experiment protocol it would be possible to construct a reliable and reproducible calibration curve and also to study the reaction *in situ* by Raman spectroscopy.

In theory better results could be obtained in the future if integration is done for longer periods of time. This approach is worth trying because the kinetics of the reaction are very slow. In the future, this work could be done at lower concentrations, so that

features for the starting material would not obliterate the salient features for the product. Another interesting approach for improving the results of this analysis would be to monitor the N-H stretching band for the product, benzamide.

In regards to the DRIFTS approach, the use of lower concentrations for the calibration standards should assist in generating a good calibration curve. This approach is suggested from implications in Figures 1-1 through 1-4. In these figures the curves are approximately linear when the alumina is loaded with benzonitrile in the concentration region of 1 to 10 millimoles. The use of a Wig-L-Bug should also help in preparing samples in which the benzonitrile is more uniformly distributed on the alumina. It was evident from the data that uniformity in sample preparation was not achieved by using a magnetic stirbar to stir the alumina/benzonitrile mixture, even though this process was carried out for quite a long time.

CHAPTER III

EXPERIMENTAL SECTION

General. Benzamide, and benzonitrile were purchased from Aldrich Chemical Co. and were used as purchased. Alumina, Brockmann neutral Activity I, was obtained from Aldrich Chemical Co.. All glassware and syringes were oven dried overnight before use.

Infrared Analysis. Infrared (IR) spectra were recorded using a Digilab Bio-Rad FTS-60A Fourier Transform Infrared Spectrometer. The diffuse reflectance attachment used was the "Praying-Mantis" model from Harrick Scientific Corporation. Spectra were recorded at 4 cm^{-1} resolution and 64 scans were co-added. The diffuse reflectance spectra were then transformed to Kubelka-Munk units. After a four-point baseline correction the intensity of the nitrile band was determined. The open beam path was used to obtain the background spectra.

Raman Analysis. The Dilor XY Raman Spectrometer was used for all data acquisition. Samples in square Pyrex cells were loaded into a furnace and Raman spectra were acquired directly in the furnace. The excitation source was a Lexel 3500 argon ion laser tuned to 514.5 nm. The laser power was set to 50 mW and the monochromator slits were set to 150 μm (equal to a 6.47 cm^{-1} band pass). While Dilor system comes with both macro and microscope stages, all the data were acquired in the macro stage. Also, while the triple monochromator system can be configured in either subtractive mode for good Raleigh line rejection or in additive mode for high resolution, the subtractive mode was used exclusively. The detector was a thermoelectrically cooled (to -70 °C) charge couple

device (CCD) detector which ha a 256 x 1024 array. In general , the foremonochromator and spectrometer were set to view a cm^{-1} interval of about 950 cm^{-1}. Typically, spectra were acquired by averaging three individual spectra, each accumulated for 60 sec. To acquire a spectrum from 350 to approximately 3400 cm^{-1} required that four individual windows be acquired and coupled one to another. Two types of spectra were recorded: (1) scans (addition of several individual windows) and (2) individual windows. Since the response of the individual pixels on the CCD is not identical, breaks occur in the baseline at the point where individual windows were coupled in the four segment spectra. The effect is the worst at high cm^{-1}, particularly if there is appreciable background signal. A furnace was placed at the macro stage of the Dilor and the sample positioned such that one area was monitored the entire time.

Sample Preparation. The samples used to study the nitrile hydrolysis by FTIR were prepared by adding via syringe 3 mmol of benzonitrile to 15 g of alumina, neutral Brockmann Activity 1. The sample was heated at 70 °C in an oil bath for 24 hours. The mixture was stirred continuously in a septum-sealed 50-mL roundbottomed flask.

In acquiring Raman spectra samples were prepared by stirring together nitrile with alumina for one hour. The material was then loaded into a square cell and capped with a septum.

Samples used in construction of the calibration curve were prepared by adding the appropriate molar amount of benzonitrile to 15 g of alumina in a 15-mL roundbottomed

flask. The flask was septum-sealed and, with the aid of a magnetic stir bar, allowed to stir for three hours.

Samples used in determining the reproducibility of the DRIFTS data were prepared by making three separate 6 mM and 12 mM benzonitrile samples. The appropriate amount of benzonitrile was added via syringe and allowed to stir for three hours.

REFERENCES

1. a) March, J. *Advanced Organic Chemistry*; 3rd ed.; Wiley-Interscience: New York,**1985**; p788 and references cited therein. b) Schaefer, F.C in *The Chemistry of the Cyano Group*; Rappaport, Z. ed; Interscience: New York, **1970**; p239.

2. Pagni, R.; Kabalka, G.; Wilgus Pala, C.; Downing, S.; Molitor, E.; Bains, S. *Tetrahedron Lett.*, **1995**, *36*, 3469.

3. a) Pagni, R. M.; Kabalka, G.; Hondrogiannis, G.; Bains, S.; Tan, L.C.; Anosike, P.; Palmer, R. *Tetrahedron* **1993**, *49*, 6743. b) Michels, J.J.; Dorsey, J.G. *Langmuir* **1990**, *6*, 414.

4. Knözinger, H.; Ratnasamy, P. *Catal. Rev. Sci. Eng.* **1978**, *17*, 994.

5. Larock, R.C. *Comphrehensive Organic Transformations*; VCH: New York, **1989**; 994.

6. Smith, B. C. *Fundamentals of Fouier Transform Infrared Spectroscopy*; CRC Press: New York, **1996**; p117.

7. Krivacsy, Z.; Hlavay, L. *Spectrochimica Acta*, **1994**, *50A*, 1, 49.

8. Krivacsy, Z.; Hlavay, L. *Spectrochimica Acta*, **1994**, *50A*, 13, 2197.

9. Griffiths, P, R.; Hamadeh, I.; Yeboah, S.; Trumball, K. *Applied Spectroscopy*, **1984**, *38*, 486.

PART 2

FTIR and Polarimetric Studies of the Lithium Ion Complexation to Carbonyl and Nitrile Functional Groups, using Crotonaldehyde , Benzonitrile and Camphor in a $LiClO_4$/Diethyl Ether System.

CHAPTER I

INTRODUCTION

Lewis acids play a pivotal role in organic chemistry. Most studies focus on their role as catalysts. They catalyze reactions such as the Diels-Alder[1] and [2+2] cycloadditions,[2] ene reactions,[3] aldol condensations,[4] Michael 1,4 additions,[5] the reaction of acetals with olefins and unsaturated ethers,[6] and Claisen rearrangements,[7] in addition to standard reactions such as the Friedel-Crafts alkylations and acylations.[8] Lewis defined acidity and basicity in a way that is appropriate to the context of the present study. Lewis considered a basic substance as "...one which may be used to complete the stable group of another atom, and that an acidic substance is one which can employ a lone pair from another molecule in completing the stable group of one of it own atoms."[9]

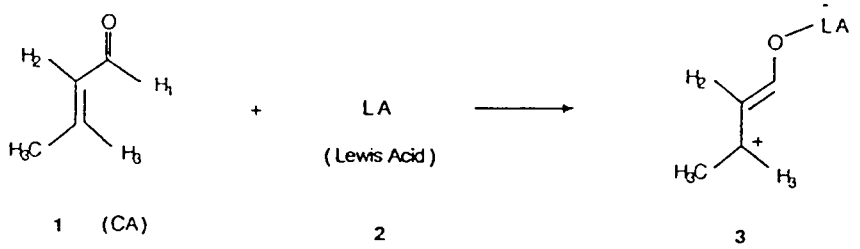
However there are other ways in which Lewis acidity maybe defined. Lewis acidity may also be defined as the ability of an acid to complex reversibly to a model compound; in these cases the equilibrium constant is a measure of the Lewis acidity. Lewis acidity can sometimes also be defined on the pH and H_o scales which are ordinarily associated with Brønsted acids. The ability of a Lewis acid to induce a chemical shift in complexed base can also be used as a measure of Lewis acidity.

In the gas phase, the lithium cation (Li^+) is an excellent Lewis acid because of its large charge density. When the lithium ion is associated with the perchlorate (ClO_4^-) counterion, as in $LiClO_4$ in diethyl ether (DE), the acidity of the lithium cation is moderated both by its complexation to the solvent and by ion pairing with the perchlorate

counterion. The lithium perchlorate-diethyl ether (LPDE) system has been shown to accelerate the rate of the Diels-Alder reaction.[10,11] Forman and Dailey[12] showed that the rate acceleration was due to catalysis by the Li^+ and not due to a solvent effect.

Since the LPDE system is so pervasive in organic chemistry, it would be useful to measure its Lewis acidity. A study of the Lewis acidity of Li^+ in the LPDE system can be approached from several angles: kinetically, stereo- and regiochemically and, thermodynamically, among others. Fourier transform infrared (FTIR) spectroscopy, nuclear magnetic resonance (NMR) spectroscopy and molecular orbital (MO) calculations can be employed as tools in studying the Lewis acidity of the LPDE system.

Childs et al.[13] made a determination of Lewis acidity for a Lewis acid by its complexation to a range of α,β−unsaturated carbonyl compounds using ^1H and ^{13}C NMR spectroscopy. The reactions were studied in methylene chloride at -20 °C. The reaction of crotonaldehyde (CA), one of the compounds studied by Childs, is shown in equation 1.



1 (CA) 2 3 (1)

Childs and coworkers defined an empirical Lewis acidity scale based on the ability of the Lewis acid to shift the H_3 and C_3 resonances of CA and related substances to lower field The magnitude of the resonance shift (Δδ) was found to be proportional to the acid

strength. Some results from Childs work are presented in Table 2-1 and Table 2-2. This method works because as shown by Laszlo and Teston[14] there is a linear dependence of the H3 chemical shift on the energy of the lowest π^* MO in the LA-CA complex. Complexation of the Lewis acid to CA lowers all of the energy levels of the molecular orbitals in crotonaldehyde. Furthermore, there should be some relationship between the energy of the molecular orbital, and the chemical shifts of the base accompanying the Lewis acid complexation. These changes parallel the catalytic activity of the Lewis acid. A Lewis acid scale based on the induced shift ($\Delta\delta$) of H3 resonance of CA on complexation with various Lewis acids was thus developed (Table 2-3).

Pagni, Kabalka and coworkers[15] made a chemical, spectroscopic and theoretical assessment of the Lewis acidity of $LiClO_4$ (LP) in diethyl ether (DE). Using the methods of Childs,[13] they were able to determine the Lewis acidity of LP by measuring the induced downfield shift of H3 of CA in LPDE at -20 °C. Their results are shown in Table 2-4.

Unlike the Lewis acids studied by Childs, where complexation was irreversible, it was found that the complexation of Li^+ was reversible. By assuming that LP only forms a 1:1 complex with CA, it was possible to fit the data in Table 2-4 to a model from which K_{eq}, the equilibrium constant for the formation of the LP-CA complex, and $\Delta\delta_\infty$, the limiting shift of H_3 were deduced. Since the limiting shift for H3 in LPDE is much smaller than for other Lewis acids such as BBr_3, $AlCl_3$ and $SnCl_4$, the Li^+ in LPDE is a

Table 2-1. ^{1}H Chemical Shift Differences ($\Delta\delta$) of Crotonaldehyde on Complexation with Various Lewis Acids[a]

	Proton $\Delta\delta$ (ppm)			
Lewis Acid	**H1**	**H2**	**H3**	**CH_3**
BBr_3	0.11	0.93	1.49	0.51
BCl_3	-0.65	0.85	1.35	0.49
$SbCl_5$	0.17	0.78	1.32	0.48
$AlCl_3$	-0.20	0.76	1.23	0.47
$EtAlCl_2$[b,c]	-0.20	0.77	1.25	0.47
BF_3	-0.27	0.74	1.17	0.44
$EtAlCl_2$[b,c,d]	-0.17	0.67	1.15	0.38
$Et_3Al_2Cl_3$	-0.15	0.69	1.14	0.39
$TiCl_4$	0.03	0.60	1.03	0.36
Et_3AlCl[b,c]	-0.15	0.55	0.91	0.30
$SnCl_4$	0.02	0.50	0.87	0.29
Et_3Al[b,c]	-0.34	0.42	0.63	0.23

Source: Reference 13.

[a]In ppm (± 0.01). Chemical shifts of uncomplexed base are: δ = 9.74 (d, 1H, H1), 6.10 (ddq, 1H, H2), 6.93(m, 1H, H3), 2.02(dd, 3H, H4 $\Delta\delta$ is positive for a downfield shift. Approximately 0.3 M solution in dichloromethane at -20 °C, unless otherwise stated.

[b]At = 60 °C. Chemical shifts of uncompleted base: δ 9.84 (H1), 6.12 (H2), 6.98 (H3), 2.05 (H4) at this temperature.

[c]Written in monomeric form for simplicity.[d]2:1 in crotonaldehyde-$EtAlCl_2$

Table 2-2. ^{13}C Chemical Shift Differences ($\Delta\delta$) of Crotonaldehyde on Complexation with Various Lewis Acids[a]

	Carbon $\Delta\delta$ (ppm)			
Lewis Acid	**C1**	**C2**	**C3**	**C4**
BF_3	8.3	-3.3	26.1	3.1
BCl_3	6.8	-3.7	31.7	4.3
$SbCl_5$	6.9	-4.0	27.6	3.7
Et_2AlCl[b]	9.4	-2.0	20.1	2.3
$SnCl_4$	7.8	-2.8	19.2	2.3

Source Reference 13.
[a]In ppm (± 0.01). Chemical sifts of uncomplexed base are: δ = 194.7 (C:), 134.4 (C2), 155.2 (C3), 10.0 (C4). As approximately 0.3 M solution in dichloromethane at -20 °C.
[b]Acid written in monomeric form for simplicity.

Table 2-3. Lewis Acid Scale Based On Δδ-values of H3 Resonance of Crotonaldehyde.

Lewis acid	Relative power
BBr_3	1.00 ± 0.005
BCl_3	0.93 ± 0.02
$SbCl_5$	0.85 ± 0.03
$AlCl_3$	0.82
BF_3	0.77 ± 0.02
$EtAlCl_2$	0.77
$TiCl_4$	0.66 ± 0.03
Et_2AlCl	0.59 ± 0.03
$SnCl_4$	0.52 ± 0.04
Et_3Al	0.44 ± 0.02

Source: Reference 13.

Table 2-4. Induced Chemical Shifts of Crotonaldehyde (H3) and Diethyl Ether in Solutions of CA in LPDE at -20°C

Initial Concentrations			Induced Shifts			
			CA		Diethyl Ether	
Entry	$[LP]_o$	$[CA]_o$	$\Delta\delta_{exp}$[a]	$\Delta\delta_{the}$[b]	$\Delta\delta CH_2$[c]	$\Delta\delta CH_3$[c]
1	0.30	0.24	0.25	0.27	0.01	0.03
2	0.45	0.36	0.33	0.32		
3	0.60	0.48	0.38[d]	0.36	0.05	0.03
4	1.00	0.80	0.44[d]	0.44	0.07	0.04
5	2.00	1.60	0.54	0.53	0.12	0.07
6	5.00	4.00	0.61	0.62	0.28	0.13

[a]Relative to $CA(H_3)$ in DE at -20°C. [b]Values obtained assuming $K_{eq} = 3.20$ and $\Delta\delta_\infty = 0.764$. [c]Chemical shifts relative to those for DE at -20 °C. [d]See reference 17.

much weaker Lewis acid. Note also that the ether resonances are also shifted on complexation with Li^+.

This study focused on finding K_{eq} for the formation of the LP-CA complex and the LP-benzonitrile (LP-BN) complex using FTIR spectroscopy. FTIR rather than NMR was preferred over NMR because differences in the time scales between the two spectroscopic techniques makes it possible to see individual bands for CA and the LP-CA complex and for BN and the LP-BN complex. With NMR, of course, one only sees a weighted average spectrum.

MNDO, a semiempirical molecular treatment was used to complement the FTIR studies. The method was used to predict theoretical values for the shifts in wave number that occur when Li^+ is complexed to either CA or BN. Differences were observed between the experimental and the theoretical values for the complexation.

In addition to studying the LP complexation by FTIR, a polarimetric analysis was performed on the complexation of LP to camphor. This analysis was performed by studying the optical rotations of solutions having a fixed concentration of camphor and varying concentrations of $LiClO_4$. It was possible to treat the data from this analysis in a manner similar to that done by Pagni and coworkers for NMR spectra.[15]

CHAPTER II

RESULTS AND DISCUSSION

Both the carbonyl (1600-1800 cm^{-1}) stretch and the nitrile (2200-2300 cm^{-1}) stretch are very sensitive to complexational and environmental effects.[16] These two absorption regions are also readily accessible in most organic solvents.

When the FTIR spectra of neat CA and BN were compared with the FTIR spectra of their LP-complexes, it was observed that an addition band/shoulder developed on either the low or high wavenumber side of the free carbonyl or nitrile stretching band respectively as the concentration of the $LiClO_4$ was increased. At low $LiClO_4$ concentrations the growth of the shoulder was linearly proportional to the amount of $LiClO_4$ present. The shoulder of the LP-BN complex appeared at higher wavenumbers and that of the LP-CA complex appeared at lower wavenumbers.

Using "Peak-Fit", a curve fitting software package from Jandel Scientific, it was possible to determine the shape, position, width and height of the infrared bands which had overlapped to give the broad band due to the various LP-complexes. The integrated area of the separate bands under the band which had been curvefitted were then used to calculate the equilibrium constants for the complexations. In most cases use of the two major bands were sufficient to give the optimum fit. However, in some cases it was necessary to use some minor bands in order to get the best fit. The minor bands did not involve species that were part of the equilibrium.

The curves were fitted to Gaussian, Lorentzian, Voigt and Pearson functions. The software employed the band width, center and amplitude as initial parameters from which initial estimates were made. A least-squares algorithm was then used to vary and optimize these parameters. The four functions are described below:

Gaussian

$$a_o \exp\left[-0.5\left(\frac{x-a_1}{a_2}\right)^2\right]$$

Lorentzian

$$a_o \Big/ 1+\left(\frac{x-a_1}{a_2}\right)^2$$

Voigt

$$\int_{-\infty}^{\infty} a_o \exp(-y^2)dy \Big/ a_3^{\,2} + \left[\left(\frac{x-a_1}{a_2}\right) - y\right]^2$$

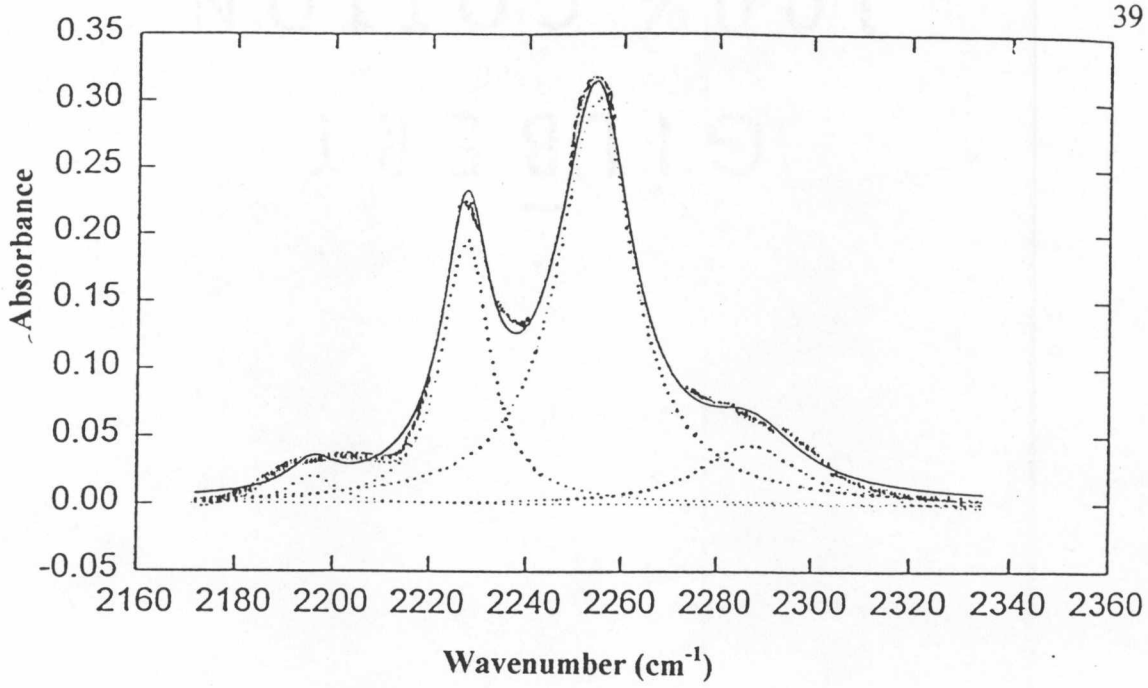
Pearson

$$a_o \Big/ \left[1+4\left(\frac{x-a_1}{a_2}\right)^2\left(2^{\frac{1}{a_3}}-1\right)\right]^{a_3}$$

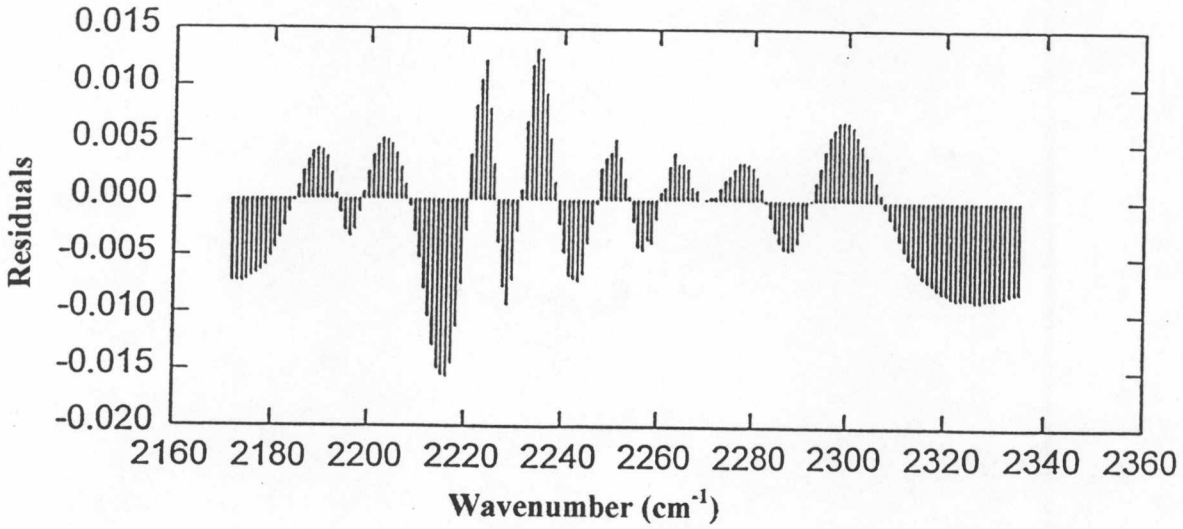
where a_o = amplitude, a_1 = band center, a_2 = width of band 1 a_3 = width of band 2, X is an individual wavenumbers and Y is an individual amplitude.

The best fits were obtained using Lorentzian and Pearson routines. A typical output is shown in Figures 2-1a and 2-1b for a Lorentzian fit of BN in LPDE. The residual plot in this Figure 2-1b is the difference between the initial spectrum and the spectrum calculated using a set of given curvefitting parameters.

The complexation of $LiClO_4$ with CA was studied by doing three separate experiments. One experiment was done using 0.04 M to 0.10 M LP with 0.10 M CA. A



a. The results of a curvefit. The sample spectrum and the calculated spectrum are nearly perfect overlaps as seen in the top of the display. In the region under these bands is shown the bands that make up the calculated spectrum.



b. A plot of the residuals from the curvefitting procedure as seen in Figure 2-1a.

Figure 2-1. The results of a curvefit and a plot of the residuals.

second experiment was done using 0.10M to 2.00 M LP with 0.28 M CA. Finally a third experiment was done for 1.00 M to 3.00 M LP with 0.28 M CA. Thus it was possible to observe the LP-CA complexation in DE at low, intermediate and high Li^+ concentrations.

Crotonaldehyde has a unique IR band in diethyl ether. This band occurs around 1700 cm^{-1} and is due to the carbonyl (C=O) stretch. A segment of the full spectrum, as shown in Figure 2-2, shows more clearly that there is only a minor contribution from DE to the carbonyl region of CA. When the ether spectrum is subtracted from the CA spectrum and expanded over a narrower wavenumber range, we get the spectrum seen in Figure 2-3. The addition of LP to crotonaldehyde causes a shoulder to develop at lower wavenumbers; this is due to the carbonyl stretch of the complex.. This behavior is seen in Figures 2-4 and 2-5, where the effect of the addition to 0.10 M LP and 0.30 M LP to 0.28 M CA is illustrated.

Even though the IR spectra seen in Figures 2-2 through 2-5 are presented as transmittance spectra, it was from the corresponding absorbance spectra that data was acquired for calculation of K_{eq} for the LP-complexation. Figures 2-6 through 2-8 show the superimposition of raw absorbance spectra acquired for low, intermediate and high concentration ranges of $LiClO_4$.

The equilibrium constants were only determined for LP concentration ranges for which the respective superimposed FTIR absorbance spectra showed an isosbestic point or at least a very close approximation of an isosbestic point. For the LP-CA complexation an isosbestic point was only observed at low LP (0.04 M to 0.10 M)

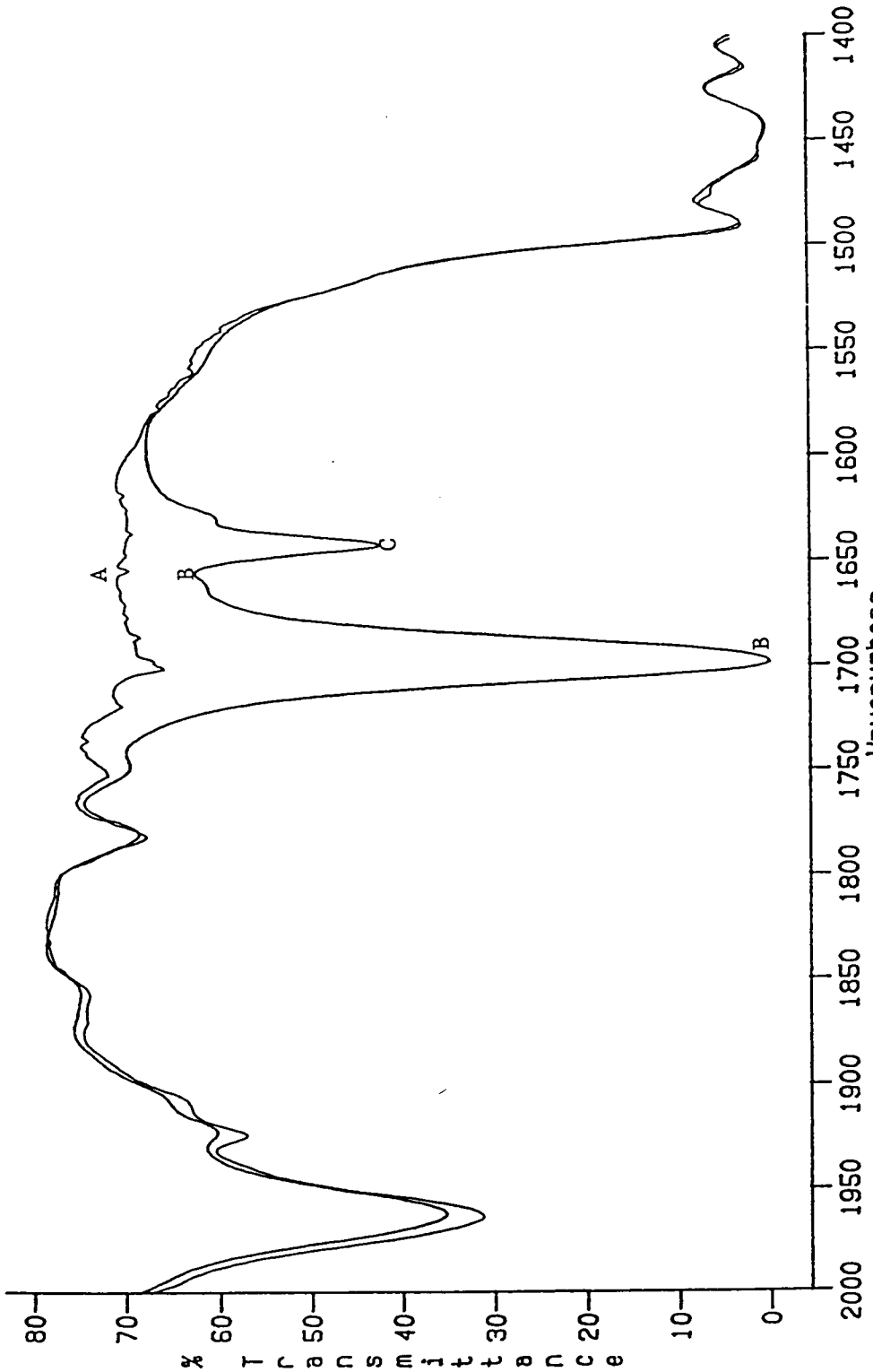


Figure 2-2. FTIR of crotonaldehyde in diethyl ether. A. Diethyl ether spectrum. B. Carbonyl (C=O) stretch (1710-1680 cm^{-1}). C. Carbon double bond (C=) stretch (1600-1635 cm^{-1}).

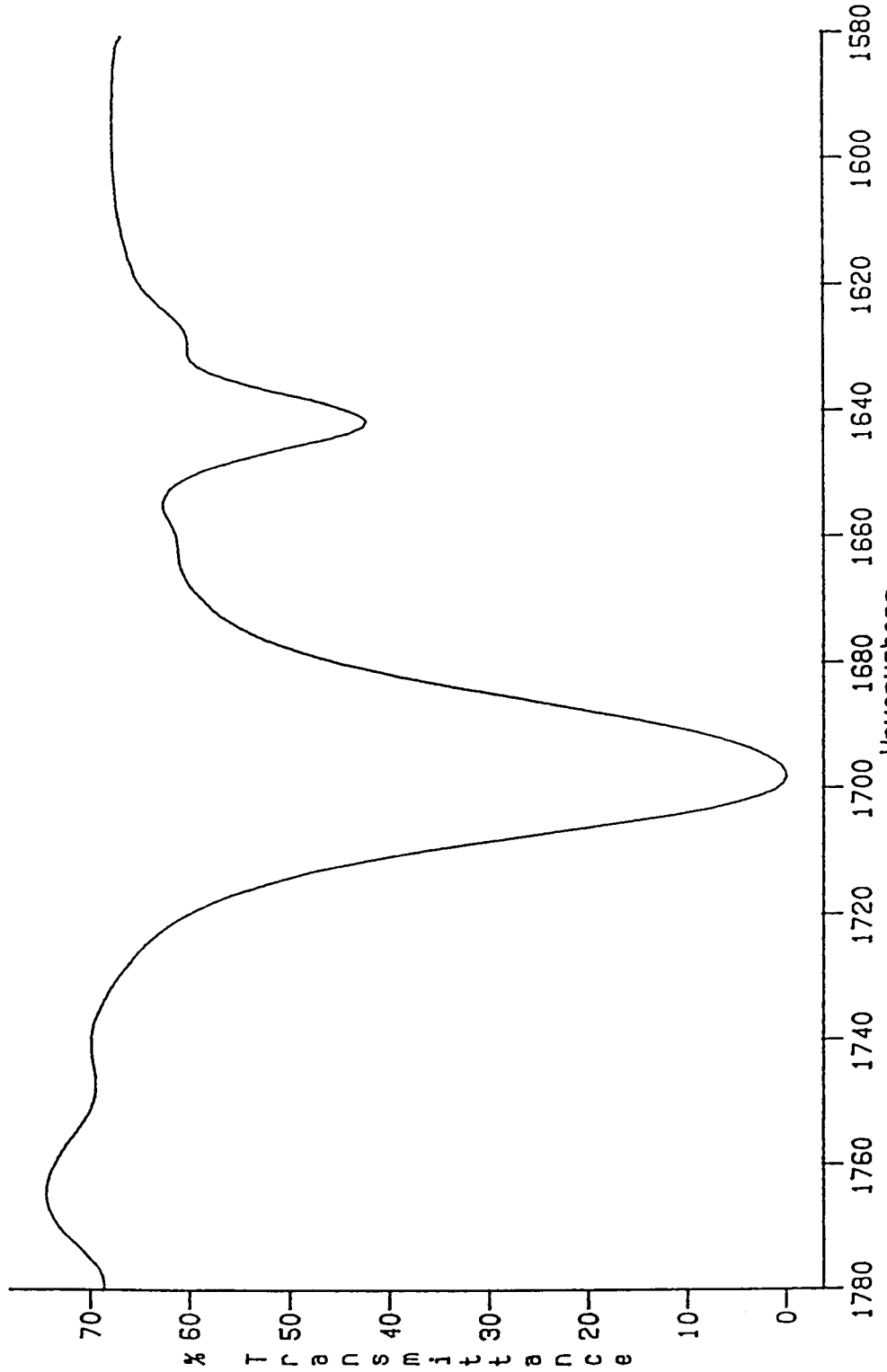


Figure 2-3. FTIR of crotonaldehyde in diethyl ether from which the spectrum of diethyl ether has been removed.



Figure 2-4. The effect of the addition of 0.10 M $LiClO_4$ to a solution of 0.285 M crotonaldehyde in diethyl ether. **A.** CA **B.** LP-CA.

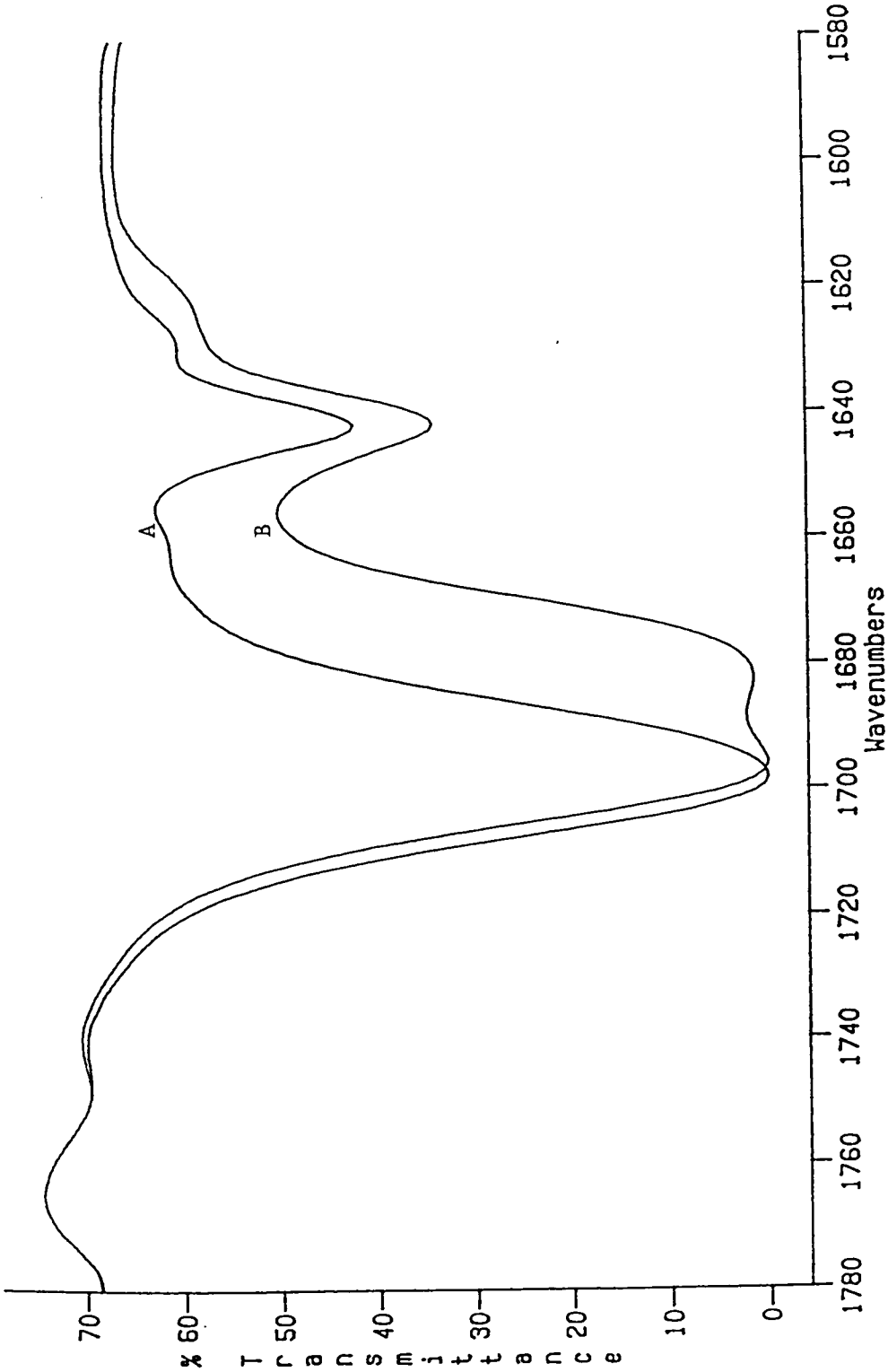


Figure 2-5. The effect of the addition of 0.30 M $LiClO_4$ to a solution of 0.285 M crotonaldehyde in diethyl ether. **A**. CA **B**. LP-CA.

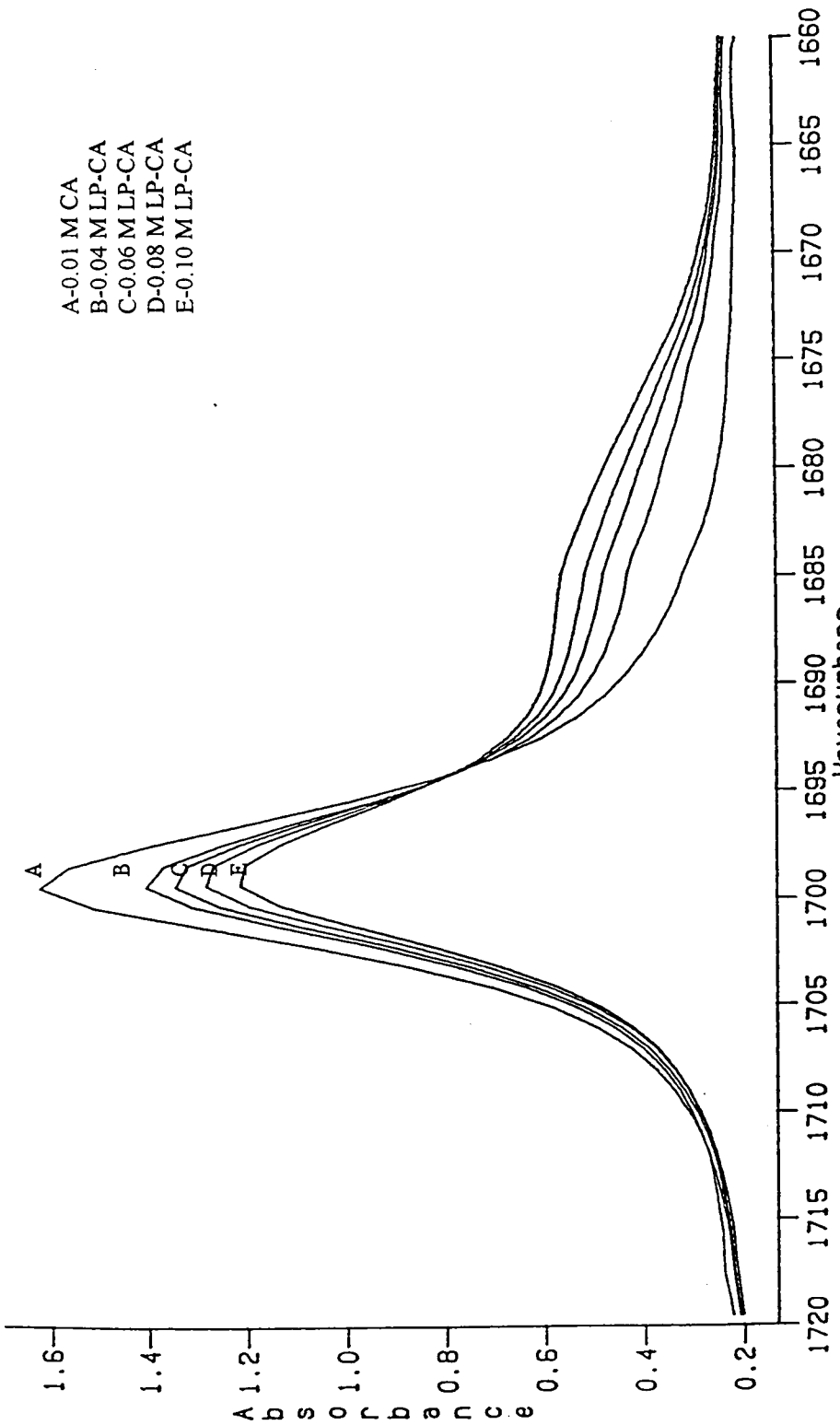


Figure 2-6. Superimposed raw FTIR spectra of 0.04 M to 0.10 M LP-CA complexes in diethyl ether.

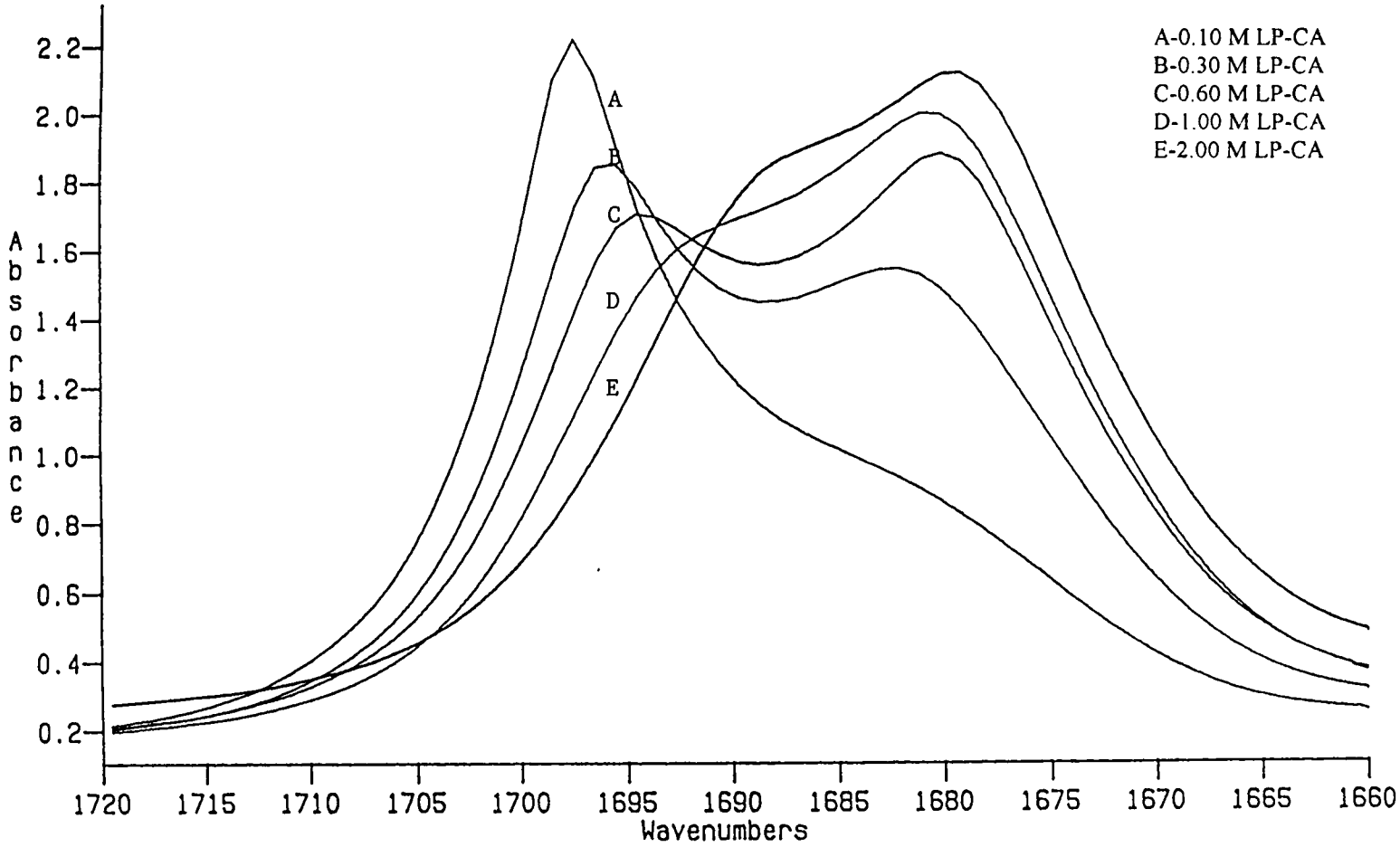


Figure 2-7. Superimposed Raw FTIR Spectra of 0.10 M to 2.00 M LP-CA complexes in diethyl ether.

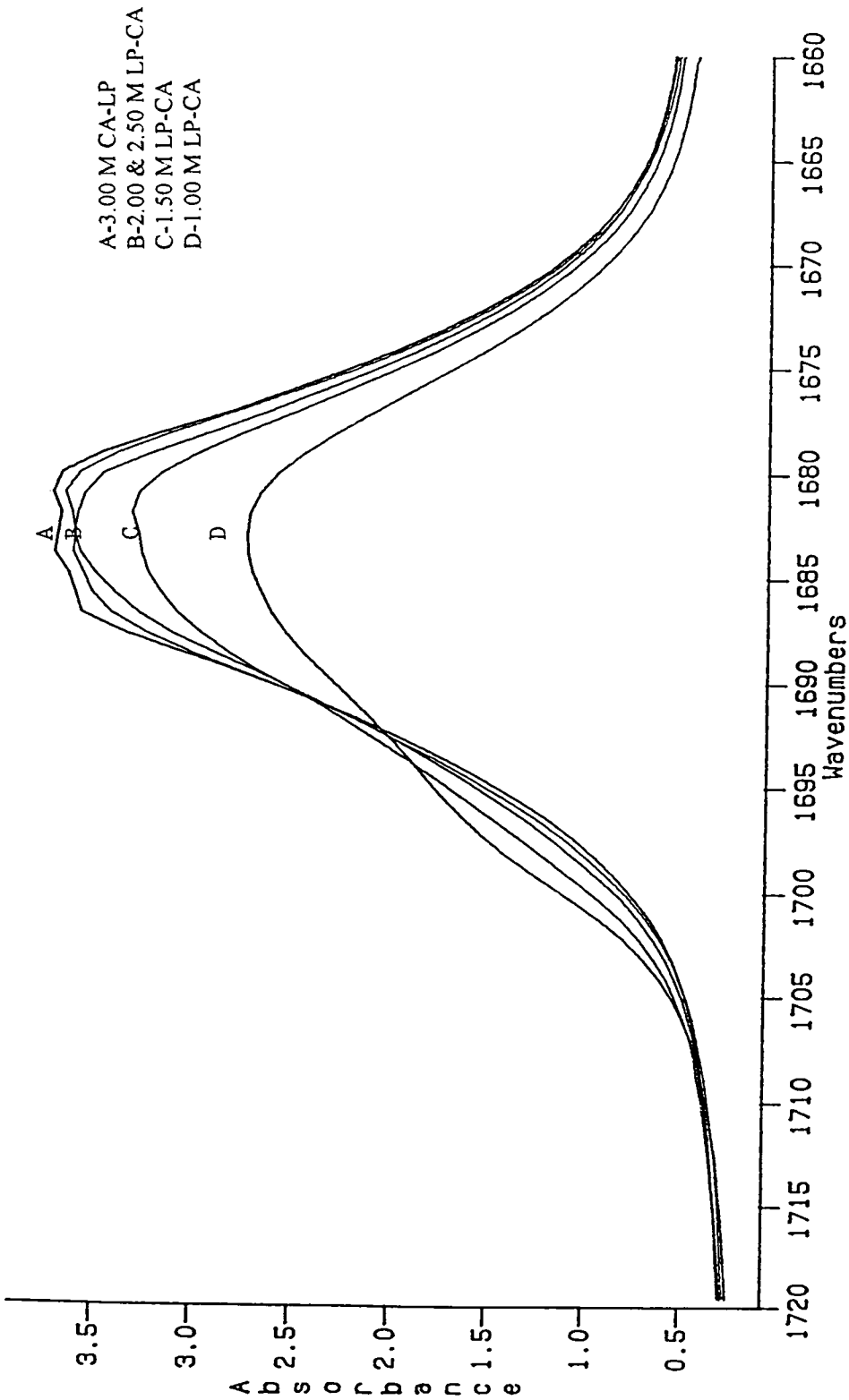


Figure 2-8. Superimposed raw FTIR spectra of 1.00 M to 3.00 M LP-CA complexes in diethyl ether.

concentration ranges. An isosbestic point [17-19] occurs when multiple spectra of varying concentration all have the same invariant intensity at some particular wavenumber. These isosbestic points occur when a unique functional group or chromophore common to both the complexed CA and the free CA absorb radiation a different frequencies. This usually results in overlapping bands in the spectrum. Clear and distinct isosbestic points then occur between the free and the complexed bands and they are only obtained when the overall concentration of the absorbing group is fixed and the molar absorption coefficients of the group in the two forms, free and complexed, are equal. It should also be noted that whenever there is a true isosbestic point the λ_{max} and the peak widths do not change with increasing LP concentration. Only the intensity of the bands change with increasing LP concentration. The presence of an isosbestic point indicates the existence of only two species in dynamic equilibrium.

The absence of isosbestic points, the rapid broadening of the absorbance bands and irregular band profile as seen in the LP-CA IR spectra for the intermediate (0.10 M - 2.00 M) and high LP concentrations (1.00 M -3.00 M) may be due to the decrease of free aldehyde and the effect of ion association. In Figures 2-7 and 2-8, which show CA spectra at "high" LP concentrations the bands show signs of beginning to coalesce. At these concentrations (0.60 M to 3.00 M) essentially all of the CA is bound to Li^+. Any further increase in LP concentration will then have very little effect on the C=O stretching band. Even though the carbonyl band ceases to respond to increasing LP concentrations, there is a band around 1960 cm^{-1} which responds in a very linear fashion

to the addition of LP in the 1.00 M to 3.00 M range. The assignment of this band, as seen in Figure 2-9, is uncertain. The band may be due to a combination or overtone stretch of the ether band.

The effect of ion pairing at high LP concentrations may also contribute to the appearance of the IR spectra of the corresponding LP-CA complexes. James and Mayes, while doing spectroscopic studies on the lithium perchlorate/N,N-Dimethylformamide[20] and the lithium perchlorate/diethyl ether[21] systems, found that at $LiClO_4$ concentrations below 2.0 M ion association is negligible. Using analysis of the band profiles for the symmetrical stretching vibrations of small polyatomic anions in conjunction with multinuclear NMR, they concluded that, "the approach of the strongly polarizing lithium ion induces an asymmetric perturbation on the ClO_4^- which is manifested by a loss of degeneracy in the antisymmetric stretching vibration, broadening of the ^{35}Cl NMR signal, and the appearance of additional components for the nondegenerate symmetrical stretching vibration." These researchers also found that the ^{7}Li NMR signal also shifted as a result of ion association. They also found that an examination of the infrared spectra showed that the antisymmetric stretching vibration undergoes a loss of degeneracy at LP concentrations above 2.5 M. From their data it was observed that the ^{35}Cl NMR signal was relatively sharp up to a concentration approximately 2 M but that rapid broadening occurred at higher concentrations. This broadening was attributed to the strong field gradient produce by the close approach of the lithium ion. The presence of an increasing number of ion pairs could lead to them absorbing some of the incident radiation. When this occurs, the behavior is known as an "inner filter effect."

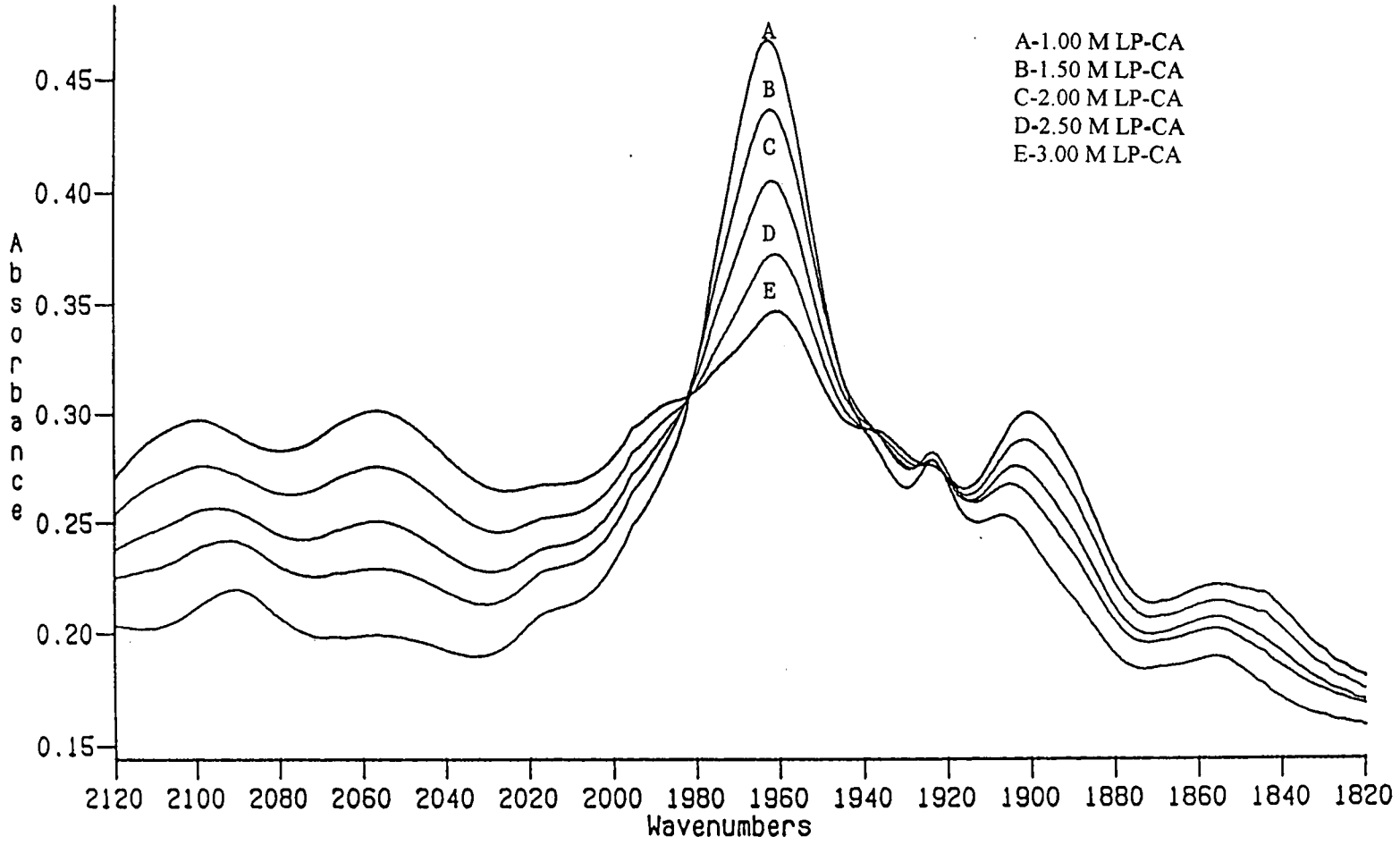


Figure 2-9. Superimposed raw FTIR spectra of 1.00 M to 3.00 M LP-CA complexes in diethyl ether with emphasis on the wavenumber region of 1940 cm^{-1} to 1980 cm^{-1}.

In contrast to Figure 2-6 where linewidths and λ_{max} do not change on with increasing LP concentration at low LP concentrations, Figures 2-7 and 2-8 show how linewidths and λ_{max} change at higher LP concentration ranges. The C=O bands for CA and the LP-CA complex shift because the solvent is becoming more polar. The bands broaden because complexation of the lithium ion to the carbonyl oxygen weakens the force constant of the double bond as a result of charge transfer from the lone pair of the oxygen atom to the Li^+ cation.. This weakening of the bond force constant results in a C=O stretch that absorbs at a lower energy. The trends in the shift of λ_{max} and the linewidths are presented in Table 2-5.

The integrated areas of the bands formed under the shoulder which appeared as a result of the Li+ complexation were found using "Peakfit". The results of curve/band-fitting the raw LP-CA complexes are presented in Tables 2-6 through 2-11. In these Tables are presented the data obtained using Lorentzian and Pearson curve-fitting functions. More than one function was used because it was necessary to see which function was best suited for modeling the complexation. The equilibrium constants for the LP-CA complexation were calculated using Lorentzian data.

Theoretically, an absorption band profile should follow a Lorentzian line shape. Excitation from a lower level to a higher level is followed by emission from the high level back to the lower level. The fall to the lower level is spontaneous, with the decay to the lower level taking a random number of pathways. The instability of the excited state

Table 2-5. Peak Centers[a] and Widths at Half-Max[b] as a Function of LP Conc.[c] For 0.10 M to 3.00 M LP-CA Complexes				
[LP]	**Center C_F[d]**	**Half-Width C_F**	**Center C_A[e]**	**Half-Width C_A**
Low				
0.04	1698.9	7.57	1686.9	28.87
0.06	1698.9	7.56	1686.0	24.33
0.08	1698.8	7.59	1685.6	23.15
0.10	1698.9	7.79	1686.1	20.70
Intermediate				
0.10	1697.2	9.14	1684.1	18.73
0.30	1695.8	10.06	1681.8	16.37
0.45	1695.0	10.47	1680.8	15.31
0.60	1694.3	11.06	1680.1	15.08
1.00	1692.2	11.96	1680.0	14.70
2.00	1688.2	12.27	1678.6	13.79
High				
1.00	1692.3	12.87	1681.8	14.74
1.50	1689.2	13.44	1680.8	13.08
2.00	1687.2	11.87	1679.8	11.84
2.50	1687.5	12.28	1679.9	11.96
3.00	1687.2	11.65	1679.8	11.75

[a,b]Measured in cm^{-1}. [c]mol/L [d]Free CA [e]Complexed CA

Table 2-6. Band-Fitting Results for 0.04M to 0.10 M LP-CA Complexes in DE (Lorentzian Fit).

	Molarity of LP[a]			
	0.04	**0.06**	**0.08**	**0.10**
Band 1				
ν^b	1686.9	1686.0	1685.6	1685.3
Amp.[c]	0.174	0.230	0.277	0.322
HW[d]	28.87	24.33	23.15	20.70
Area[e]	7.27	8.19	9.44	9.86
Fit error	0.0217	0.0229	0.0234	0.0221
r^f	0.9882	0.9863	0.9850	0.9897
Band 2				
ν^b	1698.9	1698.9	1698.8	1698.8
Amp.[c]	1.151	1.027	1.026	0.951
HW[d]	7.57	7.56	7.59	7.79
Area[e]	13.41	12.72	11.98	11.39
Fit error	0.0217	0.0187	0.0234	0.0221
r^f	0.9882	0.9909	0.9850	0.9860

[a]Molar concentration of LP in 0.10 M CA. [b]Peak center in cm^{-1}. [c]Peak amplitude in absorbance units. [d]Half-width in cm^{-1}. [e]Peak area. [f]Correlation coefficient.

Table 2-7. Band-Fitting Results for 0.04 M to 0.10 M LP-CA Complexes in DE (Pearson Fit)

	Molarity of LP[a]			
	0.04	**0.06**	**0.08**	**0.10**
Band 1				
ν^b	1687.7	1686.6	1686.1	1685.9
Amp.[c]	0.239	0.297	0.341	0.379
HW[d]	24.66	22.071	21.51	20.693
Area[e]	11.35	12.30	13.22	13.17
Fit error	0.0179	0.0187	0.0195	0.0193
r^f	0.9920	0.9909	0.9897	0.9894
Band 2				
ν^b	1698.9	1698.9	1698.9	1698.8
Amp.[c]	1.100	1.027	0.961	0.883
HW[d]	7.85	8.023	8.13	8.247
Area[e]	10.62	9.82	9.24	8.61
Fit error	0.0179	0.0187	0.0195	0.0193
r^f	0.9920	0.9909	0.9897	0.9894

[a]Molar concentration of LP in 0.10 M CA. [b]Peak center in cm^{-1}. [c]Peak amplitude in absorbance units. [d]Half-width in cm^{-1}. [e]Peak area. [f]Correlation coefficent.

Table 2-8. Band-Fitting Results for 0.10 M to 2.00 M LP-CA Complexes in DE (Lorentzian Fit)

	Molarity of LP[a]					
	0.10	**0.30**	**0.45**	**0.60**	**1.00**	**2.00**
Band 1						
ν^b	1962.3	1962.2	1962.1	1962.0	1961.9	1961.2
Amp.[c]	0.329	0.309	0.302	0.288	0.259	0.173
HW	30.78	31.23	31.74	32.31	32.50	36.78
Area[e]	14.25	13.55	13.45	13.01	11.80	8.76
Fit error	0.0057	0.0055	0.0058	0.0055	0.0057	0.0065
r^f	0.9961	0.9959	0.9954	0.9955	0.9938	0.9829
Band 2						
ν^b	1641.2	1641.2	1641.0	1641.2	1641.1	1640.9
Amp.[c]	0.215	0.243	0.288	0.310	0.268	0.327
Hwd	9.14	9.51	10.64	11.23	11.10	12.83
Area[e]	2.99	3.49	4.60	5.22	4.47	6.24
Fit error	0.0238	0.0287	0.0442	0.0388	0.0413	0.0402
r^f	0.9963	0.9955	0.9910	0.9936	0.9915	0.9933
Band 3						
ν^b	1684.1	1681.8	1680.8	1680.1	1680.0	1678.6
Amp.[c]	0.696	1.282	1.525	1.657	1.529	1.615
Hwd	18.73	16.37	15.31	15.08	14.70	13.79
Area[e]	19.4	31.47	35.09	37.57	33.79	33.54
Fit error	0.0238	0.0287	0.0442	0.0388	0.0413	0.0402
r^f	0.9963	0.9955	0.9910	0.9936	0.9915	0.9933
Band 4						
ν^b	1697.2	1695.8	1695.0	1694.3	1692.1	1689.3
Amp.[c]	1.801	1.411	1.352	1.302	0.989	1.116
HW[d]	9.14	10.06	10.47	11.06	11.96	12.27
Area[e]	25.23	21.69	21.61	21.95	17.95	20.75
Fit error	0.0238	0.0287	0.0442	0.0388	0.0413	0.0402
r^f	0.9963	0.9955	0.9910	0.9936	0.9914	0.9933

[a]Molar concentration of LP in 0.285 M CA. [b]Peak center in cm^{-1}. [c]Peak amplitude in absorbance units. [d]Half-width in cm^{-1}. [e]Peak area. [f]Correlation coefficient.

Table 2-9. Band-Fitting Results for 0.10 M to 2.00 M LP-CA Complexes in DE (Pearson Fit)

	Molarity of LP[a]					
	0.10	**0.30**	**0.45**	**0.60**	**1.00**	**2.00**
Band 1						
ν[b]	1962.4	1962.3	1962.2	1962.2	1962.2	1961.5
Amp.[c]	0.324	0.304	0.299	0.285	0.257	0.168
HW[d]	31.52	32.01	32.73	33.14	33.60	38.36
Area[e]	13.74	13.06	13.20	12.75	11.51	8.18
Fit error	0.0051	0.0049	0.0050	0.0050	0.0050	0.0061
r[f]	0.9969	0.9967	0.9966	0.9963	0.9954	0.9848
Band 2						
ν[b]	1641.7	1641.8	1641.5	1641.8	1641.8	1641.3
Amp.[c]	0.232	0.270	0.312	0.337	0.296	0.349
HW[d]	13.24	14.73	16.68	16.60	17.14	17.95
Area[e]	4.67	5.99	7.24	8.02	7.29	8.67
Fit error	0.0126	0.0129	0.0229	0.0172	0.0181	0.0277
r[f]	0.9989	0.9991	0.9976	0.9987	0.9984	0.9969
Band 3						
νb	1687.2	1681.8	1680.7	1679.9	1679.8	1678.0
Amp.[c]	0.71	1.218	1.50	1.63	1.488	1.511
HW[d]	26.94	18.32	16.98	16.30	16.38	14.89
Area[e]	20.43	25.85	30.79	33.18	29.89	31.67
Fit error	0.0126	0.0129	0.0229	0.0172	0.0181	0.0277
r[f]	0.9989	0.9991	0.9976	0.9987	0.9984	0.9969
Band 4						
ν[b]	1697.5	1696.1	1695.4	1694.6	1692.8	1689.2
Amp.[c]	1.559	1.412	1.321	1.28	0.938	1.079
HW[d]	8.24	10.73	11.84	12.56	14.37	15.53
Area[e]	21.42	22.33	19.72	20.10	15.85	20.06
Fit error	0.0126	0.0129	0.0229	0.0172	0.0181	0.0277
r[f]	0.9989	0.9991	0.9976	0.9987	0.9984	0.9969

[a]Molar concentration of LP in 0.285 M CA. [b]Peak center in cm^{-1}. [c]Peak amplitude in absorbance units. [d]Half-width in cm^{-1} [e]Peak area. [f]Correlation coefficient..

Table 2-10. Band-Fitting Reults for 1.00 M to 3.00 M LP-CA Complexes in DE (Lorentzian Fit).

	Molarity of LP[a]				
	1.00	**1.50**	**2.00**	**2.50**	**3.00**
Band 1					
ν^b	1642.0	1642.0	1641.9	1641.9	1641.9
Amp.[c]	0.385	0.435	0.483	0.462	0.477
HW[d]	9.88	11.56	14.37	13.19	13.49
Area[e]	5.74	7.54	10.29	9.08	9.58
Fit error	0.0507	0.0430	0.0325	0.0363	0.0352
r^f	0.9936	0.9966	0.9983	0.9979	0.9981
Band 2					
ν^b	1681.8	1680.8	1679.8	1679.9	1679.8
Amp.[c]	0.298	2.462	2.507	2.252	2.527
HW[d]	14.74	13.08	11.84	11.96	11.75
Area[e]	51.00	48.71	45.08	45.74	45.10
Fit error	0.0507	0.0430	0.0325	0.0363	0.0352
r^f	0.9936	0.9966	0.9983	0.9979	0.9981
Band 3					
ν^b	1692.3	1689.2	1687.2	1687.5	11687.2
Amp.[c]	1.224	1.667	2.268	2.140	2.262
HW[d]	12.87	13.44	11.87	12.25	11.65
Area[e]	23.88	33.90	40.89	39.81	40.06
Fit error	0.0507	0.0430	0.0325	0.0363	0.0352
r^f	0.9936	0.9966	0.9983	0.9979	0.9981

[a]Molar concentration of LP in 0.285 M CA. [b]Peak center in cm^{-1}. [c]Peak amplitude in absorbance units. [d]Half-width in cm^{-1}. [e]Peak area. [f]Correlation coefficient.

Table 2-11. Band-Fitting Results for 1.00 M to 3.00 M LP-CA Complexes in DE (Pearson Fit)

	Molarity of LP[a]				
	1.00	1.50	2.00	2.50	3.00
Band 1					
ν[b]	1642.3	1642.0	1642.0	1642.3	1641.9
Amp.[c]	0.289	0.454	0.470	0.469	0.477
HW[d]	19.62	14.22	15.08	14.97	13.49
Area[e]	8.04	10.17	9.86	10.61	9.58
Fit error	0.0647	0.0166	0.0228	0.0172	0.0352
r[f]	0.9897	0.9995	0.9992	0.9995	0.9981
Band 2					
ν[b]	1680.3	1680.5	1678.9	1679.0	1679.2
Amp.[c]	1.791	1.883	1.805	1.562	2.027
HW[d]	15.84	15.58	13.16	13.38	12.87
Area[e]	49.23	42.81	42.55	35.75	41.53
Fit error	0.0647	0.0166	0.0228	0.0172	0.0230
r[f]	0.9897	0.9995	0.9992	0.9995	0.9992
Band 3					
ν[b]	1689.7	1687.7	1685.8	1685.6	1686.3
Amp.[c]	1.217	1.697	2.515	2.501	2.389
HW[d]	18.69	18.44	14.82	16.30	14.20
Area[e]	24.26	33.98	43.07	46.45	40.52
Fit error	0.0647	0.0166	0.0228	0.0172	0.0230
r[f]	0.9897	0.9995	0.9992	0.9995	0.9992

[a]Molar concentration of LP in 0.285 M CA. [b]Peak center in cm^{-1}. [c]Peak amplitude in absorbance units. [d]Half-width in cm^{-1}. [e]Peak area. [f]Correlation coefficient.

energy gives rise to a range of frequencies of light that can be absorbed in producing that state. Thus the absorption profile is not infinitely narrow, but has some finite width. In 1930, the probability distribution of the absorption profile was shown by Weisskopf and Wigner to follow a Lorentzian line shape.[22] Deviations from this fit are indicative of some other types of association interactions that are occurring in the solution. The main difference between the Lorentzian and Pearson function is the a_3. or second width of band factor. This factor serves as a toggle between Lorentzian and Gaussian functions. At low values of a_3 the line shape will be more Lorentzian in character and at high values of a_3 the line shape will be more Gaussian. Some researchers[23] have found that using Lorentzian-Gaussian product functions give better curve-fitting results than pure Lorentzian or pure Gaussian functions alone. The Lorentzian function best describes the collisional broadening effect, which is ubiquitous in solution, while the Gaussian function describe perturbations due to associations such as solvent-solute interactions and H-bonding.

The equilibrium constants for the spectroscopic data were calculated using a method discussed by Bulmer[24] and McBryde.[25] In the case of the LP-CA complexation, the concentration of the free (C_F) and associated (C_A) crotonaldehyde must add up to the total, crotonaldehyde concentration (C_T)(1). Thus;

$$C_T = C_F + C_A \qquad (1)$$

Using the Beer-Lambert Law,

$$A = \varepsilon C d \tag{2}$$

(where A = absorbance, C = molar concentration, d = pathlength in cm (obtained by the interference fringe method) and ε = molar absorption coefficient), equation 2 can be restated as;

$$C_T = A_F/\varepsilon_F d + A_A/\varepsilon_A d \tag{3}$$

that can be rearranged to give:

$$A_A/C_T d = \varepsilon_A - (\varepsilon_A/\varepsilon_F)(A_F/C_T d) \tag{4}$$

Using data obtained for solutions with LP concentration in the range 0.04 M to 0.10 M, $(A_A/C_T d)$ was plotted against $(A_F/C_T d)$ to obtain a straight line with intercept (ε_A), and slope $(-\varepsilon_A/\varepsilon_F)$. Only the low concentration range of LP was used because it conformed to the linearity associated with the Beer-Lambert law. This linearity is not displayed by the higher concentration ranges. One reason for deviation from Beer's Law is that the assumption that activities can be replaced by concentrations is unreasonable at higher concentrations where deviations of activity coefficients from unity are most likely to be large. The equilibrium constant K is given by:

$$K = C_A/(C_F C_O) \tag{5}$$

where C_O is the concentration of LP, obtained from the equation:

$$C_O = C_{LP}^{\circ} - (A_A/\varepsilon_A d) \tag{6}$$

The values of the two molar absorption coefficients from (4) were obtained using a linear regression fit of the data. The correlation coefficient of this line was 0.9796. The relative area of the resolved bands are presented in Table 2-12.

Table 2-12 Resolved Bands of 0.04 M to 0.10 M LP-CA Complexes in DE[a]		
[LP]	**Area of C_A(complexed)[b]**	**Area of C_F(free)[c]**
0.04	7.27	13.41
0.06	8.19	12.72
0.08	9.44	11.98
0.10	9.86	11.39
[a]Data taken from a Lorentzian fit [b]Band ≈ 1686 cm^{-1} [c]Band ≈ 1698.9 cm^{-1}.		

The values obtained for K are summarized in Table 2-13. These values were obtained using $\varepsilon_A = 33026$ and $\varepsilon_F = 23817$, $d = 0.0078$ cm and $C_T = 0.10$ M. The values of K show little variation as the LP concentration is increased. In general, there is a decrease in the value of K as the LP concentration is increased.

Table 2-13 Equilibrium Constants for the formation of 0.04 M to 0.10 M LP-CA Complexes[a]						
[LP]	**A_A/C_Td**	**A_F/C_Td**	**A_F/ε_Fd**	**A_A/ε_Ad**	**C_O**	**K[b]**
0.04	9320.0	17192.3	0.072	0.028	0.012	32.96
0.06	10500.0	16307.0	0.068	0.032	0.028	16.81
0.08	12102.6	15358.9	0.064	0.037	0.043	13.44
0.10	12641.0	14602.6	0.061	0.038	0.062	10.05
[a]Data taken from Lorentzian band-fit. [b]Average K = 18.31						

Spectra were acquired for the complexation of LP to benzonitrile in one concentration range only. Data were obtained for solutions using 0.10 M, 0.30 M, 0.45 M, 0.60 M, 1.00 M and 2.00 M LP solution and 0.285 M BN, all in diethyl ether. Figure 2-10 shows the superimposed FTIR spectra for these solutions. From Figure 2-10 it can be seen that the λ_{max} of the complexed band occurs at higher wavenumbers than that for uncomplexed BN. This shift to higher wavenumbers occurs because the C≡N bond is strengthened on complexation to Li^+. This strengthening is possible either because of the σ-bond formed by changes in the hybridization of the bonding orbitals, or because of the strenengthing of the p_π - p_π^- or p_π - d_π[26] Strengthening of the bond is due not only to an increase of the force constant of the C≡N bond but also to a change in the vibrational mechanics of the nitrile molecule when it is bound into a complex. The trends in the shift of λ_{max} and the linewidths of the free and the complexed C≡N are presented in Table 2-14.

Table 2-14. Peak Centers[a] and Widths at Half-Max[b] as a Function of LP Conc.[c]

[LP]	Center B_F[d]	HW B_F	Center B_A[e]	HW B_A	$\Delta_{C\equiv N}$[f]
0.10	2228.0	12.26	2263.6	29.40	35.6
0.30	2227.9	12.01	2256.7	22.21	28.8
0.45	2227.5	12.33	2255.7	22.19	28.2
0.60	2227.6	11.79	2255.5	20.40	27.9
1.00	2227.3	11.47	2254.1	19.24	26.8
2.00	2226.6	11.52	2253.2	18.40	26.6

[a,b]Measured in cm^{-1}. cmol/L [d]Free BN [e]Complexed BN [f]Center B_A - Center BF

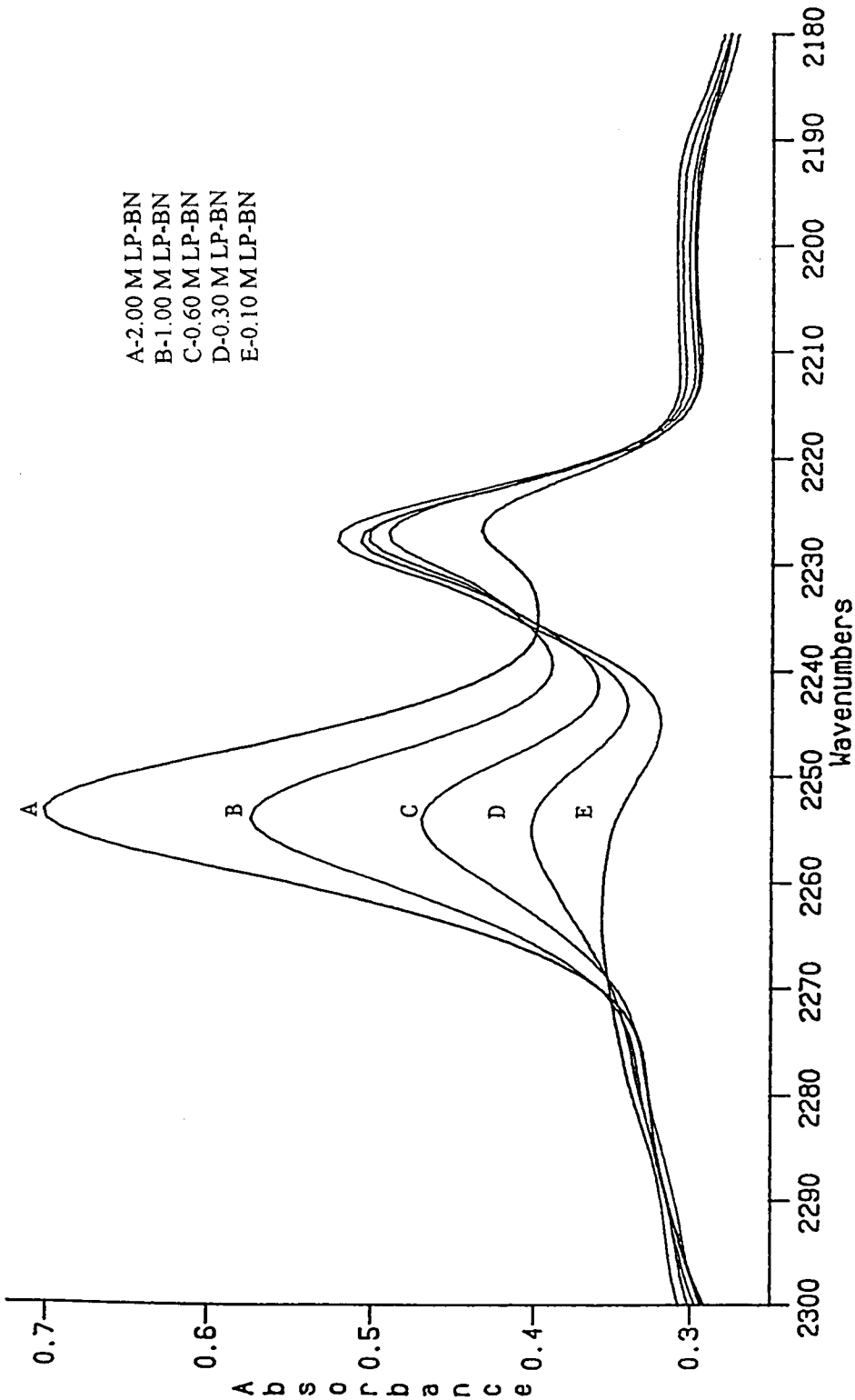


Figure 2-10. Superimposed raw FTIR spectra of 0.10 M to 2.00 M LP-BN complexes in diethyl ether.

The integrated area of the bands formed under the shoulder which appeared as result of the Li^+ complexation were found using "Peakfit". The results of the band - fitting procedures are presented in Table 2-15 and 2-16. The curves were best fitted using four peaks. The peaks which occur around 2228 cm^{-1} and 2255 cm^{-1} were assigned to the free BN and complexed BN respectively. The other two peaks are most likely overtone or combination modes of the nitrile which did not involve C≡N stretching. In general the intensity of the free BN peak decreased with increasing LP concentration and that of the complexed BN grew with increasing LP concentration.

The equilibrium constants for the LP-BN complexation were calculated using Lorentzian data. The equilibrium constants for the spectroscopic data were calculated using a method discussed by Bulmer[24] and McBryde.[25] The concentration of benzonitrile, B_F, and complexed benzonitrile, B_A, must add up to the total, benzonitrile, B_T concentration (10). Thus:

$$B_T = B_F + B_A \tag{7}$$

Using the Beer-Lambert Law,

$$A = \varepsilon C d \tag{8}$$

(where A = absorbance, C = molar concentration, d = pathlength in cm, and ε = molar absorption coefficient), equation 7 can be restated as;

$$B_T = A_F/\varepsilon_F d + A_A/\varepsilon_A d \tag{9}$$

that can be arranged to give:

$$A_A/B_T d = \varepsilon_A - (\varepsilon_A/\varepsilon_F)(A_F/B_T d) \tag{10}$$

Table 2-15. Band-Fitting Results for 0.10 M to 2.00 M LP-BN Complexes in DE (Lorentzian fit)

	Molarity of LP[a]					
	0.10	**0.30**	**0.45**	**0.60**	**1.00**	**2.00**
Band 1						
cm^{-1}[b]	2196.0	2195.9	2195.6	2195.7	2195.	
Amp.[c]	0.026	0.025	0.025	0.024	0.021	
HW[d]	12.92	12.29	13.62	12.02	11.34	
Area[e]	0.47	0.43	0.48	0.40	0.34	
Fit error	0.0064	0.0067	0.0056	0.0065	0.0062	
r[f]	0.9849	0.9877	0.9893	0.9913	0.9950	
Band 2						
cm^{-1}[b]	2228.0	2227.9	2227.5	2227.6	2227.3	2226.
Amp.[c]	0.226	0.242	0.189	0.223	0.197	0.127
Hw[d]	12.26	12.01	12.33	11.79	11.47	11.52
Area[e]	4.13	4.32	3.46	3.91	3.37	2.18
Fit error	0.0064	0.0067	0.0056	0.0065	0.0062	0.0064
r[f]	0.9849	0.9877	0.9893	0.9913	0.9950	0.9968
Band 3						
cm^{-1}[b]	2263.6	2256.7	2255.7	2255.0	2254.1	2253.2
Amp.[c]	0.075	0.114	0.129	0.194	0.301	0.439
HW[d]	29.40	22.21	22.19	20.40	19.24	18.40
Area[e]	3.07	3.63	4.12	5.71	8.42	11.79
Fit error	0.0064	0.0067	0.0056	0.0065	0.0062	0.0064
r[f]	0.9849	0.9877	0.9893	0.9913	0.9950	0.9968
Band 4						
cm^{-1}[b]	2287.6	2282.9	2283.3	2284.7	2287.1	2289.4
Amp.[c]	0.038	0.051	0.050	0.047	0.044	0.043
HW[d]	29.90	34.60	34.43	30.56	25.37	19.34
Area[e]	1.53	2.35	2.28	1.96	1.54	1.17
Fit error	0.0064	0.0067	0.0056	0.0065	0.0062	0.0064
r[f]	0.9849	0.9877	0.9893	0.9913	0.9950	0.9968

[a]Molar concentration of LP in 0.285 M BN. [b]Peak center in cm^{-1}. [c]Peak amplitude. [d]Half-width. [e]Peak area. [f]Correlation coefficient.

Table 2-16. Band-Fitting Results for the 0.10 M to 2.00 M LP-BN Complexes in DE (Pearson Fit)

	Molarity of LP[a]					
	0.10	**0.30**	**0.45**	**0.60**	**1.00**	**2.00**
Band 1						
cm^{-1}[b]	2196.9	2197.1	2197.0	2196.6	2195.9	
Amp.[c]	0.031	0.029	0.024	0.029	0.018	
HW[d]	23.89	20.67	26.20	20.61	18.89	
Area[e]	0.78	0.64	0.66	0.63	0.40	
Fit error	0.0055	0.0074	0.0079	0.0076	0.0123	
r[f]	0.9893	0.9856	0.9793	0.9883	0.9809	
Band 2						
cm^{-1}[b]	2227.9	2227.	2227.3	2227.5	2227.1	2226.6
Amp.[c]	0.227	0.238	0.184	0.218	0.185	0.132
HW[d]	13.36	13.02	13.20	12.99	14.50	11.53
Area[e]	3.85	3.68	2.97	3.36	3.16	2.58
Fit error	0.0055	0.0074	0.0079	0.0076	0.0123	0.0060
r[f]	0.9893	0.9856	0.9793	0.9883	0.9809	0.9973
Band 3						
cm^{-1}[b]	2260.7	2255.6	2254.9	2254.5	2254.0	2253.3
Amp.[c]	0.072	0.131	0.149	0.213	0.299	0.441
HW[d]	31.29	27.67	25.38	22.22	20.99	18.64
Area[e]	2.95	4.55	5.93	7.28	10.08	11.66
Fit error	0.0055	0.0074	0.0079	0.0076	0.0123	0.0060
r[f]	0.9893	0.9856	0.9793	0.9883	0.9809	0.9973
Band 4						
cm^{-1}[b]	2285.4	2286.3	2284.4	2286.3	2290.7	2290.4
Amp.[c]	0.041	0.036	0.036	0.038	0.026	0.039
HW[d]	39.60	37.63	37.47	31.99	20.62	24.67
Area[e]	1.80	1.45	1.48	1.32	0.59	1.03
Fit error	0.0055	0.0074	0.0079	0.0076	0.0123	0.0060
r[f]	0.9893	0.9856	0.9793	0.9883	0.9809	0.9973

[a]Molar concentration of LP in 0.285 M BN. [b]Peak center in cm^{-1}. [c]Peak amplitude. [d]Half-width. [e]Peak area. [f]Correlation coefficient.

When (A_A/B_Td) was plotted against (A_F/B_Td) a straight line with correlation coefficient 0.9080, the intercept (ε) and slope, $(-\varepsilon_A/\varepsilon_F)$ was obtained. The equilibrium constant, K, is given by:

$$K = B_A/B_FB_o \tag{11}$$

where Bo is the concentration of LP, obtained from the equation:

$$B_o = LP_o - (A_A/\varepsilon_Ad) \tag{12}$$

The values of the two molar absorption coefficients from (10) were obtained using a linear regression fit of the data.

An isosbestic point was observed in Figure 2-10, which shows a montage of the raw FTIR spectra of the LP-BN complexes. The presence of this isosbestic point indicates that there is a dynamic equilibrium between the complexed BN and the free BN. The relative areas of the resolved bands are presented in Table 2-17.

Table 2-17. Resolved Bands of the 0.10 M to 2.00 M LP-BN Complexes in DE[d]

[LP]	Area of B_A(complexed)[b]	Area of B_F (free)[c]
0.10	3.07	4.13
0.30	4.32	3.63
0.45	3.46	4.12
0.60	3.91	5.71
1.00	3.37	8.42
2.00	2.18	11.79

[a]Data taken from a Lorentzian fit. [b]band $\approx$ 2255 cm^{-1}. [c]Band $\approx$ 2228 cm^{-1}.

The values obtained for K are summarized in Table 2-18. These values were obtained using ε_A = 9128.4 ε_F = 2293.6, d = 0.0078 cm and B_T = 0.285 M. The equilibrium constant for the 0.10 M and 0.30 M LP-BN complexes are larger than those for the other

Table 2-18. Equilibrium Constant for the Formation of 0.10 M to 2.00 M LP-BN Complexes in DE[b].

[LP]	A_A/B_tu	A_F/B_Td	A_F/ε_Fd	A_A/ε_Ad	B_o	K
0.10	1381.0	1857.8	0.231	0.043	0.057	3.270
0.30	1632.9	1943.3	0.241	0.051	0.249	0.850
0.45	1853.4	1556.3	0.193	0.058	0.392	0.767
0.60	2568.6	1758.9	0.219	0.080	0.520	0.702
1.00	3787.7	1515.9	0.188	0.116	0.882	0.712
2.00	5303.6	980.7	0.122	0.166	1.884	0.742

[a]Data taken from a Lorentzian band fit.

complexes. These differences in the values of K may be due to the use of the data for the 1.00 M and the 2.00 M integrated areas for the calculation of the molar absorption coefficients. Since these values are much larger that other values they will have a greater effect on the value of the intercept and the slope when a linear regression is performed on the data.

An investigation was also conducted to determine the equilibrium constant for the complexation of Li^+ to camphor (CM) (Eq 13).

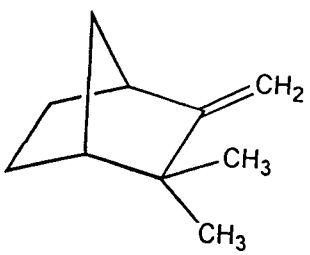
$$CM + LP \rightarrow LP\text{-}CM \qquad (13)$$

This experiment was conducted to study the change in rotation of camphor as a function of increasing LP concentration. The observed rotations for a fixed amount of camphor in DE are presented in Table 2-19. The camphor/DE solutions were prepared in a 25 mL volumetric flask.

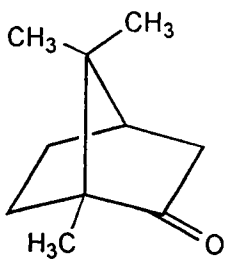
In Table 2-20 is presented the effect of increasing LP concentrations on the observed rotation of camphene **(1)**, a substrate that is incapable of functioning as a Lewis base with Li^+, but a close analogue of camphor **(2)**

Table 2-19. Camphor Rotations in Diethyl Ether as a Function of LP Conc.					
Entries	**CM (g)**	**[CM]**	**LP(g)**	**[LP]**	**Rot.**
0	2.0325	0.534	0.0000	0.0000	+ 4.236
1	2.0377	0.535	0.2610	0.0981	+ 4.053
2	2.0370	0.535	0.6643	0.2497	+ 3.557
3	2.0328	0.534	1.3390	0.5034	+ 3.083
4	2.0116	0.529	2.6631	1.0013	+ 2.428
5	2.0522	0.539	5.0630	1.9036	+ 2.247

Table 2-20. Camphene Rotations in Diethyl Ether as a Function of LP Conc.[a]				
Camphene(g)	**[camphene]**	**LP(g)**	**[LP]**	**Rotation[b,c]**
0.6855	0.5032	0.0000	0.0000	+ 0.388
0.6841	0.5021	0.1303	0.1225	+ 0.398
0.6975	0.5120	0.2503	0.2352	+ 0.369
0.6912	0.5073	0.5131	0.4823	+ 0.377
0.6830	0.5013	1.0515	0.9883	+ 0.365
0.6855	0.5032	2.1236	1.9961	+ 0.390
[a]Solutions made up using 25 mL of DE. [b]Mean = 0.381. [c]Standard deviation = 0.013.				



1



2

From the camphene rotation data, it can be inferred that increasing LP concentrations has very little effect on its optical rotation. This effect is observed because there is no place on the camphene molecule to which the Li^+ can be complexed. The changes in camphor's rotation as LP concentration is increased, as seen Table 2-19, occur because of complexation to the carbonyl oxygen of camphor. This complexation is similar to the complexation of Li^+ to the carbonyl oxygen of crotonaldehyde. It should be noted here that the rotation for the complexation of Li^+ to camphor decreases with increasing LP concentration as shown in Figure 2-11. The shape of this curve suggest that the optical rotation is reaches some limiting value at infinite LP concentration.

One explanation for the change in rotation with increasing Li^+ is that, on complexation to the C=O chromophore, the electromagnetic properties which determine the extent of optical rotation are altered. The use of the term chromophore is used here in a broader context than its definition as an atomic grouping responsible for the absorption of visible or near ultraviolet light. Charney[27] characterizes this chromophore as particles, electrons or nuclei in a given molecule that are principally involved in a chromophoric transition that was induced in a molecule by electromagnetic radiation. These chromophores not only contribute to the absorption and emission of radiation but also to the rotation of the plane of the polarization of the radiation.

Because camphor complexes to LP, reversibly, the observed rotations are a weighted average of the rotation of the complexed and the uncomplexed CM. It was thus necessary to extrapolate the data to infinite LP concentration to obtain the rotation due to

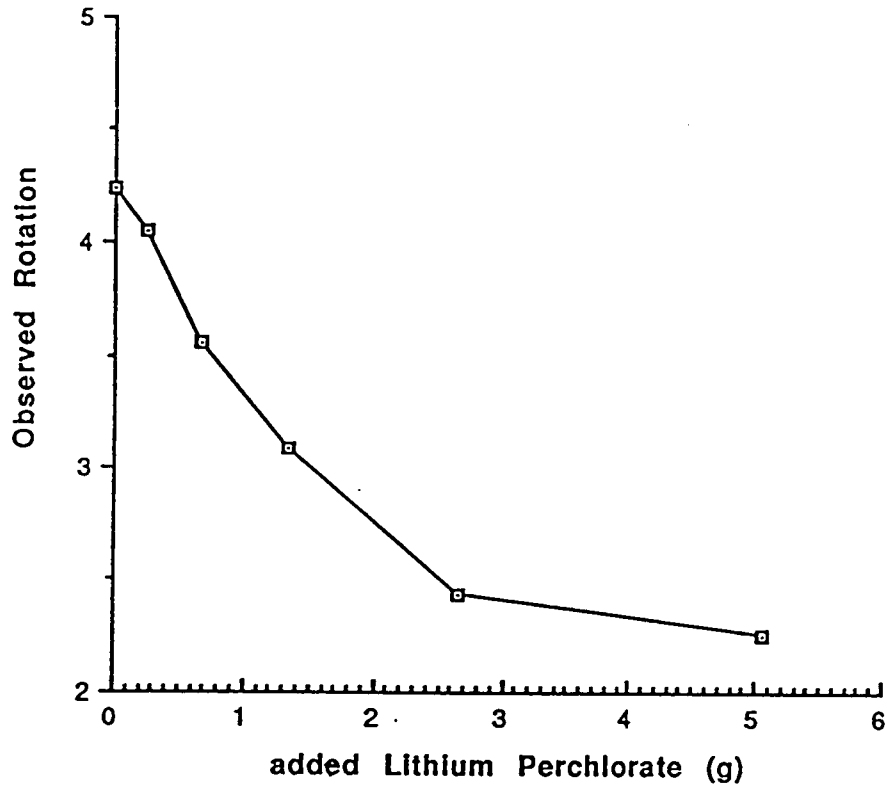


Figure 2-11. The effect of increasing LP concentration on the optical rotation of 2.00 g of camphor in 25 mL of diethyl ether.

the LP-CM complex alone. Pagni, Kabalka *et al.*[15] have developed a mathematical model by which this could be acomplished. In the model CM is assumed to complex to LP reversibly (Eq 13)

$$CM + LP \rightleftharpoons LP\text{-}CM \tag{13}$$

Therefore,

$$K_{eq} = \frac{[LP - CM]}{[CM][LP]} \tag{14}$$

Since $[LP]_o$ = [LP] + [LP-CM] and $[CM]_o$ = [CM] + [LP-CM], where $[LP]_o$ and [CM]o are the initial concentrations, one obtains

$$K_{eq} = \frac{([CA]_o - [CM])}{[CM]([LP]_o - [CM]_o + [CM])}. \tag{15}$$

Furthermore, if the observed rotation is a weighted average of the shifts due to CM and LP-CM, it follows that,

$$\delta = \frac{[CM]}{[CM] + [LP - CM]}\delta_A + \frac{[LP - CM]}{[CM] + [LP - CM]}\delta_{LP-CM} \tag{16}$$

where δ= is the rotation of pure CM in DE and $\delta_{LP\text{-}CM}$ is the rotation of the LP-CM complex. The rotation induced by the presence of Li^+, $\Delta\delta$, can be represented as,

$$\delta\Delta = \delta - \delta_A = \frac{-[LP - CM]}{[CM] + [LP - CM]} + \frac{[LP - CM]}{[CM] + [LP - CM]}\delta_{LP-CM} \tag{17}$$

Since [CM]o = [CM] + [LP-CM], rearranging Eq 17 gives;

$$\Delta\delta = \frac{[CM]_o - [CM]}{[CM]_o}\Delta\delta_\infty \tag{18}$$

where $\Delta\delta_\infty = \delta_{LP\text{-}CM} - \delta_A$ is the induced rotation of the complex. One can then combine the solution for [CM] from Eq 15 with Eq 18 and obtain, after considerable manipulation,

$$([CM]_o \Delta\delta - [LP]_o \Delta\delta_\infty)(\Delta\delta - \Delta\delta_\infty)K_{eq} = \Delta\delta\Delta\delta_\infty \qquad (19)$$

The equilibrium constants were calculated by first substituting the values for [CM]o, [LP]0, and Δδ for two entries into equation 19. Two equations of the form of equation 19 were thus obtained. By equating these two equations it was possible to eliminate K and solve for $\Delta\delta_\infty$. Once obtained, the appropriate $\Delta\delta_\infty$ was then substituted back in the appropriate equation of the form of equation 19 to find K for a given entry. The average of the two K's thus obtained are reported in Table 2-21.

Table 2-21. Results for the Calculation of K_{eq} for the LP-CM Complexation.

Entries Used[a]	$\Delta\delta_\infty$	$\delta_{LP\text{-}CM}$	K[b]
2 - 5	- 2-287	1.949	4.65
2 - 3	- 2.318	1.918	4.44
2 - 4	- 2.897	1.339	2.49
3 - 4	- 3.057	1.179	2.10
3 - 5	- 2.289	1.947	4.56
3 - 6	- 2.127	2.109	10.29

[a]Entries used. [b]Average K = 4.76.

MNDO calculations were used to predict the shift which would occur on complexation of Li^+ to the carbonyl group of crotonaldehyde and the nitrile group of benzonitrile. To do these calculations an input geometry of a given structure is first

submitted in a specified format to the program. The input geometry is then optimized by a series of iterative approximations. In order to optimize the geometry, the resultant forces on each atom in the system is first calculated and then the atoms are moved in a direction determined by these forces so as to lower the energy of the system. Once the molecular system is optimize its theoretical vibrational frequencies can then be obtained. The theoretical vibrational frequencies can be corrected by multiplying them by a factor of 0.93. This correction brings them closer to experimental values. Some water molecules were added into some of the input files to what effect the presence its presence would have on the vibrational frequencies. This was done because the reactions were done under anhydrous conditions. The solvent, diethyl ether and the reactant lithium perchlorate are both readily absorb water. The results of these calculations are summarized in Table 2-22.

Table 2-22. Comparison of IR Stretching Frequencies.

Band	Theoretical[a,b]				Experimental
	No H_2O	Corrected[f]	With H_2O	Corrected	
C=O	2110	1962	1799	1673	1700 - 1690
C=C	1828	1700	-	-	1640
C=OLi[d]	2013	1872	2066	1921	1687 - 1680
C≡N	2546	2367	-		2227 - 2225
C≡NLi[e]	2503	2327	2531	2353	2252 - 2258

[a]MNDO calculation. [b]Measured in cm^{-1} [c]Three water molecules used. [d]LP-CA complex [e]LP-BN complex. [f]Corrected by multiplying by 0.93.

The data in Table 2-22, shows that the corrected theoretical values are slightly higher than the experimental values. Also the presence of water does have some effect on the

vibrational frequencies. The altering of these frequencies by the presence of H_2O can be attributed to a solvent effect. Kirkwood,[28] Bauer and Magat[29] were among the first to investigate the influence of solvents on IR bands. They proposed the Kirkwood, Bauer, Magat (KMB) theory which relates frequency shifts to the dielectric constant of the medium. The KBM theory was later found to be inadequate. Buckingham[30] later proposed a theoretical model to explain solvent effects on the IR band frequencies and intensities. Buckingham's treatment is better than the KBM theory and holds good for interpreting solvent shifts in IR spectra as longs as there are no specific interactions.

From the results obtained from curve-fitting, it is concluded that CA and BN can exist as 1:1 complexes with LP in DE in low concentration ranges of LP. In the future these conclusions could be further strengthened by using Factor Analysis in conjunction with the band-fitting procedures.

Factor analysis[31] is a statistical technique of multivariate analysis, that was originally developed for use in the behavioral sciences. This technique deals with the structure of matrices of co-variances and correlations. Factor analysis can be used to determine the number of absorbing components in unresolved infrared absorbance band. First a matrix Q is formed from the product of the NS x NW IR absorbance matrix (A) and its transpose (A^t), where NW is the number of wavenumber data points and NS is the number of solutions of varying concentration. The next step is then to determine the number of linearly independent conditions required to fit the data.[23] This method is based on the theorems of linear algebra and assumes no particular band contour. Every

point in the absorbance matrix can be expanded as a linear sum of products:

$$A_{ij} = \sum_{k=1}^{NC} \varepsilon_{ik} C_{kj} \tag{20}$$

where A_{ij} is the absorbance of the ith data point in the spectrum of the j^{th} solution, C_{kj} is the concentration of the K^{th} species in the j^{th} solution and ε_{ki} is the molar absorption coefficient of the i^{th} data point.[24] The number of significant non-zero eigenvalues of Q is equivalent to the number of independently varying component in the system. It is proposed that in the future, this technique should be used to give the number of components which exist in the solvent systems containing LP-CA and LP-BN complexes in the presence of LP-DE.

Fawcett *et al.*[32] have proposed using attenuated total reflection Fourier-transform IR (ATR-FTIR) spectroscopy instead of transmission mid-IR techniques similar to the ones used for this study. They pointed out that transmission techniques require very small pathlengths which reduce sensitivity and make optimum flow conditions difficult if not impossible. They suggested that if one is interested in, studying the spectral of the ion-substrate complex, from those of the free substrate, that one has to overcome the problem of low solute concentration with respect to the substrate. They shown that ATR-FTIR spectroscopy by passes the pathlength/sensitivity problem and further allows one to study the ion-substrate and ion-ion interactions in detail, when these components absorb in the mid-IR region. In the future these techniques could be applied to the present study.

CHAPTER III

EXPERIMENTAL SECTION

Preparation of Reagents and Solutions. Lithium perchlorate obtained from Aldrich Chemical Co. was dried under a high vacuum trap over P_2O_5 for 24 hours in a drying piston. Ethylene glycol (B.P. 196-198°) was used as the solvent in the pot. The $LiClO_4$ was kept in a desiccator over calcium chloride until it was ready for use. All manipulations involving the use of $LiClO_4$ were done rapidly in open air conditions.

Crotonaldehyde solutions were prepared by first preparing a 2.85 M stock solution of crotonaldehyde in diethyl ether. This solution was prepared by adding 2.36 mL of crotonaldehyde (density = 0.856 g/cc) by syringe to a 10-mL volumetric flask and then diluting to the mark with diethyl ether. From this stock solution 1 mL aliquots were taken via a 1-mL pipette and then transferred to a 10-mL volumetric flask to which was subsequently added the appropriate molar amount of $LiClO_4$. Diethyl ether was then added to the mark with periodic shaking. After all the $LiClO_4$ dissolved, the solutions were then transferred to 10-mL Wheaton vials which were then septum sealed and crimped. The solutions were kept in these vials until they were ready for FTIR analysis.

All the benzonitrile solutions were prepared in a manner similar to the preparation of the crotonaldehyde solutions except that the stock solution was prepared by using 2.915 mL of benzonitrile (density = 1.010 g/cc) in order to obtain the same molar concentration.

Camphor solutions were made by placing approximately 2.0 g of camphor into a 25-mL volumetric flask to which some diethyl ether was added to effect dissolution. The appropriate molar amount of $LiClO_4$ was then added followed by addition of more diethyl ether. Dilution was made to the mark accompanied by periodic shaking. The flask was then stoppered and sealed with parafilm until polarimetric readings were taken.

Acquisition and Spectral Manipulation of IR Data. Before filling, the sealed NaCl cells, were first cleaned once with spectroscopicc grade acetone and then with anhydrous diethyl ether. The cell was then dried using a clean inert air duster. This inert gas (Enviro.Ro.Tech, Duster 1671) was obtained from Tech Spray Inc..

The solution to be analyzed was removed by syringe through the Wheaton vial's septum seal. After allowing a copious amount of the solution to flow through the cell it was capped and the outside thoroughly cleaned with acetone. This was necessary in order to remove traces of $LiClO_4$ which became deposited on the cell and its windows. After filling the IR cell the syringe had to be taken apart because residual $LiClO_4$ caused the plunger and the barrel to adhere to each other. When this occurred it was extremely difficult to move the plunger. The barrel and the plunger were then cleaned with acetone and air dried using an inert air duster. Acetone proved to be an excellent solvent for removing the $LiClO_4$ which appeared as a result of the evaporation of the diethyl ether. This acetone had to be meticulously removed by drying the syringe and the cell with the clean, inert air duster, because it was found that even minute traces of it could affect the integrity of the acquired spectra.

All data were acquired on either a Bio-Rad FTS-60A or FTS-7 Fourier Transform Infrared Spectrometer. Each spectrometer is controlled by a computer with an Idris operating system, which is a UNIX-like operating system, and the FTS 3200 data station which is the software installed on the Winchester hard drive. The software acquires and stores all the data into files. Data were acquired at a resolution of 2 cm^{-1} for 64 scans. The IR cell used to measure the absorbances of the ether solutions was a precision-amalgamated flow though cell which consisted of a lead spacer between sodium chloride plates. Luer-Lock fittings with Teflon seals permitted filling and draining the cell via luer-lock syringes. The cell path length, b, was computed by the interference fringe method for the empty cell using the following equation:

$$b = \frac{1}{2D}\left(\frac{n}{\nu_1 - \nu_2}\right)$$

where n is the number of fringes (successive maxima or minima) between two wavenumbers ν_1 and ν_2, and D is the refractive index of the sample material (1.5443 for NaCl).

The addition of lithium perchlorate to ether solutions of crotonaldehyde resulted in the appearance of a new band in the carbonyl stretching region which overlapped with the uncomplexed band. Similarly, a new band overlapping the nitrile stretching band appeared when lithium perchlorate was added to ether solutions of benzonitrile. In order to curve-fit the bands, portions of the original files were transferred to MS-DOS format and imported into DOS software packages on an IBM 386 computer. Additional Bio-Rad software was acquired for this purpose. First, a 240 cm^{-1} interval centered about the band

of interest was extracted from the original data file using the "zap" program which creates a temporary truncated spectrum. To create the temporary file, the following command was typed at the % command prompt:

% Zap -trunc -startHINO -stopLONO DATAFILE.DT temp

where HINO refers to the higher wavenumber of the interval, LONO refers to the lower wavenumber of the interval, DATAFILE.DT is the data file being truncated, and temp is the name of the temporary truncated file. A second Bio-Rad program, "dtdump2", converts the temps file into an ASCII text file. A third Bio-Rad program, "cp2pc", converts the Bio-Rad text file into a MS-DOS text file on floppy disk. Once stored on the floppy disk the file was imported into a Jandel Scientific Software package called "Peakfit". In Peakfit, the absorbance bands were first baseline corrected and then curve fitted. Several fit options were available for the data acquired here; both the Lorentzian and Pearson routines appeared to give the best correlation coefficients and the lowest standard deviations.

Polarimetric Data. The polarimetric data were collected using a Perkin Elmer M421 polarimeter. This is an automatic polarimeter with optical null balance and automatic gain control. Readings were taken at 21°C. A continuous sodium discharge lamp was used as the light source. The instrument was set at an integration time of 5 seconds for all readings. A standard glass cell with a path length of 1 dm and a capacity of 6.2 mL was used for all work.

MO Calculations. The molecular orbital (MO) calculations were carried out on a SPARC server 1000 workstation using MOPAC 6 (QCPE 581). The input geometries were obtained from molecular mechanics calculations using PCMODEL (Serena Software); 4th edition. The MO calculations were done by Dr. J. Bartmess of the University of Tennessee, Knoxville.

REFERENCES

1. a) Lamy-Schelkens, H.; Gioni, D.; Ghosez, L. *Tetrahedron Lett.* **1989**, *30*, 5887. b) Maruoka, K.; Yamamoto, H. *J. Am. Chem. Soc.* **1989**, *111*, 789. c) Midlan, M. M.; Afonso, M. M. *J. Am. Chem. Soc.* **1989**, *111*, 4368. d) Narasaka, K.;Iwasawa, N.; Inoue, M.; Yamad, T.; Nakashima, N.; Sugimori, J. *J. Am. Chem. Soc.* **1989**, *111*, 5340. e) Corey, R. J.; Imwinkelreid, E. J.; Pikul, S.; Xiang, Y. B. *J. Am. Chem. Soc.* **1989**, *111*, 5493.

2. a) Doxsee, K. M.; Farahi, J. B. *J. Am. Chem. Soc.* **1988,** *110*, 7239. b) Trost. B. M.; Yang, B.; Miller, M. L. *J. Am. Chem. Soc.* **1989,** *111*, 6482. c) Lewis, F. D.; Barancyk, S. V. *J. Am. Chem. Soc.* **1989,** *111*, 8653.

3. a) Snider, B. B. *Acc. Chem. Res.* **1980,** *13*, 426. b) Tietze, L. F.; Beifuss, V.; Ruther, M. *J. Org. Chem.* **1989,** *54*, 3120. c) Mikami, K.; Terada, M.; Nakai, T. *J. Am. Chem. Soc.* **1989,** *111*, 1940.

4. a) Ojima, I.; Kwon, H. B. *J. Am. Chem. Soc.* **1988,** *110*, 5617. b) Danishefsky, S. J.; Simoneau, B. **J. Am. Chem. Soc. 1989,** *111*, 2599. c) Hegel, G.; Thornton, E. R. *J. Am. Chem. Soc.* **1989,** *111*, 5722.

5. a) Lipshutz, B. H.; Ellsworth, E. L.; Siahaan, T. *J. Am. Chem. Soc.* **1988**. b) Lipshutz, B. H.; Ellsworth, E. L.; Siahaan, T. *J. Am. Chem. Soc.* **1989**, *111*, 1351. c) Cabral, J.; Laszlo, P.; Mahe', L.; Montaufier, M. T. *Tetrahedron Lett.* **1989**, *30*, 3969.

6. a) Povarov, L. S. *Russ. Chem. Rev. (Engl. Transl.)* **1975,** *34*, 639. b) Hosglin, R. J.; Hirsh, D. H. *J. Am. Chem. Soc.* **1949,** *71*, 3468. c) Isler, O.; Lindlar, H.; Montavon, M.; Ruegg, R.; Zeller, P. **Helv. Chim. Acta. 1956,** *39*, 249. d) Isler, O.; Montavon, R.; Ruegg, R.; Zeller, P. *Swiss Patent 317112*, **1956**.

7. a) Maruka, K.; Nonshita, K.; Banno, H.; Yamamoto, H. *J. Am. Chem. Soc.* **1988,** *110*, 7922. b) Nanoshita, K.; Banno, H.; Maruoka, K,; Yamamoto, H. *J. Am. Chem. Soc.* **1990,** *112*, 316.

8. Olah, G. A. *Friedel-Crafts and Related Reactions*; Interscience Publishers: New York, **1964**.

9. Lewis, G. N. *Valence and the Structure of Atoms and Molecules*; The Chemical Catalog Co.; Inc.: New York, **1923**.

10. Grieco, P. A.; Nunes, J. T.; Gaul, M. D. *J. Am. Chem. Soc.* **1990**, *112*, 4595.

11. a) Pocker, Y.; Cirula, J. C. *J. Am. Chem. Soc.* **1989**, *111*, 4728 and references therein. b) Braun, R.; Sauer, J. J. *Chem. Ber.* **1989**, *119*, 1269. c) Herter, R.; Fohlisch, B. *Synthesis.* **1982**, 976.

12. Forman, M. A.; Dailey, P. W. *J. Am. Chem. Soc.* **1991**, *113*, 2761.

13. Childs, R. F.; Muholland, L. D.; Nixon, A. *Can. J. Chem.* **1982**, *60*, 801.

14. Laszlo, P.; Teston, M. *J. Am. Chem. Soc.* **1990**, *112*, 8750.

15. Pagni, R. M.; Kabalka, G. W.; Bains, S.; Plesco, M.; Wilson, J.; Bartmess, J. *J. Org. Chem.* **1993**, *58*, 3130.

16. Nakamoto, K. *In Infrared Spectra of Inorganic and Coordination Compounds*, 1st ed.; John Wiley and Sons, Inc.: New York: **1993**.

17. Drago, R. S. *Physical Methods for Chemists*; Saunders College Publishing, Fort Worth, TX, **1992**, pp. 103-106.

18. Cohen, M. D.; Fisher, E. *J. Chem. Soc.* **1962**, 3044.

19. Jankowska-Nowick, *J. I. Inorg. Nucl. Chem.* **1971**, *33*, 2043.

20. James, D. W.; Mayes, R. E. *J. Phys. Chem.* **1984**, *88*, 637.

21. James, D. W.; Mayes, R. E. *Aust. J. Chem.* **1982**, *35*, 1785.

22. Winn, J. *Physical Chemistry*, Harper Collins Publishers: New York, **1995**, 678.

23. Shurvell, H. F.; Quadri, S. M. *Spectrochimica Acta*, **1995**, A51, 1335.

24. Bulmer, J. T.; Shurvell, H. F.; In *Vibrational Spectra and Structure*, Vol. 6, Durig, J. R. Ed.; Elsevier: Amsterdam, **1977**, Chap. 2, pp. 91-172.

25. McBryde, W. A. E. *Talanta. Review*, **1974**, *21*, 979.

26. a) Campbell, J. M.; Park, Y. S.; Shurvell, H. H. *Canadian Journal of Applied Spectroscopy* **1991**, *36*, 147.b) Garyanova, E N.; Gol'dshtein, I. P.; Romm. I. P. *Donor Acceptor Bond.* John Wiley and sons: New York, **1973**, p132 and references therein.

27. Charney, E. The Molecular Basis of Optical Activity, Wiley-Interscience Publications: New York, 179, pp. 165-245.

28. Kirkwood, J. G.; *J. Chem. Phys.* **1939**, *7*, 911.

29. Bauer. E.; Magat, M. *J. Phys. Radium.* **1938**, *9*, 969.

30. Buckingham, A. D. *Proc. Roy. Soc.* **1958**, A248, 169.

31. Harman, H. H. *Modern Factor Analysis*; University of Chicago Press: Chicago, **1967**.

32. Fawcett, R. W.; Lui, G.; Faguy, P. W.; Foss Jr., C. A.; Motheo, A. *J. J. Chem. Soc. Faraday Trans.* **1993**, *89*, 811.

PART 3

An Investigation of the Influence of Solvent Effects on the Optical Rotation of Camphor.

CHAPTER I

INTRODUCTION

This study focuses on the influence that solvents have on the optical activity of (1R)-(+)-camphor. The term optical activity is used to describe the ability of certain substances to rotate plane polarized light.

The phenomenon of optical activity has a history which dates back to 1811 when it was first discovered by Argo. The basic laws and concepts of optical activity were developed in the period from 1810 to 1840 by Malus,[1] Fresnel[2] and Biot.[3] Since the time of Argo, Malus, Fresnel and Biot, many theories have been developed in an effort to explain optical activity.

The development of these theories is presented in a work by Charney.[4] In this work Charney points out that the most significant contribution to our present understanding of optical activity comes from Rosenfeld[5] who developed a quantum theory of optical activity. All present-day theories of optical activity have been developed from Rosenfeld's quantum approach.

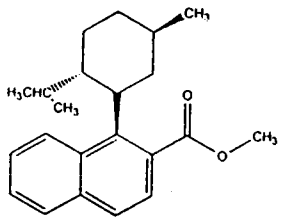
The optical activity of a sample is closely related to its refractive index.[5] In an optically active substance, right and left-handed circularly polarized light are transmitted at different velocities. Since, as previously stated, plane polarized light may be considered the resultant of two beams of circularly polarized light and opposite sense, the retardation of one or the other of these beams will produce a new resultant, polarized at a different angle from the incident beam. Retardation of one of the beams is due to a

difference in refractive index. When the refractive index of the left-handed circularly polarized light (n_L) is different from that for the right-handed circularly polarized light (n_R), the plane of polarization of the incident beam is rotated. The angle of this rotation $\delta\theta$ is given by

$$\delta\theta = (n_L - n_R)2\pi\, l/\lambda \qquad (1)$$

where λ is the wavelength of light and l. is the path length. The refractive indices differ for the two polarizations because of the helical structure that is inherent in molecules that are capable of rotating plane polarized light. If a molecule has a helical structure, its polarizability will depend on whether or not the electric field of the incident radiation follows the spiral of the molecule.

One of the earliest studies of solvent action on optical rotatory power was done by Rule and McLean.[6] They studied the influence of polar solvents on the rotatory power of 1-menthyl methyl naphthalate (**1**).

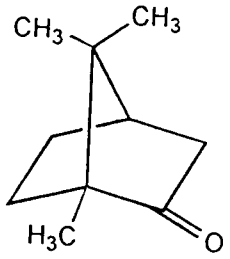


1

In their study they found that in a majority of cases the change in rotation was related to the polarity of the solvent. Rule and McLean found that polar effects are best studied by comparing solvents of the same type. In this study it was also found that for solvents of the same type a rough approximation to a smooth curve was obtained when rotating

powers are plotted against dipole moments.

In this study we were concerned about whether the dielectric constant reflected some intrinsic solvent effect or whether the solution changes the conformation of the reactant or if there is some change in the conformation equilibrium. These queries were investigated using camphor (**2**)which is a rigid molecule. Use of a rigid molecule reduces the problem to one of finding the solvent parameter or parameters which correlate best with the observed rotation.



2

We also wanted to investigate whether the specific rotation [α], was concentration dependent, as is usually assumed. The rotatory power R is given by

$$R = a(\text{conc.}) + b \tag{2}$$

for a 1-dm cell, where a and b are constants. The specific rotation [α] is given by

$$[\alpha] = a + \frac{b}{conc}. \tag{3}$$

Hence, if b = 0, [α] will not be concentration dependent unless the solvent properties are greatly affected by adding solute. If b = 0, a is then a measure of the solvent effect.

There was some concern in this study as to what the proper concentration unit in equations 2 and 3 was by which the solvent property could be related. After careful consideration molarity seems to be the appropriate concentration unit to use.

CHAPTER II

RESULTS AND DISCUSSION

The data presented in this study represent a preliminary effort to gain an understanding of the nature of solvent effects on the optical rotation of camphor. In Tables 3-1 through 3-13 are shown the data collected for the optical rotation of varying amounts of camphor in a variety of solvents. Table 3-14 contains a summary of Tables 3-1 through 3-14, with the number of grams of camphor being expressed to three significant figures. The slopes, intercepts and correlation coefficients obtained when these data are plotted as rotation versus grams of camphor is presented in Table 3-16. If the data in Table 3-14 are plotted using "Cricket Graph", the slopes, intercepts and correlation coefficients presented in Table 3-16 are obtained. In Figures 3-1 through 3-4 is shown the combined effect of concentration and nature of solvent on the optical rotation of camphor. The bar chart in Figure 3-5 gives a better visual image of the effect that the thirteen solvents used in this study had on approximately 2.00 g of camphor.

The solvent's ability to influence the optical rotation is due to one or more solvent parameters. An attempt was made in this study to see which solvent parameter best correlated to the changes in optical rotation which occurred when different solvents were used. In Table 3-18 is presented twelve solvent parameters which were considered to be potentially influential in altering the degree of optical activity. Definitions of these solvent parameters are given at the end of this chapter. As can be seen in Table 3-18 where the solvents are arranged in increasing order of the extent to which they influence

Table 3-1 Observed Rotations in Diethyl Ether		
Camphor (g)	Rotation	Rot./g
0.1246	+ 0.288	2.311
0.3729	+ 0.842	2.258
0.5089	+ 1.105	2.171
1.0401	+ 2.260	2.173
2.0028	+ 4.123	2.159
3.0066	+ 5.938	1.975
4.0228	+ 7.716	1.918
8.0582	+ 12.900	1.601

Table 3-2 Observed Rotations in Toluene		
Camphor	Rotation	Rot./g
0.1246	+ 0.213	1.709
0.2541	+ 0.426	1.677
0.5086	+ 0.846	1.663
1.0411	+ 1.700	1.633
2.0304	+ 3.259	1.605
4.0198	+ 6.072	1.511

Table 3-3 Observed Rotations in Acetone		
Camphor (g)	Rotation	Rot./g
0.1256	+ 0.250	1.990
0.2534	+ 0.501	1.97
0.5088	+ 0.993	1.952
1.0053	+ 1.920	1.910
2.0023	+ 3.722	1.859
4.0069	+ 7.003	1.748

Table 3-4 Observed Rotations in Acetonitrile		
Camphor (g)	Rotation	Rot./g
0.1255	+ 0.212	1.689
0.2500	+ 0.437	1.748
0.5016	+ 0.870	1.734
1.0037	+ 1.725	1.719
2.0076	+ 3.384	1.686
4.0079	+ 6.353	1.585

Table 3-5 Rotations in Methylene Chloride		
Camphor (g)	Rotation	Rot./g
0.1251	+ 0.233	1.863
0.2506	+ 0.455	1.816
0.5085	+ 0.899	1.768
1.0018	+ 1.780	1.777
2.0064	+ 3.448	1.719
4.0046	+ 6.490	1.621

Table 3-6 Observed Rotations in Methanol		
Camphor (g)	Rotation	Rot./g
0.1247	+ 0.210	1.684
0.2493	+ 0.381	1.528
0.5011	+ 0.757	1.511
1.0022	+ 1.501	1.498
2.0054	+ 2.937	1.465
4.0005	+ 5.572	1.393

Table 3-7 Observed Rotations in Benzene		
Camphor (g)	Rotation	Rot./g
0.1247	+ 0.197	1.580
0.2498	+ 0.387	1.549
0.5000	+ 0.767	1.534
1.0004	+ 1.531	1.530
2.0030	+ 2.989	1.492
4.0057	+ 5.888	1.470

Table 3-8 Observed Rotations in Cyclohexane		
Camphor (g)	Rotation	Rot./g
0.1242	+ 0.302	2.432
0.2495	+ 0.589	2.397
0.5004	+ 1.163	2.324
1.0006	+ 2.281	2.280
2.0033	+ 4.406	2.199
4.0039	+ 8.103	2.001

Table 3-9 Observed Rotations in Carbon Disulfide		
Camphor (g)	Rotation	Rot./g
0.1259	+ 0.214	1.700
0.2531	+ 0.429	1.695
0.5058	+ 0.826	1.633
1.0009	+ 1.670	1.668
2.0008	+ 3.263	1.631
4.0009	+ 6.144	1.536

Table 3-10 Observed Rotations in Dimethyl Sulfoxide		
Camphor (g)	Rotation	Rot./g
0.1259	+ 0.264	2.097
0.2566	+ 0.515	2.007
0.5938	+ 1.006	1.997
1.0041	+ 1.960	1.952
2.0043	+ 3.818	1.905
4.0037	+ 7.119	1.778

Table 3-11 Observed Rotations in Nitrobenzene		
Camphor (g)	Rotation	Rot./g
0.1248	+ 0.216	1.731
0.2508	+ 0.431	1.719
0.5023	+ 0.847	1.686
1.0015	+ 1.667	1.665
2.0012	+ 3.234	1.616
4.0036	+ 6.107	1.525

Table 3-12 Observed Rotations in N,N-Dimethylformamide		
Camphor	Rotation	Rot./g
0.1243	+ 0.238	1.915
0.2511	+ 0.478	1.904
0.5014	+ 0.940	1.875
1.0010	+ 1.852	1.850
2.0005	+ 3.594	1.791
4.0032	+ 6.886	1.720

Table 3-13 Observed Rotations in Hexafluorobenzene		
Camphor (g)	Rotation	Rot./g
0.1257	+ 0.307	2.442
0.2501	+ 0.625	2.499
0.5011	+ 1.231	2.457
1.0035	+ 2.337	2.329
2.0029	+ 4.469	2.231
4.0008	+ 8.230	2.057

Table 3-14 Summary of Optical Rotations of Camphor in Various Solvents.						
	Camphor (g)[a]					
Solvent	**0.13**	**0.25**	**0.50**	**1.00**	**2.00**	**4.00**
Methanol	0.210	0.381	0.757	1.501	2.937	5.572
Benzene	0.197	0.387	0.767	1.531	2.989	5.888
Nitrobenzene	0.216	0.431	0.847	1.667	3.234	6.107
Toluene	0.213	0.426	0.846	1.700	3.259	6.072
Carbon disulfide	0.214	0.429	0.826	1.670	3.263	6.144
Acetonitrile	0.212	0.437	0.870	1.725	3.384	6.353
Methylene chloride	0.233	0.455	0.899	1.780	3.448	6.490
N,N-Dimethylformamide	0.238	0.478	0.940	1.852	3.594	6.886
Acetone	0.250	0.501	0.993	1.920	3.722	7.003
Dimethylsulfoxide	0.264	0.515	1.006	1.960	3.818	7.119
sulfoxide	0.288	-	1.105	2.260	4.123	7.716
Diethyl ether	0.302	0.589	1.163	2.281	4.406	8.103
Cyclohexane	0.307	0.625	1.231	2.337	4.469	8.230
Hexafluorobenzene						
[a]The number of grams given as an approximation.						

Table 3-15 Intercepts (b), Slopes (m) and Correlation Coefficients (r) for Curves (Rot. vs. g) Using the Five Lowest Data Sets Obtained in a Given Solvent.[a]

Solvent	b	m	r
Diethyl ether	0.1087	1.9791	0.9993
Toluene	0.0244	1.5970	0.9999
Acetone	0.0383	1.8469	0.9999
Nitrobenzene	0.0332	1.6059	0.9999
Hexaflurobenzene	0.0813	2.2049	0.9997
Methanol	0.0284	1.4537	0.9999
Carbon disulfide	0.0148	1.6282	0.9999
Dimethyl sulfoxide	0.1043	1.7889	0.9992
Acetonitrile	0.0173	1.6823	0.9999
Dichloromethane	0.0313	1.7106	0.9999
Cyclohexane	0.0587	2.1806	0.9999
N,N-DMF[b]	0.0364	1.7126	0.9998
Benzene	0.0207	1.4865	0.9999

[a]Data obtained using linear regression on a Casio *f*x-7000G scientific calculator.
[b]N,N-Dimethylformamide.

Table 3-16. Intercepts (b), Slopes (m) and Correlation Coefficients (r) for Rot. vs Camphor (g) curves obtained using "Cricket Graph".[a,b]

Solvent	b	m	r
Methanol	0.0693	1.3886	0.999
Benzene	0.0314	1.4684	1.000
Nitrobenzene	0.0859	1.5112	0.999
Toluene	0.0975	1.5141	0.998
Carbon disulfide	0.0764	1.5339	0.999
Acetonitrile	0.0789	1.5872	0.999
Methylene chloride	0.0938	1.6172	0.999
N,N-Dimethylformamide	0.0787	1.7152	0.999
Acetone	0.1098	1.7425	0.999
Dimethylsulfoxide	0.1199	1.7719	0.998
Diethyl ether	0.1935	1.9036	0.998
Cyclohexane	0.1579	2.0174	0.998
Hexafluorobenzene	0.2088	2.0350	0.998

[a]A simple curve fit routine from Cricket Graph's menu was used to generate the data.bThe values for b, m, and r are slightly different from those in Table 2-15 because the number of grams used to make the plots are rouned to three significant figures instead of five as done in obtaining the data in Table 2-15.

Table 3-17. A Selection of Solvent Parameters						
Solvent	$c^{a,b}$	$\pi^{a,b}$	$\delta^{a,b,c}$	$E_T{}^b$	AN^b	DN^b
Methanol	887	285	29.8	55.4	41.5	-
Benzene	357	379	18.9	34.3	8.2	-
Nitrobenzene	-	-	-	41.2	14.8	81.0
Toluene	337	355	118.4	33.9	-	-
Carbon disulfide	410	377	20.2	32.8	-	-
Acetonitrile	590	379	15.8	45.6	18.9	-
Methylene chloride	414	408	20.3	40.7	20.4	-
N,N-Dimethylformamide	615	-	24.8	43.8	16.0	26.6
Acetone	398	337	19.9	42.2	12.5	17.0
Dimethylsulfoxide	600	-	24.5	45.1	19.3	29.8
Diethyl ether	251	264	15.8	34.5	3.9	19.2
Cyclohexane	285	326	16.9	30.9	-	-
Hexafluorobenzene	0	-	-	34.2	-	-

[a]Measured in MPa where 1 MPa = 1 $J.cm^{-3}$ = 0.2390 $cal.cm^{-3}$. [b]Source: Reference 10 and references therein.[c]Measured in $MPa^{1/2}$ where 1 $MPa^{1/2}$ = 1 $J^{1/2}.cm^{-3/2}$.

Table 3-17 (continued).						
Solvent	$\varepsilon^{a,c}$	$\mu^{d,e,i}$	$\eta^{f,g}$	β^i	α^i	π^*
Methanol	32.70	5.7	1.3290	0.62	0.93	0.60
Benzene	2.27[b]	0.00	1.5010	0.10	0.00	0.59
Nitrobenzene	34.82[b]	13.3	1.5510	0.39	0.00	1.01
Toluene	2.38[b]	1.00	1.4960	-	-	-
Carbon disulfide	2.64	0.00	1.6270	-	-	-
Acetonitrile	37.5	11.8	1.3460	0.31	0.19	0.75
Methylene chloride	8.93[b]	5.2	1.4260	0.00	0.30	0.82
N,N-Dimethylformamide	36.71	10.8	1.4310	0.69	0.00	0.88
Acetone	2.07[b]	9.0	1.3590	0.48	0.08	0.71
Dimethylsulfoxide	46.68	13.5	1.4790	0.76	0.00	1.00
Diethyl ether	4.33	3.8	1.3530	0.47	0.00	0.27
Cyclohexane	2.02	0.00	1.4260	0.00	0.00	0.08
Hexafluorobenzene	-	-	1.3770	-	-	-

[a]Given at 20 °C. [b]Given at 25 °C. [c]Source: The CRC Handbook, 67th edition. [d]Measured in 10^{-30} cm.[e]Dipole moment in Coulombmeter (Cm), measured in benzene, tetrachloromethane, 1,4-dioxane, or n-hexane at 20....30 °C. 1 Debye = 3.336·cm^{-1}. [f]Taken at 20 °C. [g]Source: The CRC Handbook, 67th edition. [h]Taken at 25 °C. [i]Source: Reference 10 and references therein.

*See notes on the following pages.

Table 3-17 (continued)

Definitions of the Selected Solvent Parameters in Table 3-17.

Cohesive Pressure. Also called cohesive energy density, the cohesive pressure, *c*, is a measure of the total molecular cohesion per unit volume. It is given by,

$$c = \frac{\Delta U_V}{V_M} = \frac{\Delta H_V - R \cdot T}{V_M} \qquad (2)$$

where ΔU_V and ΔH_V are the energy and the enthalpy of vaporization of the solvent to a gas at zero pressure, respectively, and V_M is the molar volume. The total strength of the intermolecular solvent structure is given by *c*. The more polar the solvent the higher *c* will be. Cohesive pressure is directly related to the energy required to create the cavities in a liquid during the dissolution process.

Internal pressure. The internal pressure π is defined as the change in the internal energy of a solvent which occurs when the solvent undergoes a very small isothermal expansion. It is given by

$$\pi = \left(\frac{\partial U}{\partial V_M}\right)_T \qquad (3)$$

where U is the molar internal energy, V_M is the molar volume and T is the absolute temperature. This internal pressure is created by the forces of attraction between solvent molecules that exceed the forces of repulsion

The Hildebrand solubility parameter. The Hildebrand solubility parameter, δ, is the square root of the cohesive pressure. This parameter is good for predicting the solvency of solvents for non-electrolyte solutes. Solvency is the ability of a solvent to dissolve a solute.

Dielectric constant. The dielectric constant, ε, is the ratio of the electrical capacity of a capacitor filled with the solvent to the electrical capacity of the evacuated capacitor. Polar solvents usually have high dielectric constants.

Acceptor numbers (acceptivities). Acceptor numbers, AN, are dimensionless numbers which express the acceptor property of a given solvent relative to that of $SbCl_5$. the acceptor number is given by,

$$AN = \frac{\delta_{corr}(A) - \delta_{cor}r(n-C_6H_{14})}{\delta_{cor}r(Et_3PO-SbCl_5) - \delta_{cor}r(n-C_6H_{14})} \cdot 100 = \Delta\delta corr \cdot 2.348 / ppm \qquad (4)$$

where δ_{corr} are the relative ^{31}P-NMR chemical shift values of n-hexane (reference solvent) related to those of the 1:1 adduct Et_3PO-$SbCl_5$ dissolved in 1,2-dichloroethane.

Table 3-17. (Continued)

Donor numbers (donicities). The donor number, DN, or donicity is a semiempirical measure of the nucleophilic properties of electron pair donor EPD solvents. This number is defined as the negative ΔH value for the 1:1 adduct formation between $SbCl_5$ and electron pair donor solvents (D) in dilute solutions of the reference solvent 1,2 dichloroethane. The donor number is given by

$$DN = -\Delta H_{D-SbCl_5} / (Kcal \cdot mol^{-1}) \quad (5)$$

Refractive index. The refractive index, η, is the ratio of the wavelength or phase velocity of an electromagnetic wave in a vacuum to that in the substance. When the substance is nonabsorbing and nonmagnetic at any wavelength, then η^2 is equal to the dielectric constant.

E_T(30) Values. The solvent polarity parameter, $E_T(30)$, is the transition energy for the longest wavelength solvatochromic absorption band of the pyridinium-N-phenoxide betaine dye. E_T is given by

$$E_T / (Kcal \cdot mol^{-1}) = h \cdot c \cdot \tilde{\nu} \cdot N_A = 2.859 \cdot 10^{-3} \cdot \tilde{\nu} / cm^{-1} \quad (6)$$

where h is Planck's constant, c is the velocity of light, $\tilde{\nu}$ is the wavenumber of the photon which produces the transition and N_A is Avogadro's number.

Hydrogen-bond acceptor (HBA) basicities and hydrogen-bond donor (HBD) acidities: The HBA basicities, β, are determined using UV/Vis spectral data of solvatochromic compounds. These shifts are determined for 4-nitroaniline relative to N,N-diethyl-4-nitroaniline. Only 4-nitroaniline can act as a HBD in HBA solvents; however, both standard compounds can act as HBA substrates in HBD solvents. The β-scale of solvent HBA basicities is established by taking the $\Delta\Delta\tilde{\nu}$ -value of 2800 cm^{-1} for hexamethylphosphoric triamide (a strong HBA) solvent as a single fixed reference point (β =1.00). The α-scale of solvent HBD acidities for HBD solvents is based on the same solvatochromic comparison method as the β-scale and is established by taking the $\Delta\Delta\tilde{\nu}$ -value of 6240 cm^{-1} for methanol (a strong HBD solvent) as a fixed reference point (α = 1.00).

The π* scale of solvent dipolarity/polarizability: This scale is based on the solvent effects on the π→π* electronic transitions of a group of aromatic compounds (4-nitroanisole, N,N-diethyl-3-nitroaniline, 4-methoxy-2-nitroaniline, 1-ethyl-4-nitrobenzene, N-methyl-2-nitro-*p*-toluidine, N,N-diethyl-4-nitroaniline and 4-dimethylaminobenzophenone). Initial measurements of the solvent effects on the $\tilde{\nu}_{max}$ values of this group of indicators are used to construct the preliminary π* scale. This scale is then expanded and corrected by multiple least-squares correlations with some additional solvatochromic indicators. The π*-scale of solvent dipolarity/polarizability measures the ability of a solvent to stabilize a charge on a dipole as a function of its dielectric effect.

Table 3-18 Observed Rotations of Camphor in Benzene and Methanol as a Function of Camphor's Molarity

Benzene		Methanol	
Molarity	**Rotation**	**Molarity**	**Rotation**
0.00101	+ 0.009	0.000994	+ 0.006
0.00202	+ 0.013	0.001988	+ 0.012
0.00303	+ 0.021	0.002982	+ 0.017
0.0101	+ 0.059	0.00994	+ 0.059
0.0202	+ 0.120	0.01988	+ 0.112
0.0303	+ 0.185	0.02982	+ 0.167
0.0398	+ 0.228	0.0400	+ 0.229
0.0597	+ 0.357	0.0600	+ 0.327
0.0796	+ 0.480	0.0800	+ 0.464
0.1008	+ 0.611	0.0994	+ 0.554
0.1994	+ 1.167	0.2001	+ 1.135
0.3991	+ 2.362	0.4002	+ 2.301
0.5987	+ 3.554	0.5987	+ 3.560
0.7985	+ 5.032	0.7985	+ 4.757
0.9995	+ 6.359	1.0005	+ 6.183
1.9950	+ 13.463	1.9989	+ 12.771

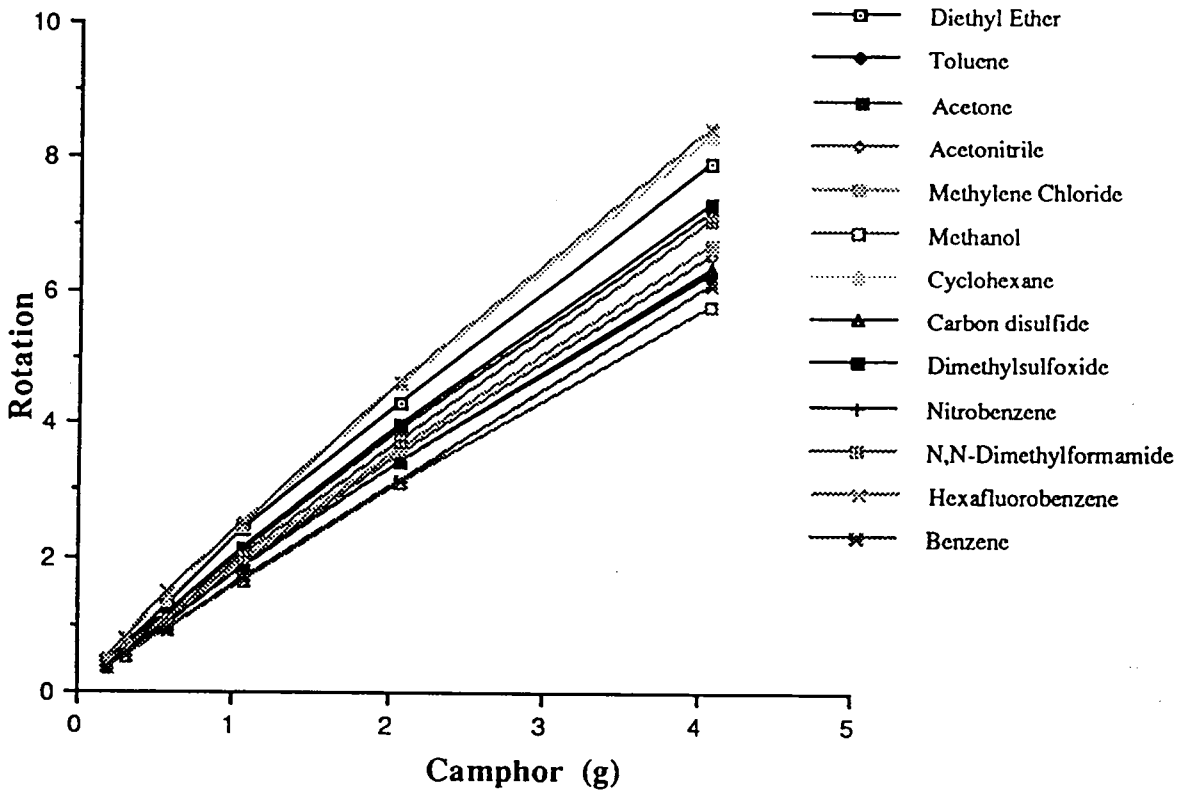


Figure 3-1. Plots of Rotation vs Camphor (g) in thirteen solvents.

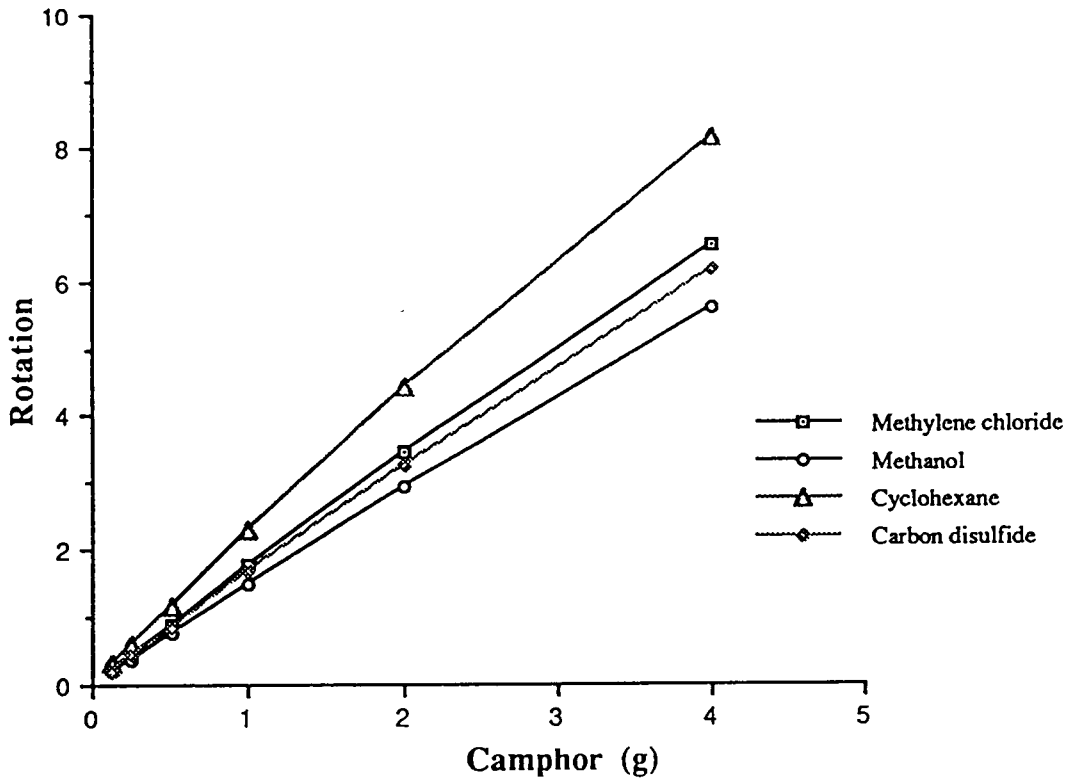


Figure 3-2. Plots of Rotation vs Camphor (g) in methylene chloride, methanol, cyclohexane and carbon disulfide.

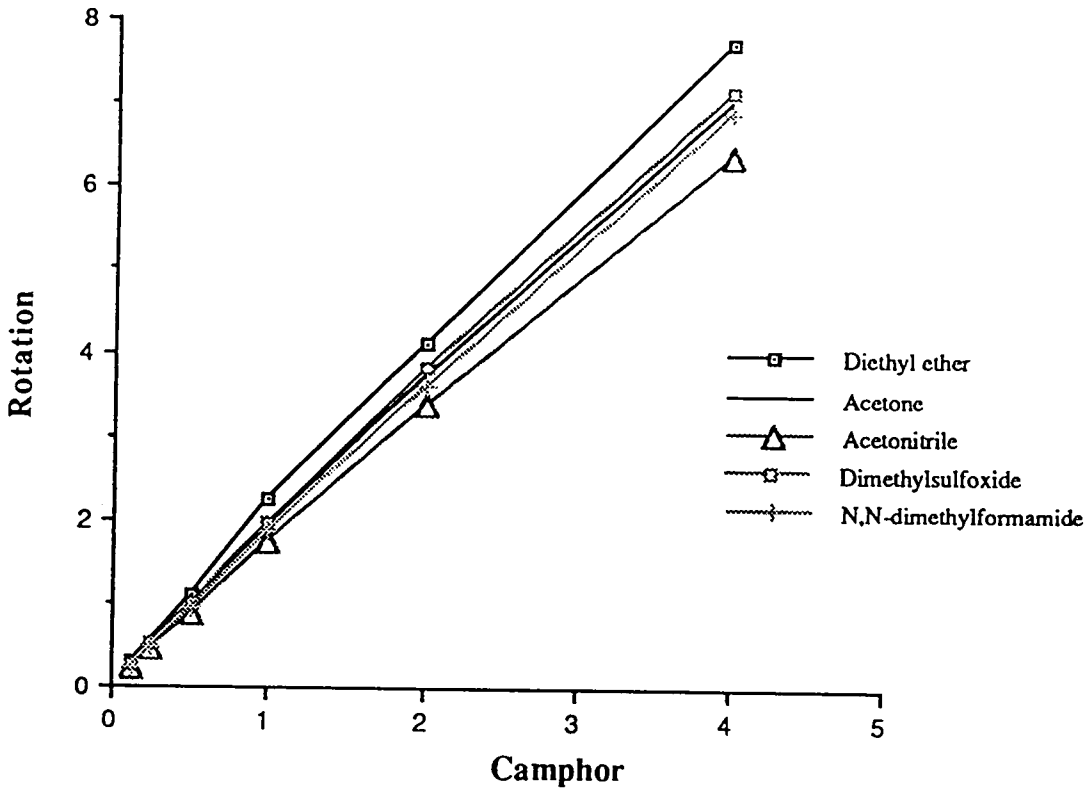


Figure 3-3. Plots of Rotation vs Camphor (g) in diethyl ether, acetone, acetonitrile, dimethylsulfoxide and N,N-dimethylformamide.

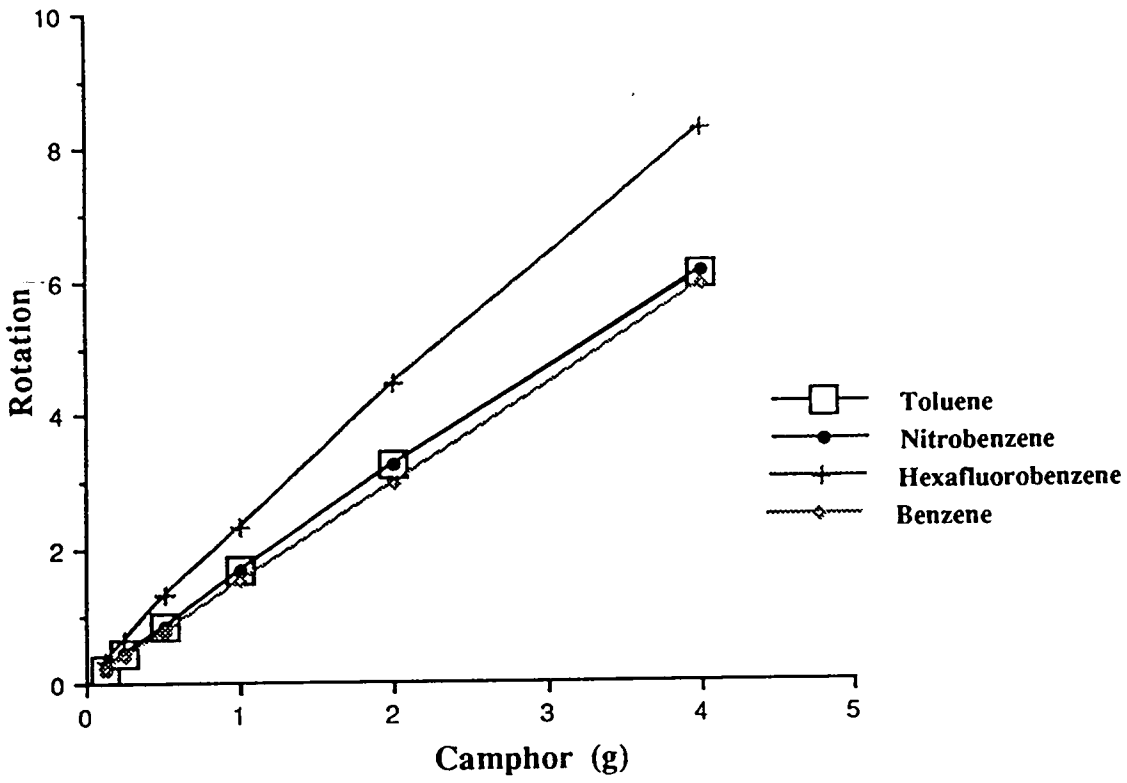


Figure 3-4. Plots of Rotation vs Camphor (g) in toluene, nitrobenzene, benzene and hexafluorobenzene.

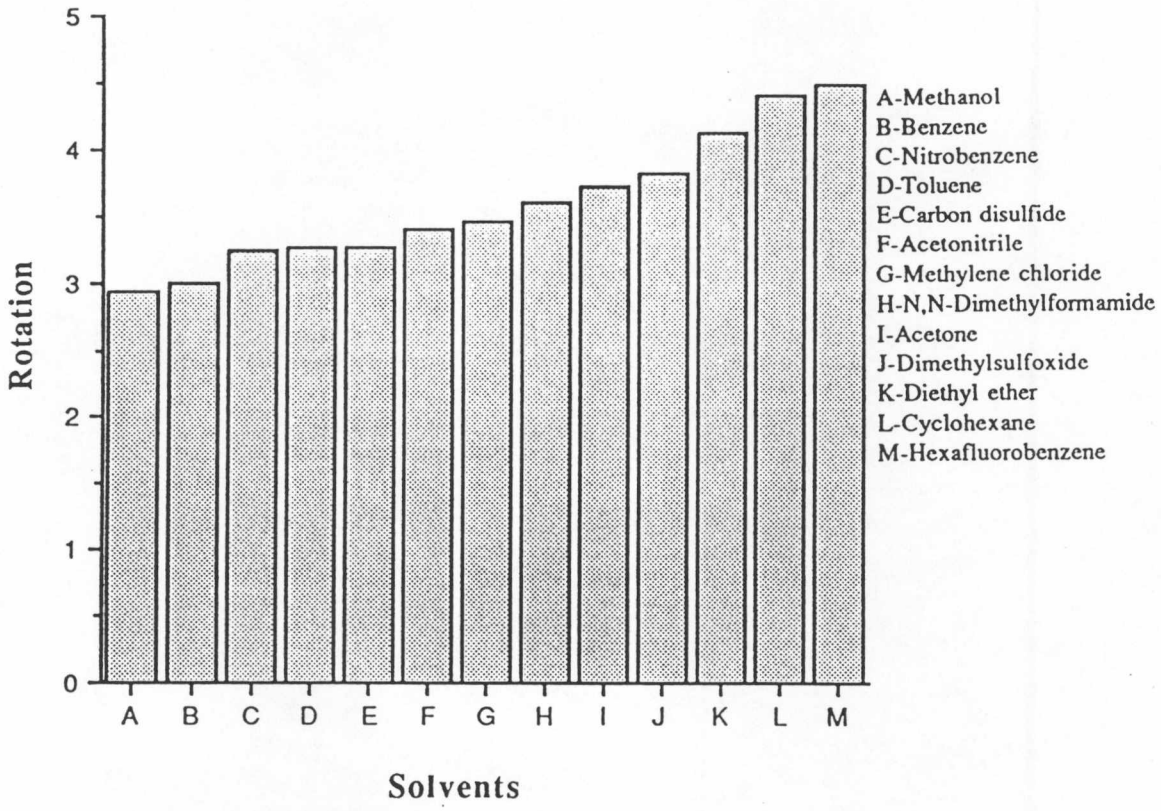


Figure 3-5. The effect of solvent on the rotation of two grams of camphor.

the optical rotation, there is no apparent correlation between the solvent parameters and the size of the optical rotation.

Rule and McLean[6] were among the first to investigate the influence of solvent on optical rotation. They concluded, after studying the relationship between the optical rotation and the dipole moment of 1-mentylmethylnaphthalate in various solvents, that the rotation was lowest in strongly polar solvents and highest in solvents whose dipole moment was zero. Beckmann, Cohen and Marks[7,8,9], showed after a vigorous mathematical proof, that the dipole moment is not the sole controlling factor in the relationship between optical rotatory and the nature of the solvent. In these papers they developed and verified a theory of solvent effects on optical rotatory power. These authors attributed the change in optical rotatory power with change in nature of solvent to deformation of the active molecule by the electrostatic field of the solvent molecules. According to Beckmann, Cohen, and Marks, this deformation is due to minute variations in the position of the virtual oscillators of the active molecule. These minute changes result in very large changes in rotatory power. Rotivity is a measure of optical rotatory power. The rotivity ,Ω, ($\Omega \equiv [\alpha]/\eta^2+2$), where $[\alpha]$ is the specific rotation and η^2 is the square of the refractive index of the medium, is a linear function of the average electrostatic field, $[F]_{AV}$, acting on the optically active molecule. The rotivity can be restated as

$$\Omega = \Omega_1 + \Omega'[F]_{AV} \qquad (1)$$

where Ω_1, is the rotivity in a zero field and Ω' is a deformability constant associated with

the active molecule. Beckmann *et al.* returned later and refined this equation to take into account the London dispersion forces and the effects of liquid structural characteristics as well as dipole forces. Beckmann and coworkers tested their general theory of optical rotatory power of liquids in a wide range of solvent systems. In all the cases studied the data were found to be in excellent agreement with the theory. The studies conducted by Beckmann and his colleagues were done using solvent systems which were formulated by the progressive replacement of nonpolar solvent by polar solvent. The following expression was derived to measure the change in optical rotatory power, S, produced by these solvents systems in the presence of an optically active molecule,

$$S \equiv (\Omega - \Omega_o)\frac{VM_\gamma}{w_\gamma} = 6\Omega'\mu_\alpha w_\alpha \frac{M_\gamma}{M_\alpha}\left(\frac{P_\alpha J_\alpha - P_\alpha^{\,o} J_\alpha^{\,o}}{w_\gamma}\right)$$

$$+6\Omega'\mu_\alpha \frac{M_\gamma}{M_\beta}\left(\frac{w_\beta P_\beta J_\beta - w_\beta^{\,o} P_\beta^{\,o} J_\beta^{\,o}}{w_\gamma}\right) + 6\Omega'\mu_\alpha P_\gamma J_\gamma = G(\alpha,\beta,\gamma) + K_{\alpha\gamma} P_\gamma,$$

where Ω is the rotivity of the solution, V, the volume of the system, M, the molecular weight, w, the weight of substance, Ω', the deformability constant of the optically active substance, P, a molar polarization and j, an integral describing the radial distribution of molecules. The subscripts α, β, and γ refer to the optically active substance, the nonpolar solvent and the polar solvent, respectively, and the subscript 0, refers to the value of the quantity when $w_\gamma = 0$. $K_{\alpha\gamma}$ and $G(\alpha,\beta,\gamma)$ are constants to which S can be reduced if the term $(w_\beta - w_\beta^{\,o})/w_\gamma$ is a constant as in ideal solutions or is linear in P_γ, as was observed experimentally by Beckmann and his coworkers. The equation for S just described above shows that the solvent effect on the optical rotatory power of an optically active

substance is not a simple correlation of solvent parameters but is a rather detailed function of solvent parameters and forces which operate at the molecular level.

In this study we were also concerned about the appropriate concentration unit to use in the expression of the optical rotation, R = a(conc.) + b, where a represent the solvent effect and where b should be zero at infinite dilution. The solvents can be placed in increasing order of optical rotatory power on the basis of the size of a which is the slope of R, the rotation, verus conc. curve However, this ordering is dependent on the concentration unit used in generating the plot. The ordering of any selection of solvents in terms of optical rotatory power should be invariant. We believe that molarity is the correct concentration unit to be used. Work is currently being done to clarify this issue. Table 3-18 contains the observed rotations when molarity is used for the methanol/camphor system and for the benzene/camphor systems. Figures 3-6 through 3-9 are plots which show the linear relationship between the molarity and the rotation. Figures 3-7 and 3-9 show how the curve approaches the origin for very dilute concentrations.

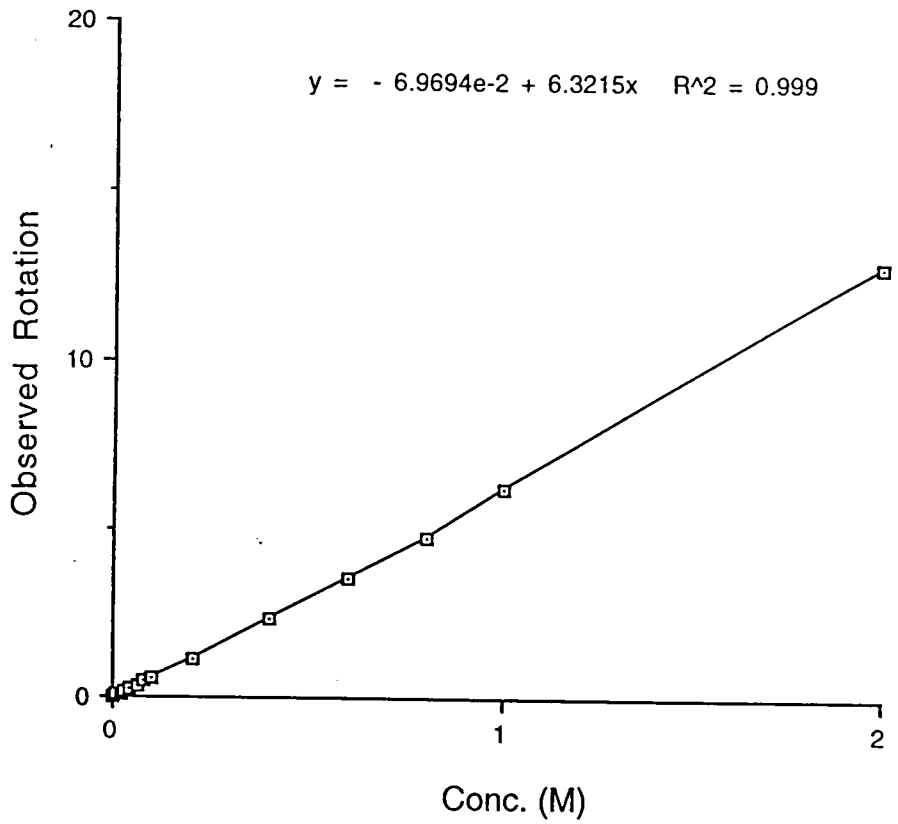


Figure 3-6. Plot of Observed Rotation vs Conc.(M) for the camphor/methanol system.

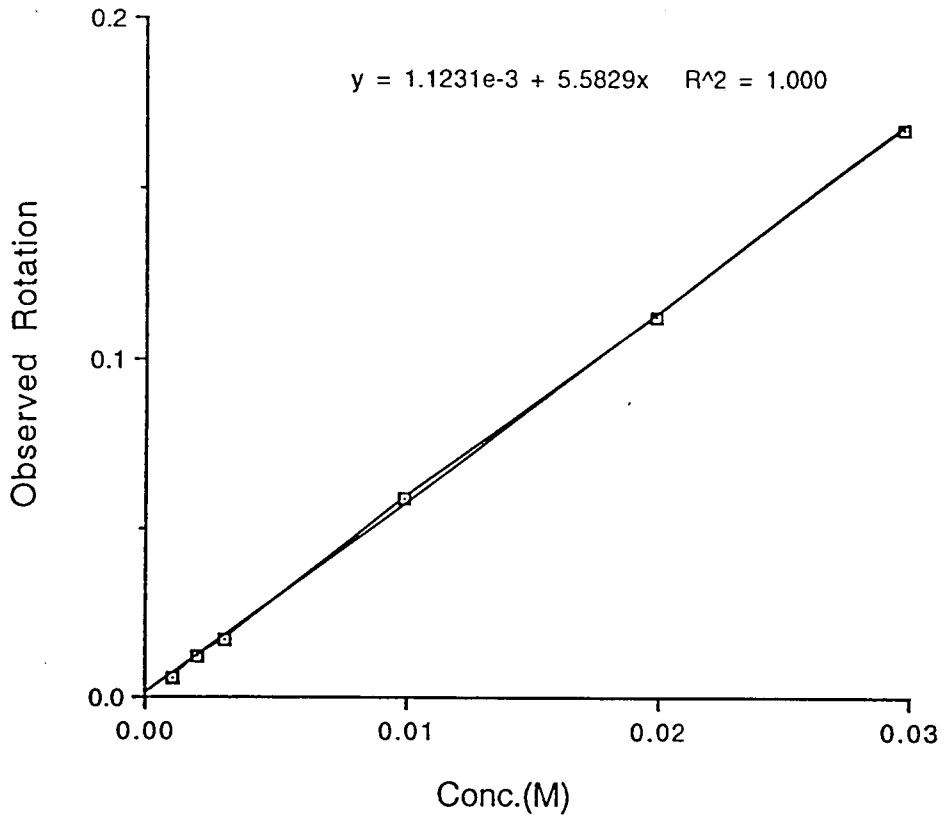


Figure 3-7. Plot of Observed Rotation vs Conc.(M)(dilute) for the camphor/methanol system.

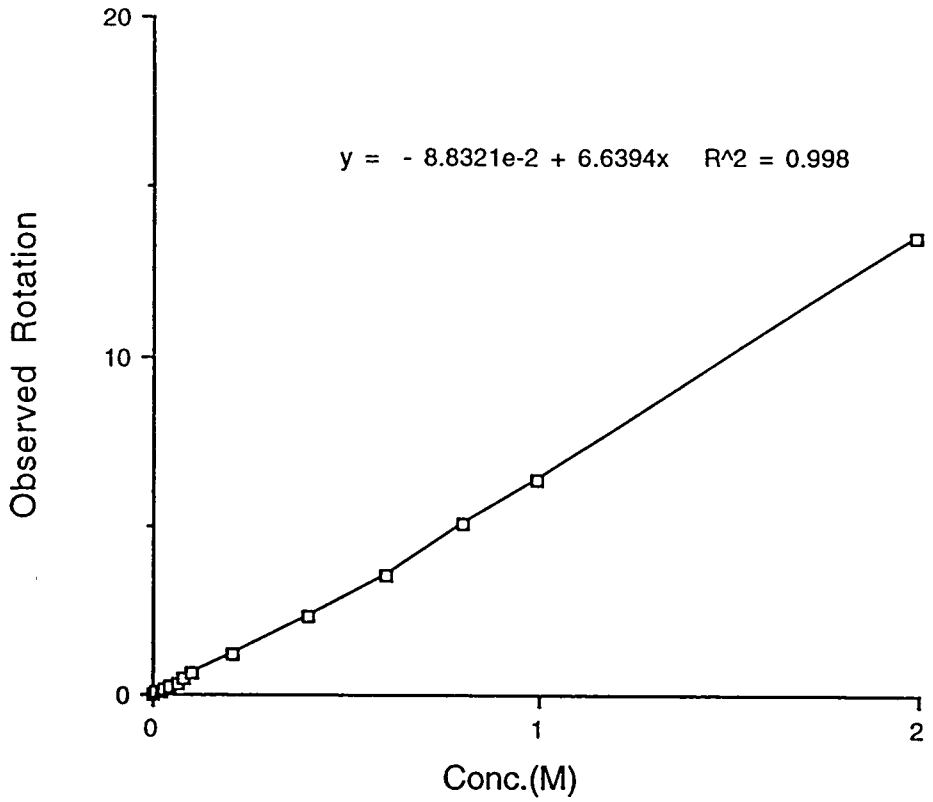


Figure 3-8. Plot of Observed Rotation vs Conc. (M) for the camphor/benzene system.

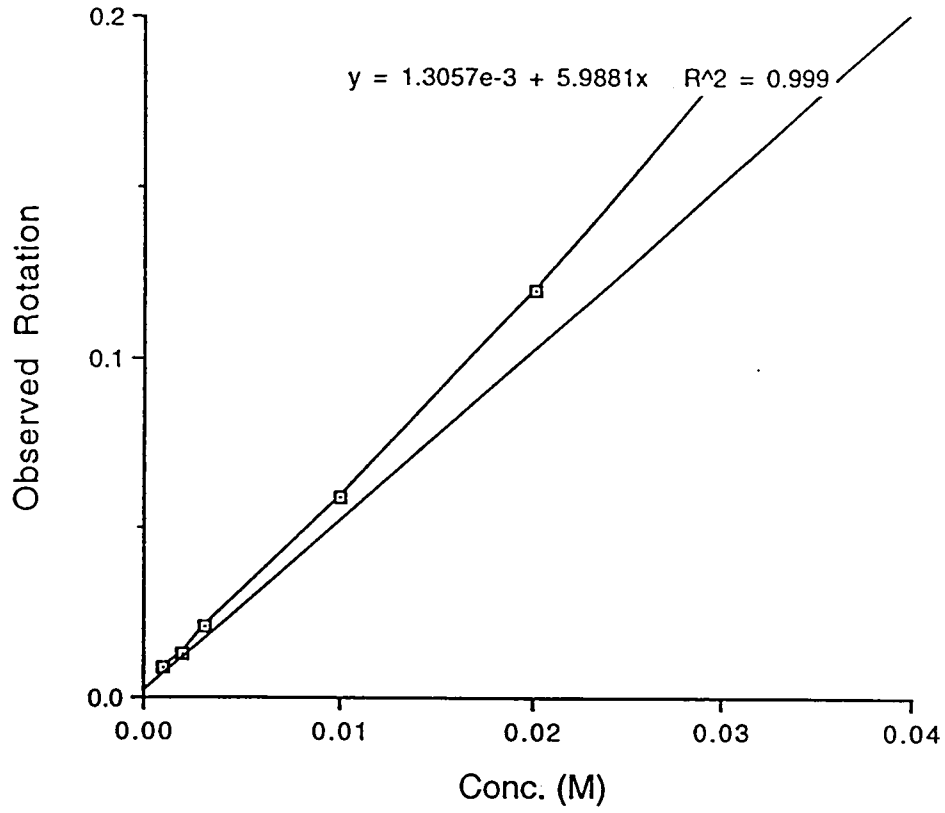


Figure 3-9. Plot of Observed Rotation vs Conc.(M) (dilute) for the camphor/benzene system.

CHAPTER III

EXPERIMENTAL SECTION

General. All glassware was oven dried overnight before use. Optical rotations were performed on a Perkin Elmer model M421 polarimeter. Carbon disulfide, cyclohexane and dimethyl sulfoxide were purchased from Aldrich Chemical Co.. They were used as received. Nitrobenzene, methanol, diethyl ether, toluene and benzene were obtained from Fisher Scientific and were used as purchased. Acetonitrile, methylene chloride and acetone were obtained from Mallinckrodt and were used as purchased. N,N-Dimethyl formamide was obtained form Matheson Coleman and Bell and was dried over molecular sieves for two days before use. Hexaflurobenzene, obtained from Oakwood Products Inc., was used as purchased. (1R)-(+) Camphor (99%, M.P. 179 - 181°, $[\alpha]^{25}$ +44.1°) was purchased from Sigma Chemical Co. and was used as received.

Preparation of solutions. All solutions except for molar solutions were prepared by adding to a 50-mL volumetric flask, containing a weighed amount of camphor, 25 mL of the selected solvent. The solvent was measured out in a 25-mL volumetric flask. The resulting solution was shaken to dissolve the camphor and was subsequently stoppered until ready to be used in taking optical rotations. Molar solutions were prepared by adding the molar amount of camphor to a 10-mL volumetric flask, which was then diluted to the mark with the selected solvent.

Polarimetric Data: All polarimetric readings were done at 21^0C and were taken using a standard glass cell having a path length of 1 dm and a capacity of 6.2 mL. All volatile

solvents were handled in a hood. The glass cell was cleaned with acetone between changes of solvent. It was then dried using the laboratory air supply. When using a given solvent, readings were taken in increasing order of camphor concentration. The polarimeter was set at an integration of 5 seconds and a sodium lamp was used as the monochromatic light source.

REFERENCES

1. a) Biot, J. P. *Bull. Soc. Phil.* **1815**, 190. b) Lowry, T. M. *Optical Rotarory Power*, Longmans Green: London, **1935**, p20.

2. Fresnel, A. *Ann. Chim. Phys.* **1825**, *28*, 147.

3. Malus, E. L. *Mem. Soc. Arcueil*, **1808**, *1*, 113.

4. Charney, E. *The Molecular Basis of Optical Activity*, John Wiley and Sons: New York, **1979**, pp. 1-10.

5. Atkins, P. W. *Physical Chemistry*, 4th ed.; Freeman and Company: New York, **1990**, 653.

6. Rule, G. H.; McClean, A. *J. Chem. Soc.* **1931**, *1*, 674.

7. Beckmann, 0. C.; Cohen, K. *Journal of Chemical Physics*, **1936**, *4*, 784.

8. Beckmann, O. C.; Marks, H. C. *Journal of Chemical Physics*, **1940**, *8*, 827.

9. Beckmann, O. C.; Marks, H. C. *Journal of Chemical Physics*, **1940**, *8*, 831.

10. Reichart, C. *Solvents and Solvent Effects in Organic Chemistry*, 2nd ed.; VCH: New York, **1990**.

VITA

Gerald Henderson Springer was born in St. Lucy, Barbados. He attended the Coleridge and Parry Secondary School and later took advanced level courses in physics, chemistry, biology and mathematics at the Barbados Community College. In June 1993, he graduated with honors from Oakwood College in Huntsville Alabama with a Bachelor of Science degree in Chemistry with a minor in Mathematics. In January 1994, he accepted a teaching assistantship from The University of Tennessee, Knoxville and received the Master of Science degree in Chemistry in May 1997. In January 1997, he accepted a teaching assistantship to pursue study towards a Ph.D. in Materials Chemistry at Kansas State University in Manhattan Kansas. Gerald is an accomplished pianist and violinist, who enjoys playing the works of Bach and Chopin and who also enjoys jazz and other contemporary styles.